Characteristics and origin of black breccia and its relation to adjacent facies within the Martha hill deposit, Waihi

A thesis presented in partial fulfillment of the requirements for the degree of

Masters of Science (Research)

in

Earth Sciences

Gianluca Domenico Salsano

THE UNIVERSITY OF
WAIKATO
Te Whare Wānanga o Waikato

The University of Waikato
School of Science
New Zealand

December 2022

Abstract

The Coromandel Volcanic Zone [CVZ] was an active continental volcanic arc between 18 – 1.9 Ma that was responsible for bimodal andesitic–dacitic–rhyolitic volcanism. Following the emplacement of these volcanic formations, some became locally hydrothermally altered to generate ≈ 50 low sulphidation Au–Ag deposits within the CVZ (Hauraki Goldfield). The Martha Hill deposit is a rift–low sulphidation adularia–sericite gold deposit situated in the township of Waihi, New Zealand. Notably, the origin of a black breccia appearing in core logs at the Martha Hill deposit was previously unknown. The focus of this study was to identify the origin of the black breccia through analyses of three separate drill cores (pertaining to the black breccia), and to discover its significance in the paleo–geothermal field at Martha. Analytical techniques included core logging, microscopy, x–ray diffraction [XRD], x–ray flourescence for geochemical majors [XRF] and scanning electron microscopy [SEM]. Initial core logging and analyses recognised 10 new facies relating to the black breccia. These recognised facies fell under three separate categories; two facies for the weakly altered, five for the highly altered and three for the breccia facies. One of the weakly altered facies best reflects the andesite country rock of the Waipupu Formation. The other weakly altered facies is a foreign clast inclusion of a breccia deposited during the original emplacement of the andesite lavas. The five highly altered facies are related to the varying degrees and overprinting events of the paleo–hydrothermal fluid. One of the breccia facies related to the original emplacement of andesite lava as an autobreccia, whilst the other breccia facies was the product of hydraulic fracturing in the sub–surface. Based on core logging, petrographical and geochemical analyses, the black breccia was discovered to be related to diatreme formation. Diatreme formation can vary among deposits due to the post–eruptive hydrothermal environment (high versus low sulphidation) and the nature of the mechanism utilised to generate the diatreme (phreatomagmatism or hydrothermal eruption). However, the poorly sorted, matrix supported nature of the black breccia that was observed during core logging is widely associated with volume expansion (a hydrothermal brecciation mechanism responsible for diatreme formation). Diatreme formation is the result of an increase in temperature or depressurisation. Facies that may suggest the presence of a feeder dike responsible for generating volume expansion and phreatomagmatism was not observed during core logging, but may be present at greater depths or in other drill core. A more likely scenario for the formation of black breccia was due to depressurisation and volume expansion in the near surface due to hydrothermal eruptions. Indeed, initial steam bursts may have ejected cover materials at the surface resulting in depressurisation and boiling in the near–surface. Brecciation and fragmentation would have likely continued and propagated further downward until the steam supply rate was insufficient to further brecciate and uplift rock fragments. Carbonate veins (calcite) that were present during core logging indicates that the paleo–geothermal field reset after the formation of the black breccia and associated diatreme. The presence of adularia indicated by XRD analyses within the black breccia matrix, signifies that the paleo–hydrothermal fluid temperatures after the emplacement of black breccia was ≈ 180 – 350°C.

Acknowledgements

I would like to thank everyone who has contributed to this study and who has had a positive impact on myself during my time undertaking this research at The University of Waikato.

First off, a massive thank you to my supervisor Dr.Adrian Pittari, for your mentorship, patience and optimism throughout the duration of my project. I am truly grateful for all the time you have spent checking and providing suggestions for my chapters.

Thank you in particular to Shannon Richards for suggesting the idea for this project and for taking the time to provide intellectual conversations and assist with access to cores and data.

Thank you to the School of Science technical staff; Kirsty Vincent, Helen Turner and Annette Rodgers for your training and assistance on all of the petrographical and geochemical equipment used during the course of my research.

Thank you AUSIMM for the MSc Education Endowment Trust scholarship.

Thank you to my family Mum, Papa, Ciro and Jess for all the love and support you have given me over the years.

Cheers to my friends; Caleb, Carlos, Kaea and Will and everyone in The Tron disc for the laughs, banter and company.

Thanks to all the new colleagues and friends I have made while undertaking my research and Unirec gym for providing the equipment needed to keep myself physically fit and mentally healthy.

Contents

List of Tables

List of Figures

Chapter 1
Introduction

1.1 Overview

The Coromandel Volcanic Zone [CVZ] is a continental volcanic arc that was active between 18 and 1.9 Ma (Christie et al., 2007; Nicholson et al., 2004). During this time, it was dominated by bimodal andesitic-dacitic-rhyolitic volcanism. The CVZ can be regarded as the successor to the Northland volcanic zone [NVZ] and a precursor to the currently active Taupo Volcanic Zone [TVZ]. The CVZ serves as a major geological interest within North Island of New Zealand, due to its economic value with the presence of gold bearing Miocene aged andesite host rocks. As such, the CVZ is also referred to in literature as the Hauraki Goldfield, which likely reflects its gold bearing qualities. Previous studies have been based on the gold bearing andesite host rocks found within the area (Brathwaite & Faure, 2002; Brathwaite et al., 2006; Christie et al., 2007) and the wider tectonic-forming processes including those associated with the migration of volcanism to the TVZ (Julian, 2016, and references therein). The Hauraki Goldfield is a north-south-oriented belt, extending 200 km long and 25 km wide (Skinner, 1986). It has been divided into three provinces (northern, eastern and southern) based on factors such as host rock and geologic settings (Fig. 3.2) (Christie et al., 2007). Around 97% of past gold production was from deposits hosted within rocks from the Coromandel Group. To date the majority of gold production has been carried out on the world-class Martha Hill deposit in Waihi (John, 2011). Through 2009, total production from both underground and open-pit mining was approximately 66% and 89% of total Gold [Au] and Silver [Ag] production respectively (John, 2011; Spörli & Cargill, 2011). Veins forming within the Martha Hill deposit are hosted almost entirely within a lower andesite unit which begins to pinch out in the upper andesite (Shannon & Lorrance, 2022). However, southeast of the Martha deposit, veins are hosted solely within an upper andesite unit at Favona, which challenges the previous assumption of preferential mineralisation within the lower andesite unit. Furthermore, such discoveries reinforce the idea that despite an extensive mining history of over 127 years, there are more economic veins to be discovered. Within core logs of the epithermal Martha vein system, a type of hydrothermal breccia appears which is denoted by geologists at OceanaGold as the carbonaceous black breccia. During this project, 3 drill cores previously logged by OceanaGold were studied with a focus on sections containing the black breccia and its surrounding facies. These sections were logged, sampled and analysed petrographically and geochemically. Through understanding the significance of the black breccia deposit, its presence in future core logs can potentially prove invaluable to the discovery of new epithermal gold deposits.

1.2 Research aim & objective

This study aims to interpret the geological processes involved in the creation of the black breccia to better understand its significance within the hydrothermal vein system at the Martha Hill deposit in Waihi. Secondly, spatial associations and a potential relationships between the black breccia and

other facies will be determined.

Therefore, the objectives for this study will;

- Identify and log sections containing the black breccia including, its transitional surrounding facies.
- Document the petrographic and geochemical characteristics of the deposits.
- Identify the origin of the black breccia and generate assumptions on the processes involved in generating the deposit.

The objectives will be carried out using three separate drill cores (800SP3MN1216, 920SP2MN1164, EMP16RG1842), provided by OceanaGold from the Martha Hill deposit. These drill cores were selected as they were previously logged to contain black breccia.

1.3 Location of Study

The study was undertaken within the township of Waihi, located on the Coromandel Peninsula, within the North Island of New Zealand. Core sampling was carried out in the core shed for OceanaGold at; 43 Moresby Avenue, Waihi 3610 (fig. 1.1). In total, sections of core pertaining to the black breccia were taken from three separate drill holes. These core samples were then taken back to The University of Waikato to be logged and petrographically and geochemically analysed.

1.4 Thesis Structure

Chapter 2 reviews literature that covers relevant processes involved in epithermal mineral alteration through hydrothermal activity. This chapter covers what hydrothermal alteration is and how each style of alteration and its zones affects mineralisation. Furthermore, the effects of volcanism, tectonism and structural settings will be discussed, followed by expected deposit characteristics within arc and rift low sulphidation environments. Chapter 3 encapsulates an in depth literature review of current research of the known tectonic and geological history of the Waihi region. Furthermore, regional variations and similarities are investigated among the different Hauraki goldfield provinces and an overview of the Waihi veining system is given. An assessment of the identified facies and drill core descriptions following core logging on 3 separate drill holes is given in Chapter 4. Petrography and geochemistry analysis on the recognised facies will be given in chapter 5. Facies analysis within this chapter covers microscopy, X-ray flourescence [XRF] (and portable XRF), X-ray diffraction [XRD] and scanning electron microscopy [SEM]. Chapter 6 discusses the data collected in Chapters 4 and 5. This includes a brief description of the petrograhpic and geochemical indicators for alteration found in Chapter 5. Relationship and origin of the 10 different facies based on data from Chapters 4 and 5 is provided next. Finally, an in depth discussion pertaining to the origin implications of the black breccia based on my uncovered data is provided last. Chapter 7 details the key findings of this study and suggests further work. A reference list covering all of the literature is provided last, followed by an appendices of all the raw data generated during the study.

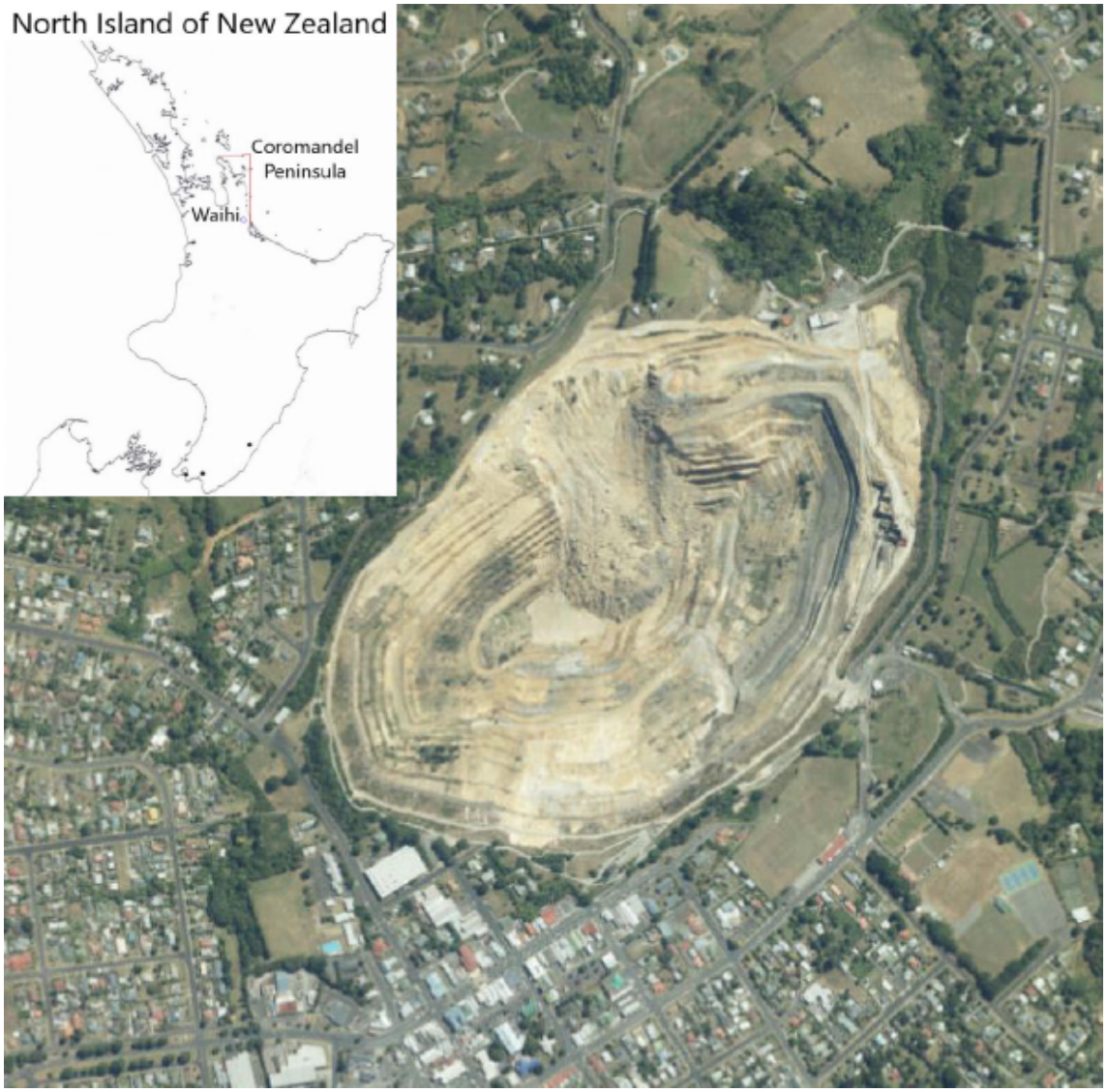

Figure 1.1: Figure showing the study area of Waihi, located on the Coromandel Peninsula in the North Island of New Zealand.

Chapter 2
Epithermal gold deposition

2.1 Introduction

Epithermal deposits are economically valuable deposits that are responsible for the precipitation of precious metals such as gold. The word epithermal comes from the Greek word 'epi' and 'thermal' meaning shallow heat. Lindgren (1933) defined the term 'epithermal' from mineralogical and textural observations and deduced the pressure and temperature (depth) conditions for this style of mineralisation (White & Hedenquist, 1990). Simmons and Browne (1997) highlights that epithermal mineral deposits form in the shallow parts of hydrothermal systems where sharp, temperature, pressure and chemical gradients favour the precipitation of metals. Previously, the presence and deposition of precious metals found within these systems had been known (Weissberg, 1969). However, it was not until the discovery of the scale of such deposits (up to 6 wt % Au, 30 wt % Ag) on the back pressure plates of geothermal wells (Brown, 1986) that the depositional potential of such systems became recognised (Simmons & Browne, 1997).

This chapter covers what hydrothermal alteration is and the subsequent different styles of alteration caused. Furthermore, the different epithermal deposit environments and the effects of igneous, tectonic and structural controls are discussed. Lastly, gold deposit classes found in low sulphidation arc and rift environments are discussed. We recognise the transitional differences within these classes as the system begins to telescope outward and upward further from an intruding magmatic source.

2.2 Hydrothermal alteration

Hydrothermal alteration is the process occurring between a hot aqueous fluid interacting with and circulating through a host rock. There are observable mineralogical, chemical and textural changes within the host rock causing a change in primary volcanic minerals altering into other secondary minerals. Often, the formation of alteration halos are observed extending from a magmatic heat source into the sites of mineralisation and beyond the limits of mineralisation (fig. 2.1). Proper identification for sites of mineralisation and accurate reconstruction of past hydrothermal systems, are crucial processes during exploration as they assist in narrowing the prospective sites of mineralisation. Temperature, pressure, host rock composition, fluid geochemistry and the duration of activity, are observed as strong controllers for the formation of hydrothermal minerals (Browne, 1978) As these controls evolve over time and distance from the magmatic heat source, a change in the styles of alteration and subsequent mineral assemblages can be observed (fig. 2.1).

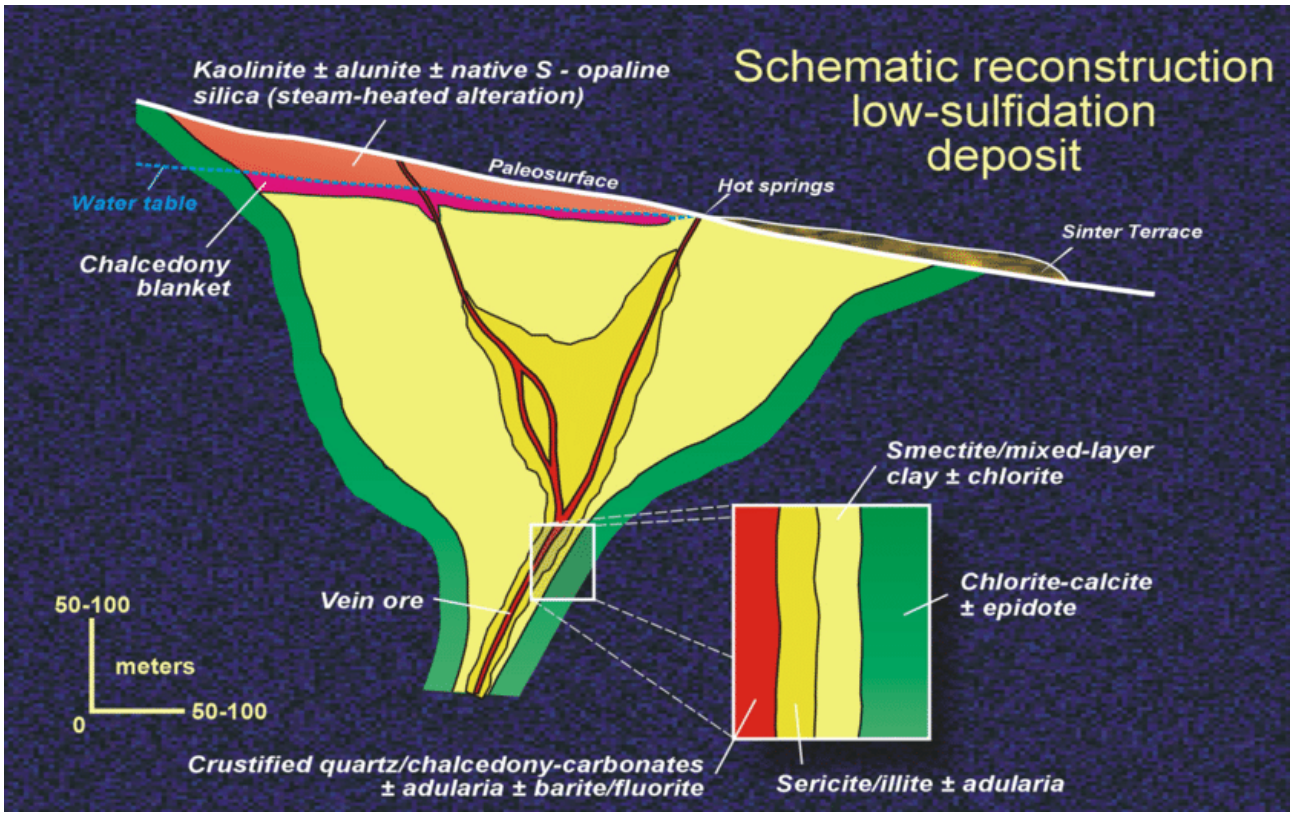

Figure 2.1: Figure showing the outward and upward zonation of different mineral assemblages in low sulphidation environments (from Arribas et al., 2000).

2.2.1 Fluid geochemistry and alteration styles

· There are three end member hydrothermal solution compositions that exist in the geothermal-epithermal environment (Simmons & Browne, 1997): chloride water (near neutral fluid), bicarbonate waters (alkaline fluid) and acid sulphate waters (acidic fluid). These different water types are attributed to the differences in temperature, pH and gas contents and in turn are responsible for the formation of specific mineral assemblages (Simmons & Browne, 1997). Hydrothermal mineral assemblages are only stable over a limited range of pH and temperatures and as such, their characteristics can be used to reconstruct the thermal and geochemical structure of a past hydrothermal system (fig. 2.2; Sillitoe, 1994; Simmons & Browne, 1997).

Propylitic alteration

In low sulphidation systems, the chloride waters are responsible for transporting metals into the epithermal environment. During periods of activity, the chloride waters produce quartz (chalcedony and amorphous silica), illite, adularia, albite, epidote, chlorite, calcite and pyrite (Simmons & Browne, 1997). This order of mineral assemblage is referred to as the propylitic alteration portion of mineral assemblages within the low sulphidation epithermal environment. Propylitic alteration is typical of low temperature conditions usually $< 200°C - 250°C$. This extends laterally away from the ore body, with quartz, illite, adularia and pyrite predominating in the vicinity of mineralisation (Simmons & Browne, 1997).

Argillic alteration

Argillic alteration assemblages consist of minerals formed at relatively low temperatures $< 200°C - -250°C$. Argillic alteration occurs in the shallowest parts of the hydrothermal system where it overprints propylitic alteration – particularly adjacent to veins and fractures (Christie et al., 2007). Typical mineral assemblages are smectite, illite–smectite, kaolinite, quartz and pyrite. At the Waihi Martha deposit, marginal and shallow bicarbonate waters are assosciated with illite, smectite, calcite and siderite, which account for widespread argillic halos found at shallow levels (Simmons & Browne, 1997). Acid–sulphate waters are associated with surficial pocket depositions of kaolinite, alunite and pyrite, which form at the paleo–water table and represent boiling above it (Simmons & Browne, 1997). Complex mineral relationships do exist due to successive alteration mineral replacements and overprinting events, complicating distinct subdivision of argillic and propylitic alteration types (Christie et al., 2007).

Advanced argillic alteration

Advanced argillic alteration is characteristically formed within acidic conditions with a pH < 4 and associated with high sulphidation environments. Advanced argillic alteration consists of greater temperature conditions than argillic alteration at temperatures $> 250°C$. Advanced argillic style is characterized by kaolinite, pyrophyllite or dickite and alunite together with lesser quartz, topaz and tourmaline (Singh, 2015). Sulphides and amorphous clays may also be present in variable concentrations.

Phyllic alteration

Phyllic alteration occurs at low to intermediate temperatures $< 200°C$ – $350°C$ and generally characterizes the deeper margins of epithermal deposits. Sericite is the most dominant alteration mineral present with kaolinite and chlorite group minerals (Corbett & Leach, 1998). Typical mineral assemblages consists of quartz–sericite–pyrite and accessory chlorite, quartz and pyrite with some trace amounts of calcite, zoisite and albite. Phyllic alteration can be observed to grade into either low temperature argillic or high temperature potassic alteration types with increasing amounts of clay minerals or K–feldspar respectively (Singh, 2015, and references therein).

Potassic alteration

Potassic alteration is abundant within the deeper parts of the epithermal system and is commonly associated with high temperature and pressure conditions than other alteration types $\approx 850°C$ – $550°C$. This alteration type characteristically consists of a neutral to alkaline conditions. Typical minerals present are K–feldspar, quartz, magnetite, iron sulphides and sulphide minerals such as pyrite, chalcopyrite and galena.

2.3 Epithermal environments

The term 'epithermal' is attributed to the range of temperature versus depth (pressure) conditions responsible for ore formation within much larger (mainly subaerial) hydrothermal systems (Simmons et al., 2005). It describes Au ± Ag ± Cu deposits formed in magmatic environments at elevated crustal settings, typically above the level at which porphyry Cu–Au deposits are formed (< 1 km) and often associated with subvolcanic intrusions (Corbett, 2002). Chemical changes in these environments are caused by sharp pressure and temperature gradients ranging from $\approx 150°C$ to $\approx 300°C$ at depths from $\approx$ 50 to 1500 m below the water table (Simmons et al., 2005). Whilst these physical controls define the epithermal environment, ore genesis is still heavily reliant on the composition of the hydrothermal solution responsible for the transportation and endowment of metals (Simmons et al., 2005). The origin and composition of such metal–transporting solutions differ among deposits. As such, over a dozen classification schemes have been used since the late 1970s to describe the wide range of features associated within epithermal ore–bodies (Table. 2.1) (Simmons et al., 2005). Most notably, epithermal deposits are classified as having been derived from two principle styles of alteration, low or high sulphidation. Low and high sulphidation are distinguished using a criteria of varying gangue and ore mineralogy deposited by the circulation of different hydrothermal ore fluids within host rocks (Corbett, 2002; White & Hedenquist, 1990).

2.3.1 High versus low sulphidation

Hedenquist (1987) proposed the terms low and high sulphidation referring to the redox state of sulphur present in the mineralising fluid (fig. 2.1). Epithermal gold deposits from a low sulphidation environment are derived from reduced, near neutral pH, dilute fluids. These low sulphidation fluids are developed by the interactions of different magmatic components within deep circulating ground waters with sulphur species reduced to H_2S. In comparison, high sulphidation environments are developed both in the epithermal and the upper parts of the underlying porphyry environments up to 2 km in vertical depths. High sulphidation environments develop from the interaction between host rocks and hot acidic magmatic fluids often generating advanced argillic lithocaps (fig. 2.4). These are created by absorption of large amounts of magmatic volatiles within groundwater, which in turn generates significant volumes of acidic fluid (Sillitoe, 2000). The result is the development of an ore system comprised of high sulphur and Au + Cu + Ag deposition, Characteristics of high sulphidation environments include a pyrite rich high sulphidation–state sulphide assemblages typified by enargite, luzonite, digenite and advanced argillic assemblages of quartz, alunite, kaolinite/dickite and massive sulphide bodies of replacement origin dominated by pyrite, melnikovite and marcasite (Singh, 2015, and references therein).

2.4 Characteristics of low sulphidation epithermal deposits

Epithermal deposits comprise epigenetic ores that are generally hosted by coeval and older volcanic rock and/or underlying basement rocks that cover areas that range from <10 to >100 km^2 (Simmons et al., 2005). Host rock lithologies and structures control the diverse shapes of ore–bodies and represent zones of paleopermeability within shallow parts of the hydrothermal system (Simmons et al.,

Table 2.1: Evolution of classification schemes used to describe epithermal deposits (modified after Simmons et al., 2005, and references therein)

Sillitoe (1977)	Acid		Alkaline			
Buchanana (1981)	Epithermal					
Ashley (1982)	Enargite gold					
Giles and Nelson (1982)			Hot-spring type			
Bonham (1986, 1988)	High sulfur		Low sulfur		Alkalic deposits	
Hayba et al. (1985)	Acid sulfate		Adularia-sericite			
Heald et al. (1987)						
Hedenquist (1987, White and	High sulfidation		Low sulfidation			
Hedenquist (1990, 1995)						
Berger and Henley (1989)	Alunite-kaolinite		Adularia-sericite			
Albino and Margolis (1991)			Type 1 adularia-sericite		Type 2 adularia-sericite	
Sillitoe (1989, 1993a)	High sulfidation		Low sulfidation			
			High sulfide + base metal		Low sulfide + base metal	
White and Poizat (1995)	High sulfidation		Low sulfidation			
	Au-Ag-Cu deposits with vuggy quartz alteration	Au-Ag-Cu deposits with pyrophyllite-sericite alteration	Sn-Ag-base metal deposits	Ag-Au-base metal deposits	Au-Ag deposits: With calc-alkaline volcanic rocks	Au-Ag deposits: With alkaline volcanic rocks
Hedenquist et al. (2000),	High sulfidation		Intermediate sulfidation		Low sulfidation	Alkalic
Einaudi et al. (2003),						
Sillietoe and Hedenquist (2003)						
Cooke and Deyell (2003)	Descriptive nomenclature based on ore metals, deposits form, diagnostic hypogene gangue and alteration minerals, and dominant Cu-bearing mineral					

2005). Typically, these ore–bodies will form in veins with steep dips that formed through dilational and extensional processes (Simmons et al., 2005). Some ore–bodies may be hosted within major faults, however, they are more commonly associated with minor faults (second or third–order structures) (Simmons et al., 2005). Ultimately, the optimum structural development of the ore–bodies is dependent on rock rheology and brittle failure. Rock lithology is also important (e.g. contrast between porosity and permeability), by its ability to focus fluid flow though specfic units, along rock contacts, or through permeable masses of brecciated rock (Simmons et al., 2005). Factors such as faults and fracture networks, breccias, coarse clastic rocks and intensely leached rocks (formed from either volcanic or hydrothermal processes), all contribute to the ore–forming process and dictate whether an ore will occur in veins or become disseminated within rock units (Bodger, 2015). The ore forming process can extend laterally for 100s to 1000s metres and vertically by 10s to 100s of meters (Simmons et al., 2005). Quartz is the dominant gangue mineral, resulting in epithermal ores being hard and having a general resistance against weathering. Pyrite is the dominant sulphide mineral, with the volume of sulphide content ranging from < 1 to > 20 % (Simmons et al., 2005). By using mineral assemblages we are able to construct paleoisotherms which are useful for locating conduits of paleoflow. The significance of paleoflow is that it is the area within the hydrothermal system in which major ore accumulates. These paleoflows range from 180°C to 280°C with depths of 100 m to 800 – 1500 m. Typically within low sulphidation systems, the best indicators of paleotemperatures are areas dominated by clay minerals with variations in their basal spacing (White & Hedenquist, 1995). Commonly, a progressing thermal stability is observed through a clear upward and outward zonation of minerals (Fig. 2.1 & 2.3).

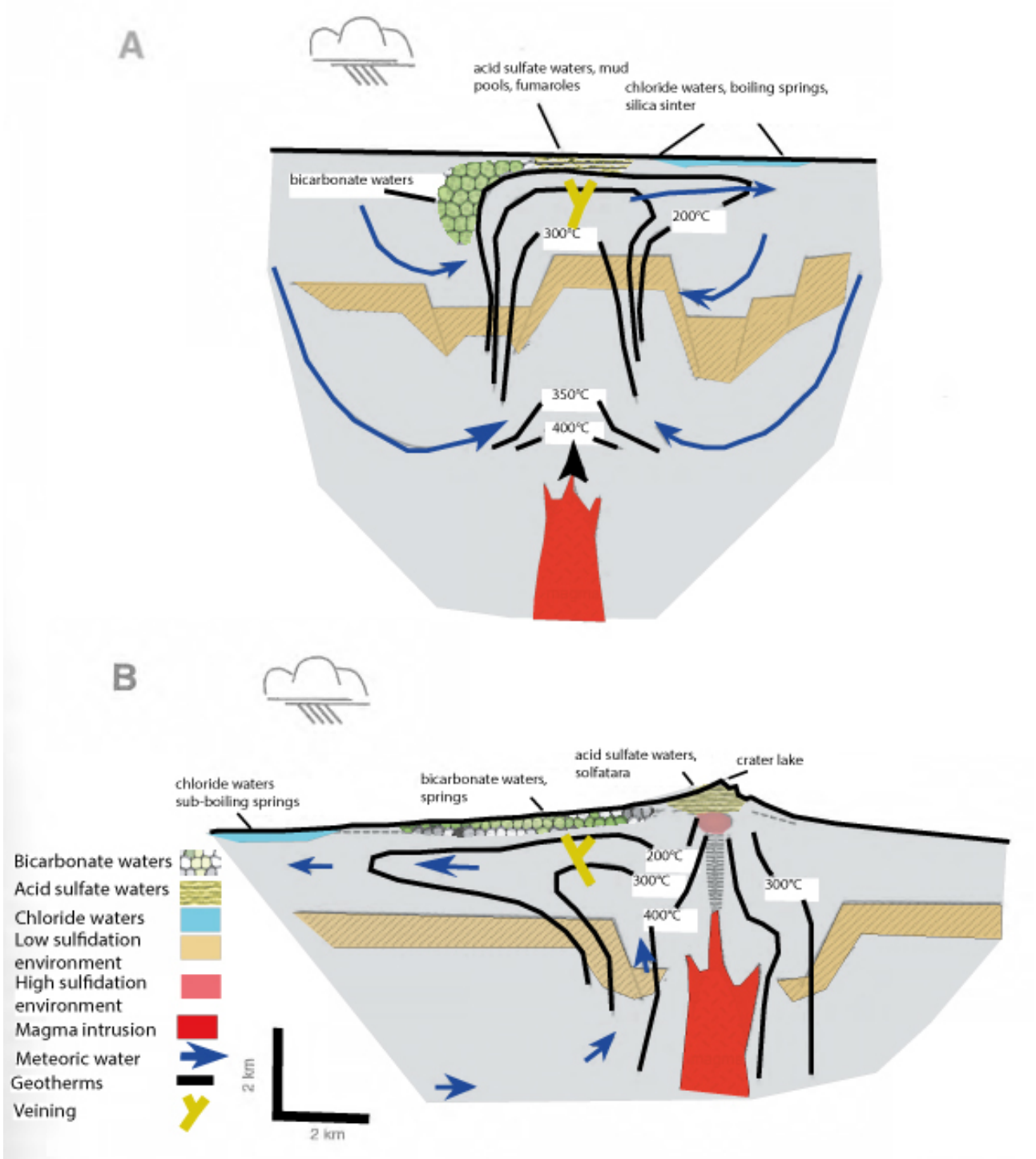

Figure 2.2: Conceptual model showing typical low sulphidation environments. A. rift low sulphidation environment B. arc low sulphidation environment. (modified from Simmons & Browne, 1997)

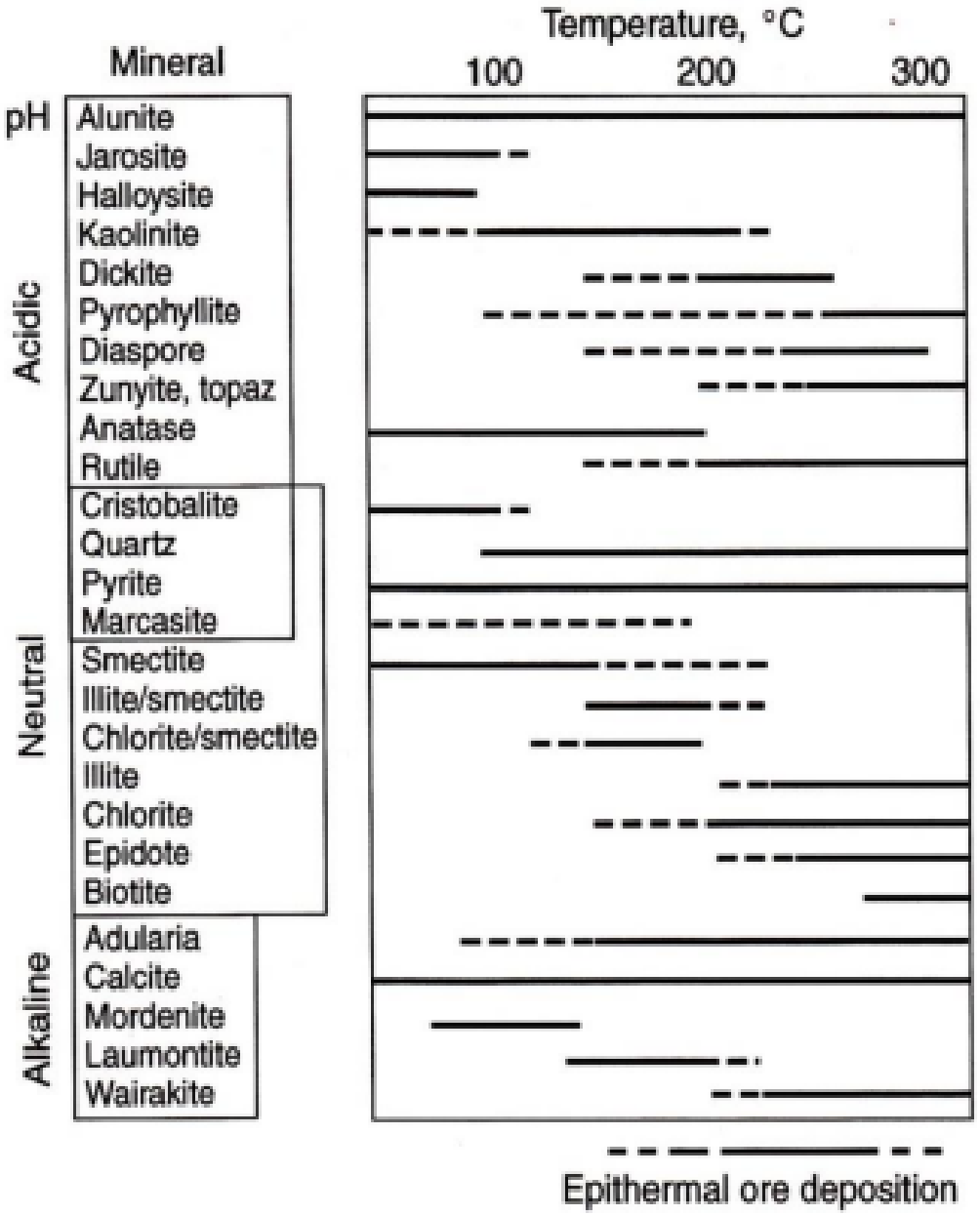

Figure 2.3: Figure showing the association between fluid pH conditions, minerals present and temperature within epithermal systems. A solid line indicates a mineral is present, a dotted line indicates a mineral may be partially present and absence or termination of a line indicates a mineral will not be present at those temperatures. Typical temperature conditions responsible for epithermal ore deposition are also labelled on the bottom right hand corner. (from Pirajno, 2009)

2.5 Epithermal settings

Igneous setting

Epithermal deposits form a close temporal and spatial association with subaerial volcanic rocks and their related subvolcanic intrusions (White & Hedenquist, 1990). Even in areas where deposits formed prior to volcanism, the significance of igneous activity within epithermal settings is in it's ability to provide the heat necessary in generating a hydrothermal convection cell. Furthermore, magmas may contribute some component of gases into the overlying hydrothermal system (Giggenbach, 1986; White & Hedenquist, 1990). There is a central to proximal relationship between the volcanic setting and hosted epithermal deposits. Epithermal deposits hosted in volcanic settings are typically associated with effusive or pyroclastic rocks. These volcanic setting deposits are abundantly located in intermediate to acid volcanic settings, with calc–alkaline to alkaline suites potentially containing significant deposits. Hydrothermal activity associated with modern volcanic environments can be classified into silicic depressions, (calderas or grabens), andesite stratovolcanos, cordilleran volcanism and oceanic islands (White & Hedenquist, 1990, and references therein). Essentially, these classifications are based on the characteristics of the hydrological regime through it's effects on controlling; the discharge and recharge of the hydrothermal system, the distribution of conduits and hydrothermal alteration products and potential sites of deposition of ore minerals.

Tectonic setting

Subaerial volcanism associated with tectonic settings occurs mainly as volcanic arcs in convergent boundary settings (White & Hedenquist, 1990). Within tectonic settings, back–arc basins may evolve into a marine back arc basin. Back arc basins, which have become marine back arc basins, are no longer prospective for epithermal deposits, but rather develop massive sulphide deposits instead (Cathles, 1983). The Basin and Range region of western U.S and New Zealand's Taupo Volcanic Zone and Coromandel Peninsula are examples of wide back–arc rifts which are extensively mineralised with epithermal deposits (White & Hedenquist, 1990, and references therein). There are some subaerial volcanic settings which have not yet been found to be prospective for epithermal deposits. Regions of both tholeiitic or alkaline, continental flood basalts do not contain epithermal deposits and instead create small near surface heat anomalies which preclude any major development of shallow hydrothermal systems. This may reflect their deep and/or small magma chambers and narrow conduits. Oceanic ridges do not appear prospective for epithermal deposits due to being submarine. Primitive island–arc settings (Tonga-Kermadec chain) appear unprospective, as large magma chambers required to generate the necessary heat–flow conditions for any major hydrothermal activity have not yet developed. A subaerial oceanic ridge in Iceland has extensive geothermal activity involving meteoric waters. However, it is not apparent whether this setting may be prospective. Additionally, given the nature of its rare setting in the geological record, it may not be significant for exploration purposes.

Structural setting

Geological structures such as fractures, cause a permeability enhancement effect in the near surface and are considered a major component for controlling gold deposition. Epithermal deposits are regionally

associated with volcanic structures (Rytuba, 1981), with a close association observed among felsic and andesitic vent complexes. Furthermore, regional faulting acts as a control for epithermal deposits by potentially guiding and emplacing the magmatic heat source responsible for hydrothermal activity (Hedenquist, 1986). Whilst major faults may act as an important control on the localisation of deposits, mineralisation is often focused on subsidiary faults or fault splays (White & Hedenquist, 1990). Within prospective areas, minor structural features such as, bedding planes, joints and joint intersection will have an effect on the permeability and subsequent distribution of mineralisation in epithermal deposits.

2.6 Epithermal deposit classes architecture

Low sulphidation deposits are categorised into two groups according to; mineralogy, formation styles at differing crustal levels and relationships with possible magmatic source rocks (setting) (Corbett, 2002). Deposits displaying mineralogies derived dominantly from magmatic source rocks are commonly observed at arc low sulphidation environments (fig. 2.2). Deposits with mineralogies dominated from circulating geothermal fluid sources are associated with rift low sulphidation environments (fig. 2.2).

2.6.1 Arc low sulphidation

Arc low sulphidation epithermal deposits display a close relationship with an inferred magmatic source. Each deposit class can be broadly separated based on distinct characteristics such as, the appearance or termination of different gangue minerals or the difference in vein composition and styles. Arc low sulphidation epithermal deposits are listed below as increasing depths from the inferred magmatic source (Corbett, 2002). Transitional zones between deposits may display characteristics from more than one class of deposits.

Quartz–sulphide gold ± copper

At the deepest crustal levels, there is a transition between porphyry and epithermal gold deposits, whereby, some low sulphidation quartz–sulphide gold ± copper formed at deeper crustal levels begins to transition in to porphyry Cu – Au – locally termed wall rock porphyry deposits by some workers (fig. 2.4; Corbett, 2002). These quartz–sulphide gold ± copper deposits comprise dominantly iron sulphides and quartz, mostly as veins and vein breccias respectively.

Polymetallic gold silver veins

Polymetallic Au – Ag class are a recognisable transitional phase between quartz–sulphide gold ± copper and carbonate–base metal gold (fig. 2.4; Corbett, 2002). It can be distinguished from the low sulphidation carbonate base metal gold systems by a general paucity of carbonate as a predominate gangue mineral phase linked to the environment of formation (Corbett, 2002). Polymetallic veins comprise dominantly quartz, pyrite, galena, sphalerite, lesser chalcopyrite, some carbonate (mostly calcite) and a variety of lesser mineral phases including many silver minerals.

Carbonate–base metal gold

Carbonate–base metal gold occurs at higher crustal levels than quartz–sulphide gold ± copper system (fig. 2.4). Gangue minerals consist of carbonate > quartz > pyrite > sphalerite > galena > chalcopyrite as fracture/vein/breccias (Corbett & Leach, 1998). Carbonate–base metal gold deposits are characterised by extremely irregular gold grades with bonanza grades. Bonanza veins vaguely describe rich ore veins with gold grades > 30 g/t. Some carbonate–base metal gold deposits contain overprinting bonanza epithermal quartz gold–silver ores and others which are telescoped (juxtaposed or overprinting early deep mineralisation) (Sillitoe, 1994) upon deeper level quartz–sulphide ± copper mineralisation (Corbett, 2002).

Epithermal quartz gold–silver

Within the arc low sulphidation group, epithermal quartz gold–silver deposits occur at the highest crustal level, furthest from the inferred intrusion source rock than other deposit classes (fig. 2.4; Corbett, 2002). Corbett and Leach (1998), characterised as having a presence of bonanza gold grades possibly hundreds of g/t, giving rise to significant alluvial gold deposits. Veins are comprised of quartz and vary from crystalline opal/chalcedony, while chlorite and illite–smectite are also common constituents (Corbett, 2002). A number of alkaline systems contain vanadium illite, roscoellite and significant secondary K feldspar, mainly as wall rock alteration and in veins (Corbett et al., 2001). Mineralisation typically occurs as fracture/vein/breccias, locally overprinting earlier veins upon which they are telescoped. Mineral deposition is the product of a mixing meteoric fluid with oxidising near–surface groundwaters, typically from oxygenated meteoric or collapsing acid sulphate (low pH) waters.

2.7 Rift low sulphidation; adularia–sericite epithermal gold–silver

Like the low sulphidation arc epithermal quartz gold–silver deposits, adularia–sericite deposits occur at shallow crustal depths far from an inferred intrusion source (fig. 2.4; Corbett, 2002). Adularia–sericite deposits are silver rich with typical Au:Ag ratios greater than 1:10. The Waihi, Martha mine is one example of an adularia–sericite gold silver deposit. Adularia–sericite deposits display more of a close association with extensional structures and rift settings than intrusional source rocks (Corbett, 2002). They often occur in fossil back arc rifts (e.g. Taupo Volcanic Zone) where a geothermal fluid is able to circulate through dominantly felsic volcaniclastic sequences (Corbett, 2002). Assosciated gangue minerals within adularia–sericite deposits are quartz (mostly chalcendony), adularia, quartz pseudomorphing carbonate and dark sulphidic material (ginguro bands). Cooling and traditional boiling models are typically reliable for the deposition of gangue minerals and some gold while the mixing of rising pregnant fluid with oxygenated or collapsing low pH groundwaters favour the development of bonanza gold–silver grades. Boiling forms lattice textured bladed calcite which is replaced by quartz as the system cools (Corbett, 2002). In a system lacking erosion, the paleosurface deposit is marked by silica sinters (Hedenquist et al., 2000). The adularia–sericite gold–silver typically occurs as banded fissure veins and local vein/breccias consisting of dominant colloform banding. Fissure veins displaying colloform banding may form at depths of up to 1 km and are the main gold producers in areas such as Pajingo and Waihi (Corbett, 2002). Calcite represents a major constituent of some veins where

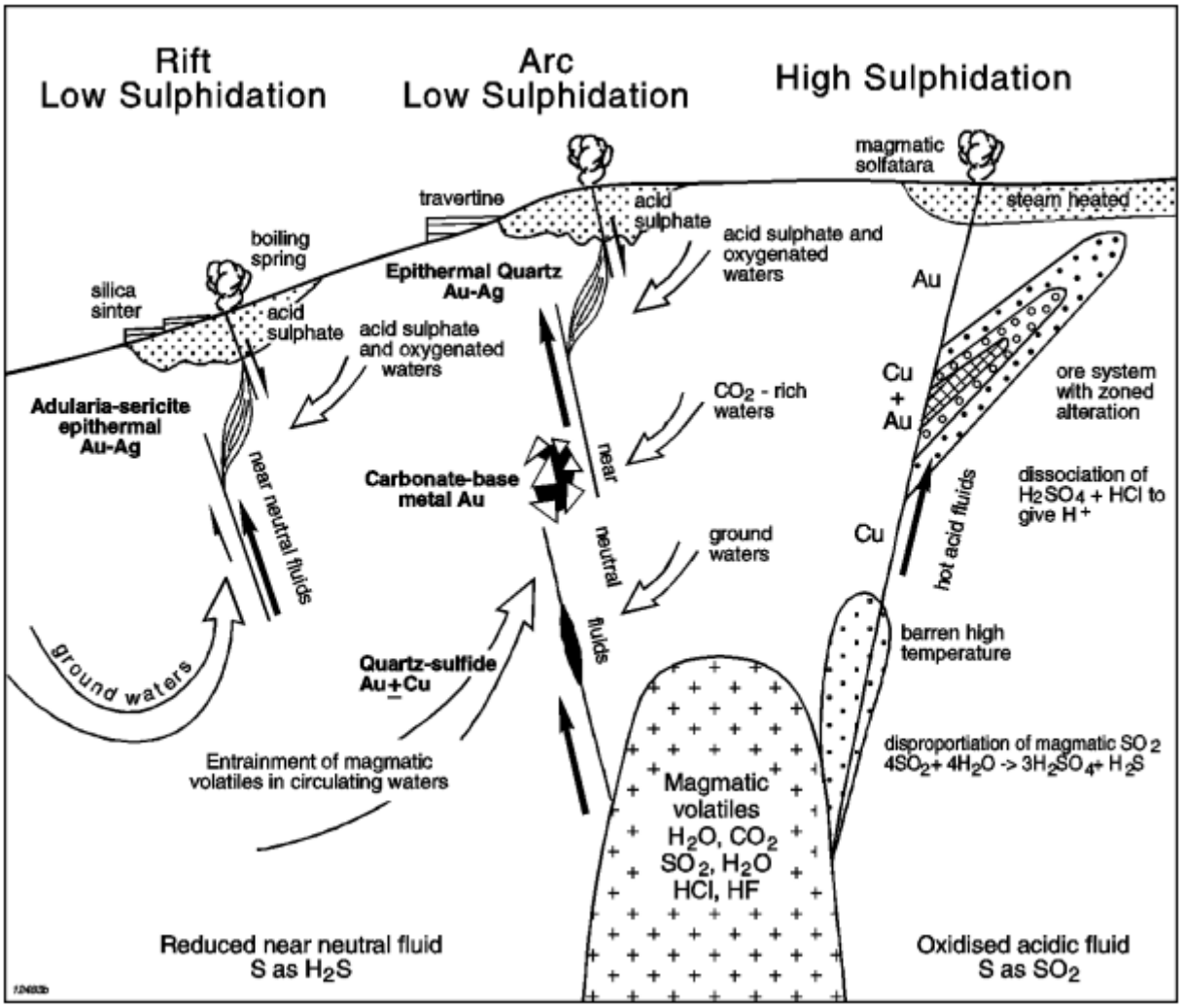

Figure 2.4: Figure showing arc and rift low sulphidation and high sulphidation environments. Common system features are labelled, such as the typical corresponding deposit classes at different environments and varying depths (from Corbett, 2002)

it is generally deposited as a late cutting quartz or infilling remaining open space. Vein systems also consist of anomalous copper as chalcopyrite, mercury as cinnabar and antimony as stibnite (Corbett, 2002). There are multi–episode vein breccias which may reflect hydrothermal eruptions at surface as a result of pressure release. Some of the eruption breccia systems cap sheeted veins can extend into the breccia, while others cap mineralised fissure veins. Structure and host rock competency are important ore controls in adularia–sericite vein systems, whereby only brittle rocks which fracture well are capable of hosting veins (Corbett, 2002).

The research within this thesis is conducted on hydrothermally altered rock within a known epithermal system. The focus of this study is a rift low sulphidation epithermal system as an adularia–sericite gold–silver deposit. The purpose of this chapter was to investigate these concepts to better understand the effects of hydrothermally altering our host rock formations discussed in the next chapter.

Chapter 3
Coromandel Peninsula

3.1 Introduction

New Zealand is positioned along a convergent plate boundary zone between the subducting oceanic Pacific plate and the over–riding Indo–Australian continental plate (Davey et al., 1995). As a result of the interaction between the two plates, a continental margin volcanic belt has formed. Over the past 25 Ma this volcanic arc has migrated within the North Island (Stevens, 2010) and formed the CVZ as the predecessor to the presently active TVZ (Julian, 2016). The results of the past 25 Ma of plate subduction can be constrained into three major time and spatial groups in accordance with the shift in the locus of volcanism (Fig. 3.1) (Adams et al., 1994; Mauk et al., 2011). The north– to northwest–trending Northland Volcanic Arc was dominated by basaltic–andesitic eruptives and active between 25 and 15 Ma. The Coromandel Volcanic Zone was active between 18 and 2 Ma and transitioned into the currently active northeast–striking Tonga–Kermadec–Taupo Volcanic Zone arc. Both Coromandel and Taupo Volcanic arcs are dominated by andesitic–rhyolitic eruptives (Adams et al., 1994; Briggs et al., 2005; Mauk et al., 2011).

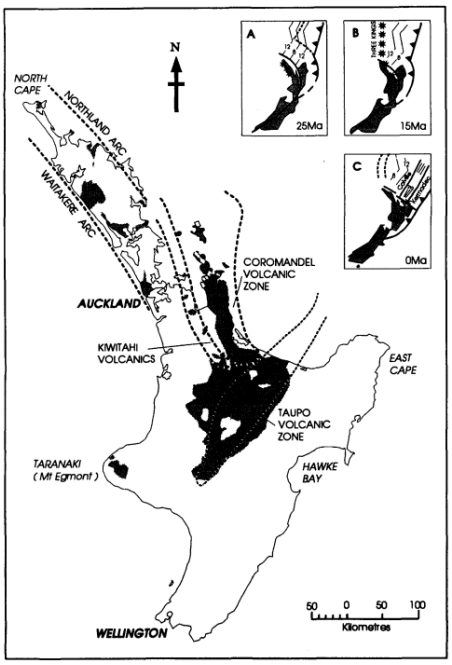

Figure 3.1: Map of the North Island showing plate boundary migration and the resulting volcanic zones (Adams et al., 1994)

This chapter outlines the tectonic and geological setting of the Coromandel Peninsula and discusses the factors responsible for separating the Hauraki Goldfield into three separate provinces. A description on the local controls and features responsible for the mineralisation and alteration of the Waihi vein system will also be given.

3.2 Tectonic and geologic setting

This section describes current literature on the known history of the Coromandel Peninsula. Relevant ages for the paleo tectonic environment responsible for the creation of different lithological formations are described in the tectonic setting subsection. The lithology and stratigraphy subsection details the percentage of different surface lithology groups exposed. Furthermore, the suggested ages for the lithology formations and any stratigraphic relationships are given. Displacement caused by major and

minor structures within the Coromandel Peninsula are outlined in the structure subsection.

3.2.1 Tectonic setting

The oldest rocks on the Coromandel Peninsula are late Jurassic (c. 163 Ma – c. 145 Ma) low grade metagreywacke sequences of the Manaia Hill Group (Fig. 3.3) (Adams et al., 1994). Brathwaite and Skinner (1997) maintain that the greywackes were accreted onto the Gondwana continental margin during the Mesozoic. These greywackes form the basement of Cenozoic volcanic rocks and can be observed in outcrop at the northern and western part of the Coromandel Peninsula (Skinner, 1972). The separation of New Zealand from Gondwanaland by the opening of the Tasman Sea is dated around c. 82 Ma (Christie & Brathwaite, 1997). Laird (1996) suggests extension and rifting began 20–25 Ma earlier at about 105 Ma superseding a period of convergent margin tectonics. This deformation resulted in block faults forming in the greywacke basement, some of which were rejuvenated in the overlying Tertiary rocks (Skinner, 1986). Uncomformably overlying these greywackes are thin sequences of Paleocene to Miocene coal measures, carbonates, mudstones and sandstones, such as the Colville formation of the Waitemata Group (Brathwaite & Skinner, 1997; Dix & Nelson, 2004; Skinner, 1976). The Oligocene–Miocene boundary (formed c. 25 Ma) is marked by several major events and ultimately highlights the initiation of volcanic arcs in the northern North Island by the subduction of the Pacific Plate (Adams et al., 1994; Christie & Brathwaite, 1997). Therefore, some of these early Miocene sediment formations, such as the Colville formation, can be used as an indicator for the initiation of volcanism on the peninsula (Adams et al., 1994).

The suggested history of volcanic activity within the CVZ during the Cenozoic varies, but the general consensus is that activity commenced early to mid Miocene (c. 18 – 16 Ma) and halted in the late Miocene to Pliocene (c. 4 – 1.8 Ma) (Adams et al., 1994; Nicholson et al., 2004; Skinner, 1986; Spörli & Cargill, 2011). During this time, from early to late Miocene, the Coromandel Group volcanic sequence erupted. This eruption was andesitic to dacitic in composition and formed a continental volcanic arc more than 200 km long and 35 km wide (Fig. 3.3) (Skinner, 1986). Around mid Miocene, c. 15 Ma, a major change occurred with the cessation of volcanism in Northland and rejuvenated volcanism in the Coromandel (Christie & Brathwaite, 1997). Following this change was an observable shift in the focus of volcanism moving west to east–central sector of the Coromandel peninsula during the late Miocene, resulting in a continuous evolution along the length of the Coromandel Peninsula through the late Cenozoic (c. 18 ma to 4 Ma) with regional time breaks no more than 2 Ma (Adams et al., 1994; Nicholson et al., 2004). This shift is characterised within the CVZ by the transition of stratovolcanos to rhyolitic calderas, typified by widespread ignimbrite sheets, rhyolite dome complexes and some localised basaltic–andesitic cones and flows in the northeast forming the Whitianga Group (Fig. 3.3) (Adams et al., 1994). The late Miocene – early Pliocene Whitianga Group underlies and merges with volcanic rocks ejected from the TVZ whilst broadly overlapping early Miocene to late Miocene andesitic to dacitic volcanic rocks from the Coromandel Group (Skinner, 1986). The volcanic history of the Coromandel peninsula ended in the late Pliocene when volcanism shifted to the TVZ and continues to the present day (Adams et al., 1994; Christie & Brathwaite, 1997).

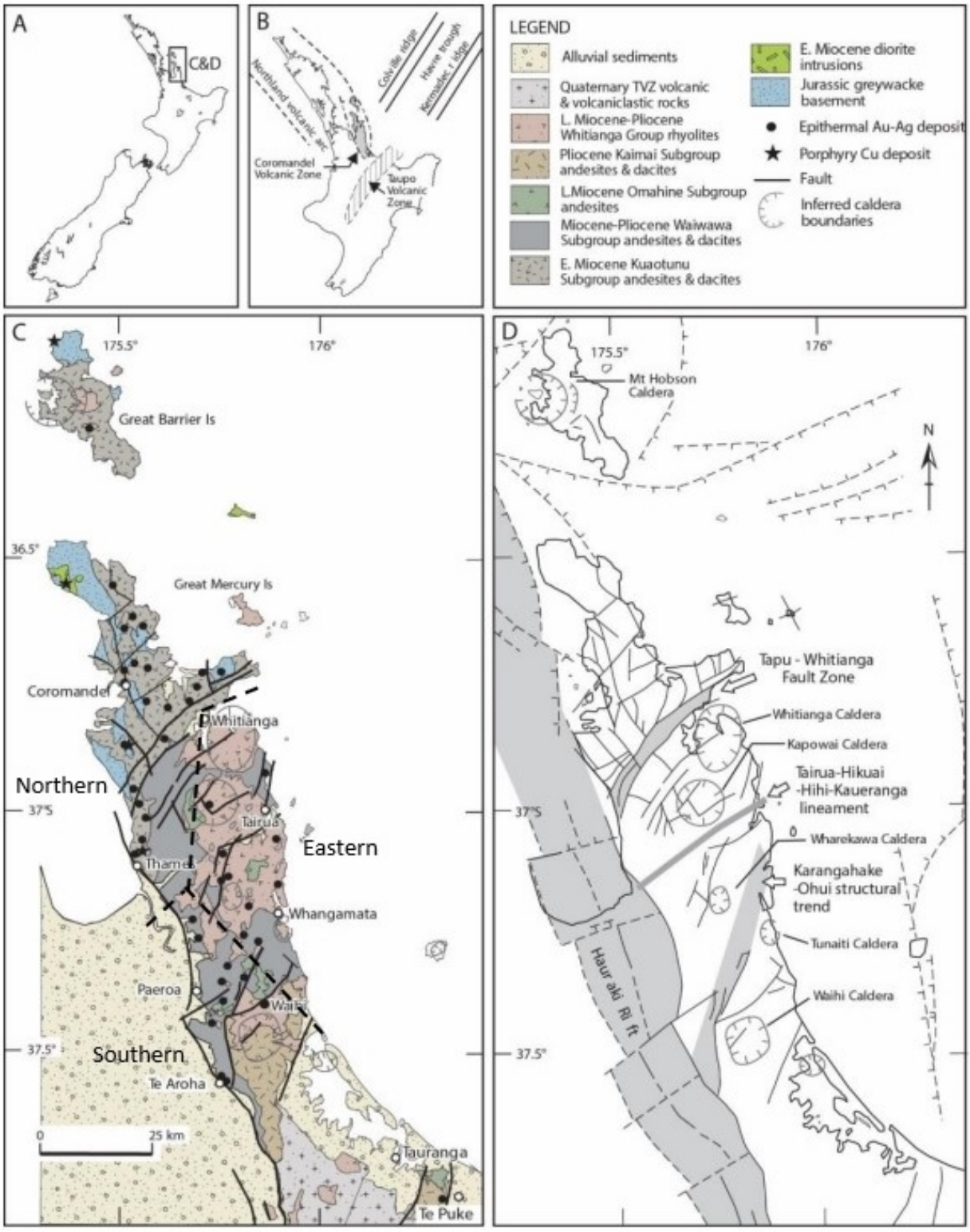

Figure 3.2: Figure showing the different elements of the Coromandel Peninsula. (A) The square box indicates the geographical position of the Coromandel within the larger context of New Zealand. (B) Shows the positioning of the Hauraki Goldfield and the different volcanic arcs formed from subduction. (C) Details showing surface geology, mineral deposits and the three Hauraki provinces. Working legend given in the top right corner. (D) Structural features of the Hauraki Goldfield and CVZ such as the Hauraki Rift. (from Bodger, 2015)

.

3.2.2 Lithology and stratigraphy

The CVZ is comprised predominantly of calc–alkaline, medium K volcanic rocks (Adams et al., 1994; Skinner, 1986). The Coromandel Group, consisting of andesitic – dacitic eruptives, make up 61 percent of the main rocks exposed (Christie et al., 2007). Dacite, rhyolite and rhyodacite eruptives of the Whitianga Group make up 30 percent, whilst greywacke from the Manaia Hill Group make up 9 percent (Fig. 3.2 C & 3.3). Additionally, there are exposed basalt and basaltic andesite units of the Kerikeri Volcanic Group (Mercury Basalts), which make up <0.1 percent (Christie et al., 2007) and erosional remnants of Waitemata Group exposed on the northern part of the peninsula (Adams et al., 1994; Brathwaite & Christie, 1996). Christie et al. (2007) found two key features of volcanism within the region; a southward to eastward progression of younger volcanic units and a separation of westward andesitic dominated volcanism versus eastward rhyolitic dominated volcanism (Fig. 3.2).

The Coromandel Group is described by Skinner (1986) as consisting dominantly of pyroxene or pyroxene hornblende andesite, with lesser dacite and rhyodacite (Brathwaite & Christie, 1996). The andesite and dacites of the Coromandel Group are subdivided into four subgroups: the Kuatonu (early to middle Miocene), Waiwawa (middle to late Miocene), Omahine (late Miocene to Pliocene) and the Kaimai (late Miocene to Pliocene) subgroups, which are separated by periods of volcanic quiescence and erosion (Adams et al., 1994; Brathwaite & Christie, 1996; Skinner, 1986). The Kuatonu subgroup consists of alternating pyroxene andesite and hornblende pyroxene and is found above the Colville formation (Waitemata Group) (Adams et al., 1994). In contrast, the Waiwawa and Omahine subgroups are predominantly pyroxene andesites. Adams et al. (1994) suggests a 1–2 Ma hiatus between Waiwawa and Kuatonu Subgroups, from which the Waiwawa Subgroup can be separated by an unconformity from the older Kuatonu Subgroup. The Omahine Subgroup is for Coromandel Group formations which post–date mid–Taranakian (late Miocene) rhyolite and ignimbrites of the Whitianga Group (Brathwaite & Christie, 1996; Christie et al., 2007). The Kaimai Subgroup includes Miocene to Pliocene, basaltic to dacitic, volcanic and volcaniclastic strata of the Kaimai Range (Brathwaite & Christie, 1996; Houghton & Cuthbertson, 1989). The Whitianga Group, described by Schofield (1959), can be subdivided into the Minden Rhyolite, Coroglen and Ohinemuri Subgroups (Skinner, 1993). The Minden Rhyolite Subgroup describes older, calc–alkaline to alkaline eruption centres characterized by flow and dome–building rhyolites (Adams et al., 1994; Christie et al., 2007). The Coroglen Subgroup is for ignimbrite, pumice breccia and associated sediments. These Subgroups are most abundant in the central and southern parts of the eastern Coromandel peninsula (Fig 3.4). The Ohinemuri Subgroup represents the youngest units of the Whitianga Group and is exclusive to three ignimbrite formations in the Waihi Basin of late Pliocene age. The Kerikeri Volcanic Group (Mercury Basalts) are localised smaller volumetric rhyolite–basalt assemblages on offshore islands and within the northeastern part of the Coromandel peninsula (Fig. 3.3) (Spörli et al., 2006).

3.2.3 Structure

As in other areas of New Zealand (King, 2000), faults formed within the greywacke basement during the Cretaceous to early Tertiary are assumed to have reactivated within overlying Tertiary volcanic rocks in the CVZ (Skinner, 1986). Prominent faults located throughout the Coromandel peninsula, strike northeast–north–northwest with some south–striking faults which include major fault zones (Spörli & Cargill, 2011). Map patterns in the northern part of the peninsula are strongly

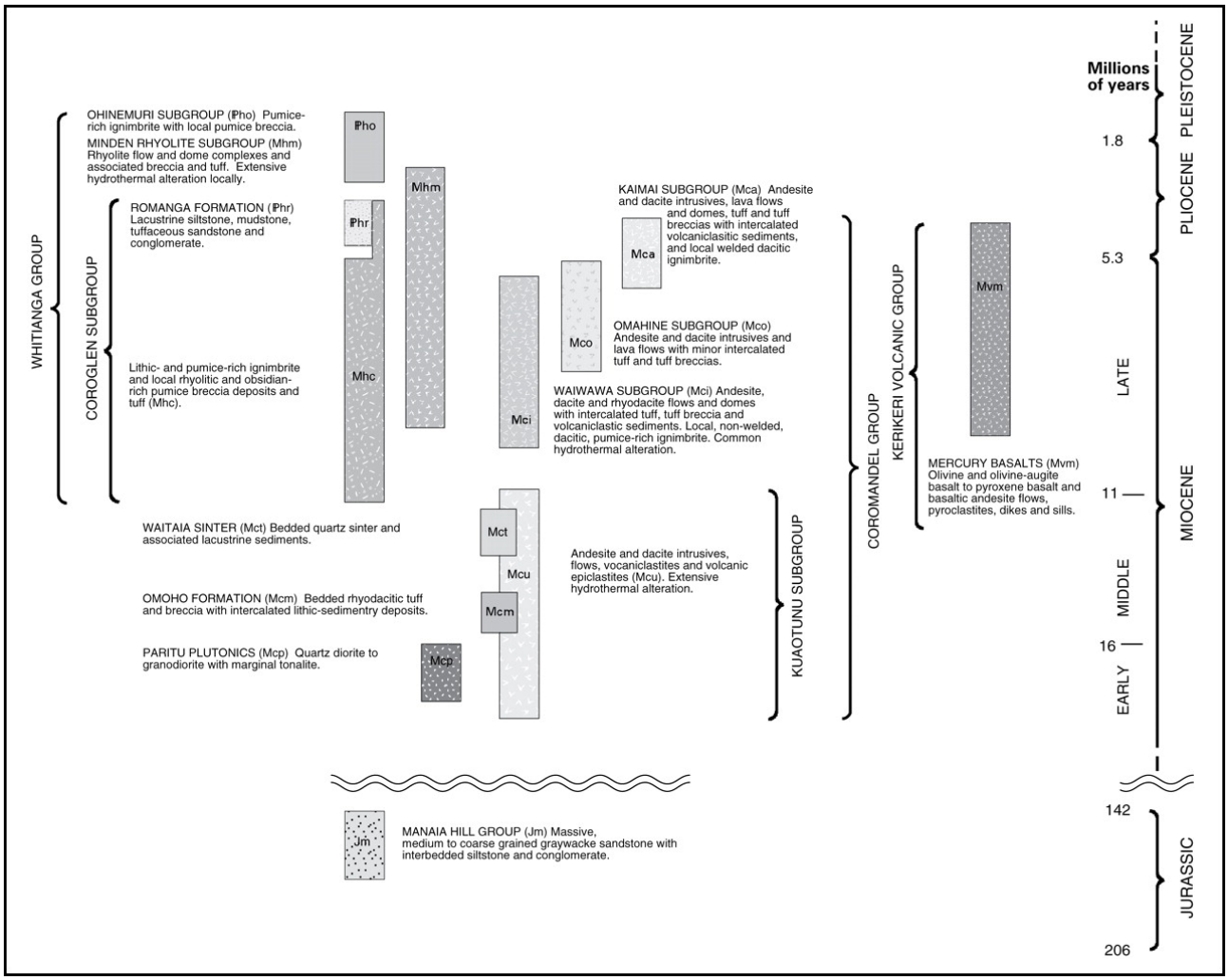

Figure 3.3: Figure showing stratigraphy and percentage of rocks exposed at surface. (from Christie et al., 2007)

influenced by post–Miocene, eastward and southward block fault tilting (Spörli et al., 2006). The displacement caused by northeast and east–northeast striking faults has resulted in the lowering of the Jurassic greywacke basement and a progressively thickening volcanic sequence to the south, towards the TVZ (Christie et al., 2007). The north–northwest striking faults tend to form horst and graben patterns whilst northeast striking faults are predominantly downthrown to the south (Skinner, 1986). Minor faulting within the peninsula include several hundred meters to kilometers in extent, some of which are hosts to epithermal quartz veining (as cited in Bodger, 2015). Spörli and Cargill (2011) identifies an association between the north–northwest–striking belt of calderas occurring along the eastern Coromandel peninsula and younger Whitianga Group rhyolites (Christie et al., 2007). The north–south–striking Hauraki rift is a continental rift and a major active tectonic feature of the region (Fig. 3.2). Depending on its age of inception, it may have had a significant tectonic influence on the development of the Hauraki Goldfield (Hochstein & Ballance, 1993). The Hauraki rift extends over 300 km from north of Little Barrier Island to the TVZ and is buried under late Pleistocene ignimbrites (Briggs et al., 2005). Evidence suggesting the timing of the initial formation of the Hauraki Rift varies; 30 Ma (Dix & Nelson, 2004), 10 – 7 Ma (Hochstein & Ballance, 1993), 3 – 5 Ma (Hayward et al., 2006) which has resulted in downthrown Miocene to Pliocene volcanic rocks by 1–3 km (Briggs et al., 2005; Hochstein & Ballance, 1993). The Hauraki Rift forms the western margin of the CVZ and theHauraki Goldfield (Fig 3.2) (Christie et al., 2007; Spörli & Cargill, 2011).

3.3 Hauraki goldfield

The Hauraki Goldfield is another name given to the gold producing region of the Coromandel Peninsula. The Hauraki Goldfield encompasses an area, 200 km long, up to 40 km wide, spanning from Great Barrier Island to Te Puke (Fig. 3.2) (Christie et al., 2007). There are prominent north–northwest and north–northeast striking faults and fractures within the Hauraki Goldfield which generate steep to moderate dips at regional scale to strike lengths of only a few hundred meters (Spörli et al., 2006). Christie et al. (2007) suggests the Hauraki Goldfield contains approximately 50 adularia–sericite–epithermal Au–Ag deposits occurring in a north–south–trending belt along the Coromandel peninsula. Additionally, these deposits have been broadly subdivided into three provinces (Fig. 3.2 C), (northern, eastern, southern), displaying differing characteristics in the host rocks, veining features and relative abundance of key minerals (Christie et al., 2007). The deposits within the northern province are hosted in andesite and dacite formations of the Kuatonu Subgroup (Coromandel Group), and locally in the greywacke basement of the Manaia Hill Group (Christie et al., 2007). Deposits found within the eastern province occur primarily in rhyolite of the Whitianga Group, but in local instances (e.g. Broken Hills and Neavesville) are hosted by, or extend downward into, andesite and dacite of the Waiwawa Subgroup (Christie et al., 2007). Deposits found within the southern province are primarily hosted in andesites and dacites of the Waiwawa Subgroup (Coromandel Group), with exceptions (e.g. Karangahake) which extend upward into overlying rhyolitic rocks of the Whitianga Group (Christie et al., 2007). The Southern Province is responsible for over 80 percent of the Au recovered within the Hauraki goldfield (Mauk et al., 2011). It is here, in which the Waihi vein system is situated, within the late Miocene Waipupu Formation.

3.4 The Waihi vein system

This section focuses on the Waihi vein system itself. The host rock name, mineral composition and preferred ages are described first along with the boundary and evolution of the Waihi vein system. Fault orientations responsible for the generation of the different vein zones are described later.

3.4.1 Stratigraphy

The Waihi Vein system is a quartz vein system located within the Waiwawa Subgroup on the southern Hauraki Goldfield province. The preferred age for Martha Hill mine deposit was found to be c. 6.16 ± 0.06 Ma based on $^{40}Ar/^{39}Ar$ plateau dates of adularia from quartz veins (Mauk et al., 2011). The vein system is hosted within late Miocene, hydrothermally altered andesites and dacites of the Waipupu Formation (Brathwaite & Faure, 2002). The system encapsulates the Martha Hill deposit, Union–Gladstone Hill deposits and the Favona deposit (Brathwaite & Faure, 2002; Brathwaite et al., 2006); and is considered a major producer of epithermal Au–Ag within the Hauraki Goldfield, accounting for approximately 66 percent of the total Au and 89 percent of the total Ag production in the region (John, 2011; Spörli & Cargill, 2011). The main rock type is plagioclase–porphyritic two–pyroxene andesite with SiO_2 contents of 60 to 63 percent (anhydrous composition) indicating high Si andesites, characteristic of the Waipupu Formation (Brathwaite & Faure, 2002). Expected phenocrysts typically found within the unaltered andesite include; plagioclase, augite, hypersthene, minor quartz and local hornblende with accessory magnetite, apatite and zircon (Brathwaite & Faure, 2002). Additionally, beds of dacitic lithic and crystal tuff are found between some flows. The composition of these tuffs are lithic clasts (andesite, dacitic tuff, pyritic siltstone) and broken crystals of plagioclase, quartz and altered pyroxene or biotite (Brathwaite & Faure, 2002). There are also thin carbonaceous lake beds found within the sequence. To the northeast of the Martha Hill deposit, where the Favona vein is hosted, the upper andesitic host rock formation is dominated by dacitic tuffs and tuff breccias with only minor andesite flows. To the east of this, the andesitic and dacitic host rocks become unconformably overlain by unaltered hornblende dacite of the Uretara Formation of the Kaimai Subgroup (late Miocene to early Pliocene age) (Brathwaite & Faure, 2002; Brathwaite et al., 2006). The findings of Brathwaite and Faure (2002) for the evolution of the Waihi epithermal system, was subdivided into three stages: (1) initial vein filling with platy calcite, quartz, pyrite and adularia, associated with alteration of the andesite wall rock; (2) a main stage of quartz and sulphides ± electrum vein filling; and (3) a final stage deposition within the veins by minor amethyst. The final deposition during the amethystine stage is minor but significant as it marks the last event in the vein deposition sequence (Brathwaite & Faure, 2002). The veins within Waihi can be considered to be deposited as a thick package of upper and lower andesites, separated texturally by an upper horizon lacking the presence of quartz and a lower quartz bearing horizon. (Shannon & Lorrance, 2022; Singh, 2015). Veins forming the Martha and Correnso veins were hosted almost exclusively within the lower andesite, pinching out into the upper andesite. With the discovery of the Favona vein, the belief of preferential host rock mineralisation at Martha was challenged by the Favona vein being hosted almost entirely within the upper andesite.

3.4.2 Structure

There are four main subparallel quartz lodes or vein zones (Martha, Welcome, Empire and Royal) within the Martha vein system (Fig. 3.4 & 3.5). These form an intricate braided pattern of veining in plan and cross section with predominant northeast strikes and steep dips (Christie et al., 2007). The Martha lode dips at 70° to 80° southeast, whereas most of the other lodes dip steeply northward and converge with the Martha lode at depth (Fig. 3.4 & 3.5 (Brathwaite & Faure, 2002; Brathwaite et al., 2006). Spörli and Cargill (2011) notes that individual vein strikes are predominantly northeast–southwest, but the Waihi vein system appears to transect a west–northwest–east–southeast trend (Fig. 3.4). Sets of less continuous veins striking east–west are associated with north striking faults. The hanging walls of the Martha, Empire and Royal lodes are bound toward their tops by fault zones. The north striking faults predate the formation of the major lodes (Cargill, 1994). The Waihi vein system is host to an extensive fault–fracture system in which the Martha Hill deposit is being hosted in (Brathwaite, 1989). This vein system is considered a fault–fracture mesh in which the Martha lode is the principal fault in a greater array network of linking and rejoining splays being formed between it and the principal wall fault splays hosting the Welcome, Empire and Royal lodes (Fig 3.4) (Brathwaite et al., 2006). Additionally, mutual vein cross–cutting relationships indicate that vein formation was broadly synchronous, although northeast–striking veins commonly cut east–striking veins (Brathwaite et al., 2006; Cargill, 1994).

3.4.3 Mineralisation and alteration

The style of alteration inferred by the presence of different mineral assemblages can be useful for the reconstruction of past paleoenvironments and the recognition of different ore bodies. Here the different styles of alteration are identified and a scheme used for ore zonation based on the subdivision of mineral assemblages is recognised. The change in vein texture and paragensis with depth is then discussed.

Alteration

At Martha Hill, potassic, propylitic and argilic alteration are the three main types of alteration recognised (Christie et al., 2007). Brathwaite and Faure (2002) broadly subdivided alteration features into three alteration zones based on petrography and XRD samples from drill holes in the central and eastern part of the vein system. The scheme used was similar to the works of Brathwaite (1989) but with subdivisions differing based on phyllosilicate minerals. The recognised zones were; (1) the smectite zone (smectite–chlorite–calcite–pyrite), (2) interlayered illite–smectite zone and (3) an illite zone with an adularia–quartz–illite subzone to adjacent quartz lodes.

Mineralisation

Vein paragenesis alters with depth at the Martha Hill deposit (Brathwaite & Faure, 2002). Microcrystalline quartz deposition during vein filling typically occurs as crustiform and colloform banding within the shallow parts of Martha and Welcome lodes (RL 1,000 m). Bands occuring with adularia typically occur in contact with the wall rock indicative of the early stages of vein filling in the deposition sequence (Brathwaite & Faure, 2002). There are deposits of minor kaolinite which line cavities

and act as partings between quartz bands, possibly a product of descending acid–sulphate waters (Brathwaite & Faure, 2002). The colloform quartz contains many of the main ore bearing minerals such as electrum and acanthite, and associated minerals such as pyrite, sphalerite, galena, tetrahedrite and chalcopyrite (Brathwaite & Faure, 2002; Panther et al., 1995). With increasing depths, colloform quartz begins to grade into crustiform comb quartz interbanded with hydrothermal breccias. These crustiform combs are typically comprised of fine– to medium–grained quartz, with sulphides making up 3 – 80% of the bands and creating cockade overgrowths around fragments (Brathwaite & Faure, 2002).

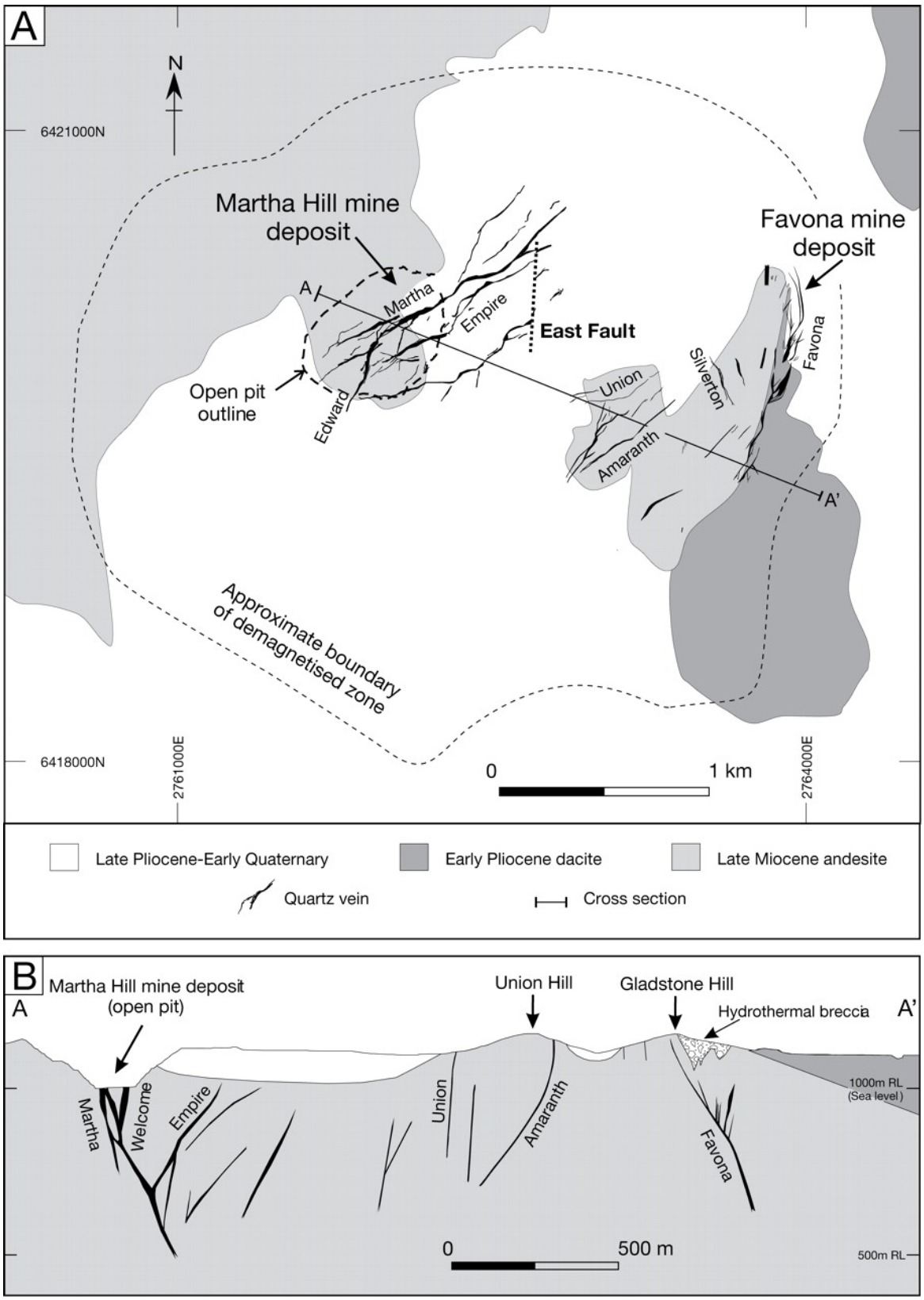

Figure 3.4: (A) Geological surface map displaying the ages of host rocks and identified veins. There is an observable pattern of northeasterly vein lodes situated across a west to northwest, east to southeasterly trend of deposits. The demagnetised boundary represents the Waihi up–flow system (B) Cross section made from A – A' in (A) (from Spörli & Cargill, 2011, modified from Simpson & Mauk, 2007)

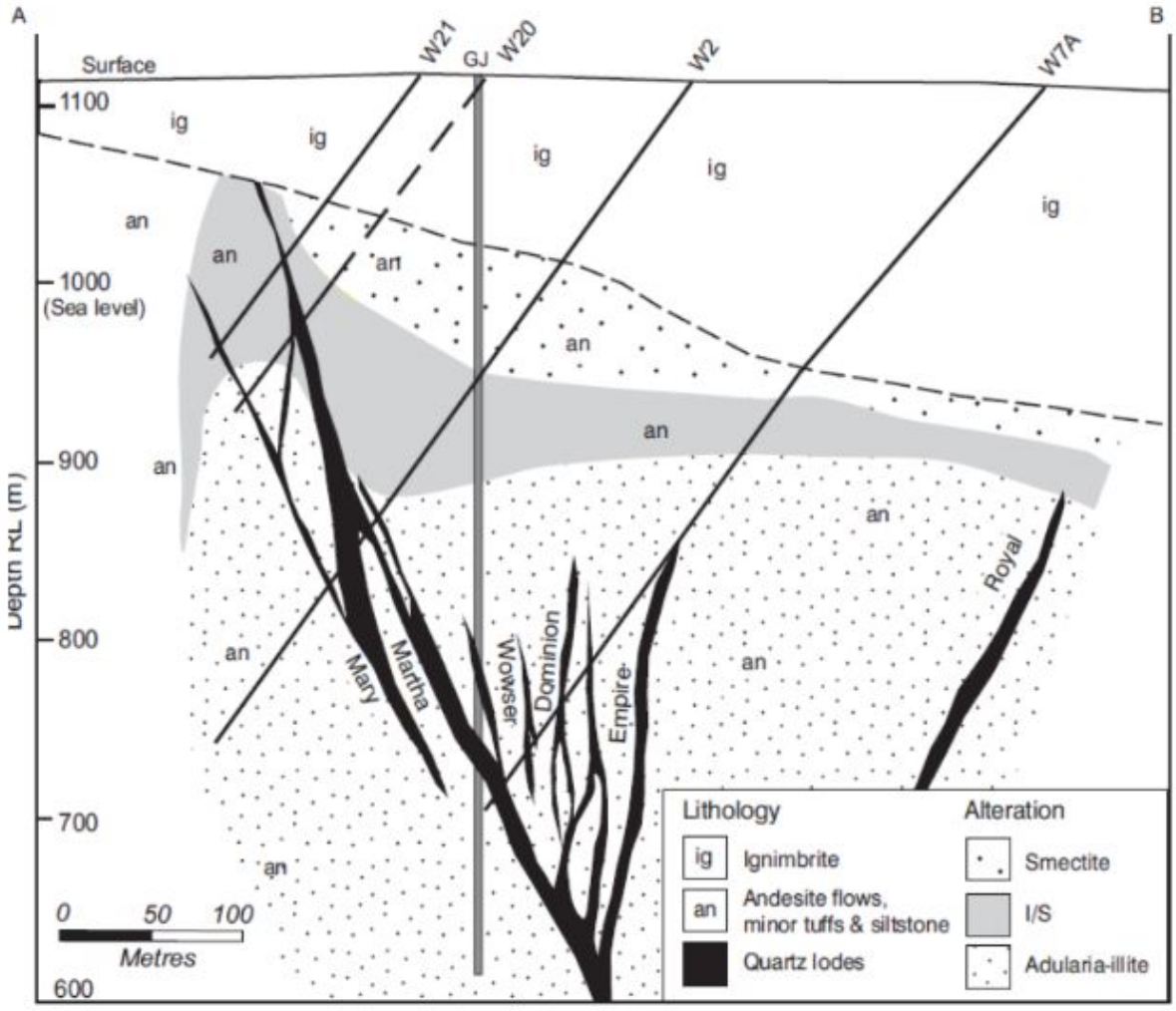

Figure 3.5: Cross section A–B at 2160 m E (mine grid), showing the main lithologies, lodes and alteration zones of smectite, interlayered illite–smectite (I/S) and adularia–illite. Also shown are the location of drill holes and the Grand Junction shaft (GJ) for former underground workings (from Brathwaite et al., 2006)

Chapter 4

Facies and drill hole descriptions

The main focus of this study was on the black breccia and any potential relationship among the outer weakly altered halo zone. To begin understanding these relationships, sampling and core logging was carried out in areas containing and surrounding the black breccia facie. The methods and results of 112 m of core logging are detailed below.

4.1 Sampling

Sampling began with the review of existing facies and their distribution within the Martha ore body using 3D geological software. Hard rock samples were collected from drill core areas, provided by OceanaGold, which had been identified as containing the black breccia or weakly altered sections. These hard rock sample specimens were distributed among three separate drill holes (800SP3MN1216, 920SP2MN1164, EMP16RG1842) and 112 m of core was physically collected from OceanaGold's core shed and logged at The University of Waikato.

4.2 Core Logging

Core logging was carried out on hand samples collected from three separate drill holes. Core was logged at a scale of 5 cm to 1 m of core (0.05 : 1). The core log colour was given as a descriptive colour name (e.g. whiteish grey) and was interpreted after applying water to provide a wet colour. Core log descriptions were based on three primary categories which noted observable texture, compositional structure changes in primary volcanics, brecciation or alteration features. Typical descriptions for primary volcanics included: difference in crystal sizes; crystal percentages relative to groundmass; average feldspar abundance, shapes and sizes; average mafic abundance, shape and size; and groundmass colour and features. Breccias were defined by: the vertical extent of individual breccias or brecciation; typical sizes of individual breccia clasts; breccia volcanic description or matched to an existing facies; and other notable features. Additionally, the degree of brecciation was recorded in areas where entire sections had become brecciated. A strongly brecciated section contained large breccia clasts supported within a well-defined matrix. This matrix often contained very fine 1-5 mm breccia clasts, fine phenocrysts and disseminations/infilling from silicified veining. Weakly brecciated sections often defined areas that alternated between breccia clasts with minor matrix fill and whole rock with a well defined groundmass. Alteration was logged based on how well primary volcanic textures were preserved and by the appearance of secondary minerals mostly as veins or colour changes between rock facies. Vein descriptions were made on the average vein abundance, thickness (measured in mm from the foot of the vein) and styles (crustiform, colloform, combs, stringers or bands). Following vein and rock descriptions, rock facies were given a broad descriptive marker indicating whether that facies was strongly altered ($> 75\%$), altered ($\approx 50\%$) or weakly altered ($< 25\%$). A strongly altered section did not preserve volcanic textures very well and involved the replacement of primary volcanics

by secondary minerals and large comb, crustiform and colloform veins. A weakly altered section preserved the original volcanic textures well and displayed characteristics similar to typical andesite formations. In contrast to the strongly altered sections, the weakly altered sections contained smaller feldspar phenocrysts with a higher of percentage mafic phenocrysts, stringer veins and hard coherent darker coloured sections with minor to absent brecciation. Lastly, contacts were noted at observable changes and breaks in the core lithology. A strong contact was noted where an abrupt change in rock lithology was observed. A gradational contact was logged whereby a gradual change in rock lithology (e.g. colour, phenocryst/alteration amount) was observed. A brecciated contact was observed where a previously logged coherent section changes to a brecciated section and was often transitional.

4.3 Facies definition

A facies description is a way to separate and group sections of rock that display similarities or differences in their characterstics, composition, formation or other notable features. Generating facies were crucial in early stages of core logging as it attempted to generalise large sections of lithology that often varied significantly in just a matter of several meters. A typical process followed for generating facies involved providing an early description of primary volcanics, alteration and brecciation (as discussed in section 4.2). In an effort to generate a basic model for the facies, I devised three facies assosciations of which, 10 facies were classified. The following facies assosciations - altered and coherent, weakly altered and coherent and brecciated classes - are detailed further below, alongside their respective facies.

4.4 Highly altered facies

The highly altered facies was a facies assosciation that encapsulated facies that were completely or partially altered using the criteria discussed in section 4.2. For simplicity, the facies under this class were all given the letter A to signify facies that had been moderately – highly affected by alteration. The highly altered facies class is further subdivided into their respective facies in numerical order, to produce facies – A1, A2, A3, A4 and A5 – and are discussed further below.

Facies A1 (Greyish white feldspar rich)

Facies A1 was porphyritic and typically contained ≈ 65% phenocrysts in a fine–grained greyish white groundmass (see fig 4.1). The observable ground mass appeared as a 'washed out' greyish white colour. Phenocrysts were predominantly feldspars and subhedral, 1 – 6 mm with an average size of ≈ 4 mm present. The boundaries of feldspar phenocrysts were not well defined in some areas with some containing a low degree of hardness. Veining was present as crustiform / colloform veins. Some visible grey sub – rounded shaped inclusions (likely an alteration feature) often encased other phenocrysts and a stain of orange brown surrounded these. There was an apparent lack of mafic phenocrysts present.

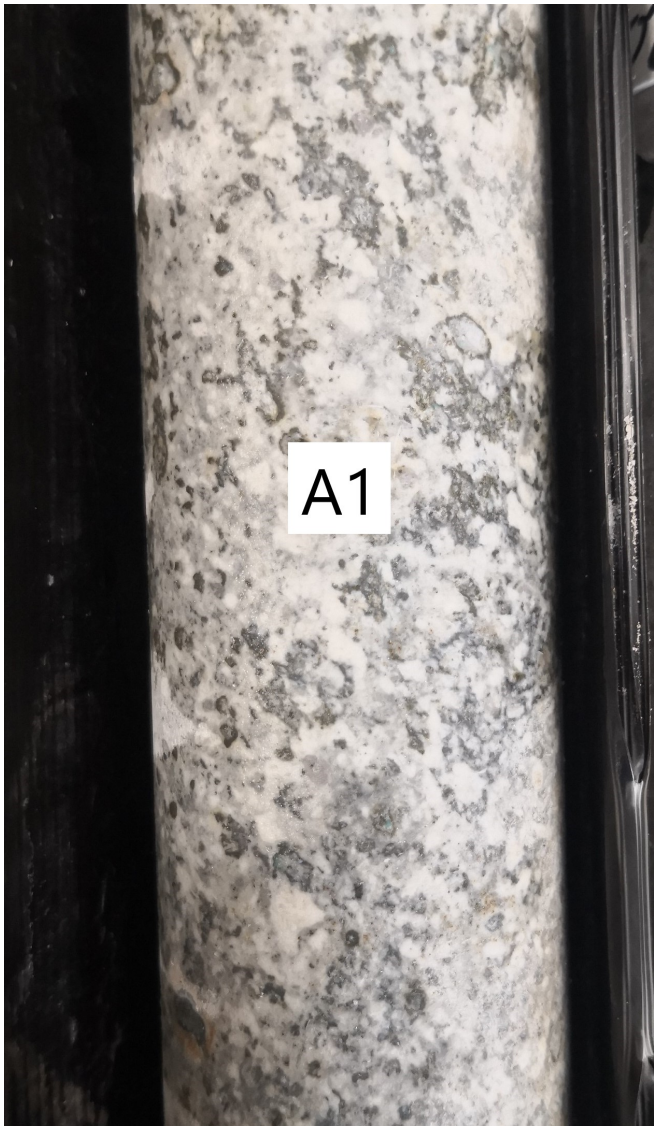

Figure 4.1: Figure showing A1 facies

Facies A2 (Feldspar rich in dark grey)

Facies A2 was porphyritic ≈ 60% phenocrysts in a grey groundmass (see 4.2). Feldspar phenocrysts were ≈ 40% and 1 – 6 mm in size with an average size of 2 mm (fig 4.2). There were some (< 5%) sub – angular 2 – 4 mm mafic phenocrysts present. This facies was classed as altered with the feldspar phenocrysts displaying similar properties to A1, albeit, they were quite well defined within the grey groundmass (the boundaries between the groundmass and phenocrysts were not obscured). Some veins were present and typically > 10 mm in size. A2x was a breccia clast found within A2 (see fig 4.3). It was an 80 mm thick breccia with 15% sub–rounded – rounded feldspar phenocrysts that were <1 mm – 3 mm thick and on average 1 mm. Other notable features were specks of green–blue phenocrysts.

Figure 4.2: Figure showing A2 facies

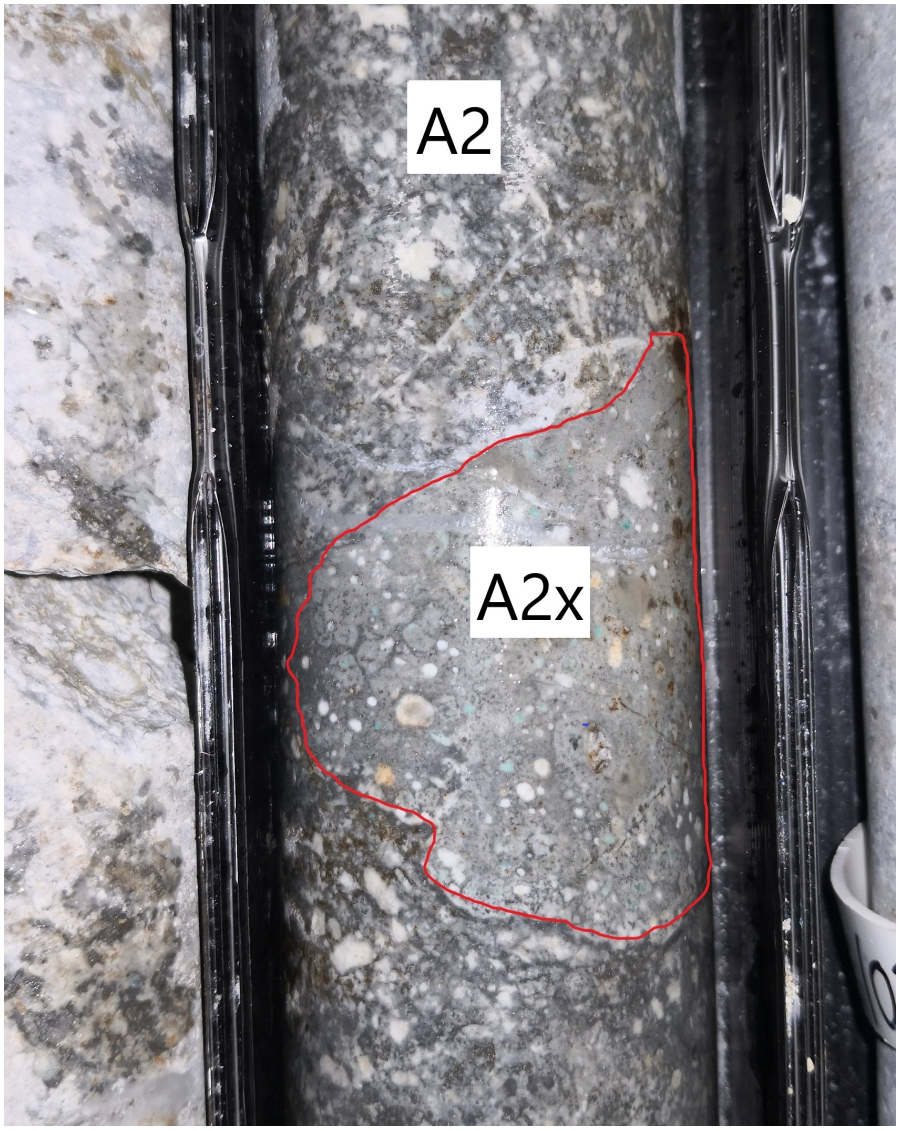

Figure 4.3: Figure showing A2x facies (an A2 breccia clast) within the drawn red boundary

Facies A3 (White alteration patches)

Facies A3 was porphyritic with ≈ 25% phenocrysts present in a grey groundmass. Feldspar phenocrysts ranged from angular to sub - angular $< 1 - 4$ mm with an average size of 1 mm. Phenocrysts were well defined within the groundmass. Mafic phenocrsysts were present at around $5 - 10\%$ with a range size of $1 - 2$ mm and an average size of 1 mm. Facies A3 characteristically showed patches of alteration highlighted by the red circle in fig 4.4. Some minor quartz veining (typically ≈ 2) mm was also present.

Figure 4.4: Figure showing A3 facies. Red circle demonstrates observed patches of alteration. Blue circle is an example of quartz veining present within the facies.

Facies A4 (Dark grey, quartz disseminated)

Facies A4 was porphyritic with 10% feldspars that were euhedral to subhedral shaped in a dark grey groundmass. Feldspar phenocryst sizes ranged from 1 – 4mm with the average being 2 mm. The groundmass had a coarse appearance with many very fine <1 mm micro phenocrysts visible within the groundmass. There were also ≈ 5% subhedral mafic phenocrysts. Some sporadic stringer veining 0.5 mm – 2 mm thick were present (fig 4.5) and irregular groundmass quartz disseminations.

Figure 4.5: Figure showing A4 facies. Blue circle is an example of abundant quartz stringer styled veining present in the facies

.

Facies A5 (Feldspars in a smoke light grey)

Facies A5 was porphyritic with subhedral feldspar phenocrysts ≈ 20% in a smoky light grey groundmass. These phenocrysts were predominantly white, 1 – 4 mm in size with an average size of 2 mm. Some orange brown staining was apparent on the faces of the core. There were also <5% sub – angular mafic phenocrysts were present, which were a darker grey colour than the surrounding groundmass. Stringer veins were present (fig 4.6).

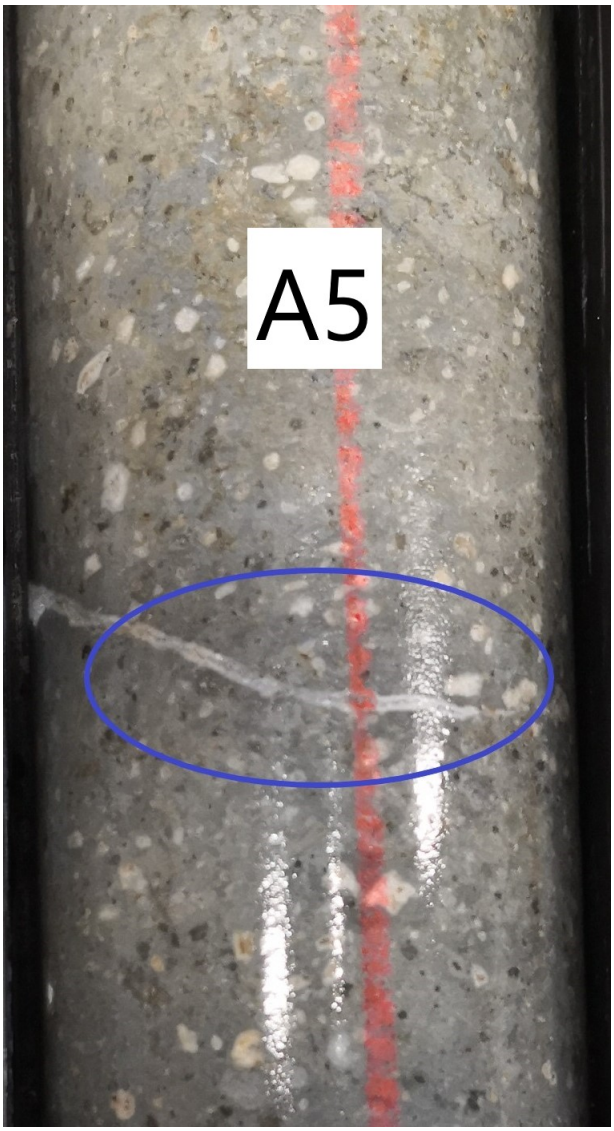

Figure 4.6: Figure showing A5 facies. Blue circle demonstrates quartz veining present in the facies.

4.5 Weakly altered facies

The weakly altered facies consisted of facies that appeared to have little alteration. They were defined using the criteria discussed in section 4.2. The facies labelled weakly altered were all given the letter B and separated into their respective facies in numerical order to produce facies B1 and B2. The weakly altered facies B1 and B2 are described further below.

Facies B1 (Country rock andesite)

Facies B1 was porphyritic and reflected the original andesitic texture the most. 10% feldspar phenocrysts were present with a size range of 1 – 4 mm with an average size of 1 mm. There was also 15% mafic phenocrysts <1 – 2 mm with an average size of 1 mm in a dark blue-grey groundmass. Irregular and sporadic 0.5 – 2 mm stringer veins (fig 4.7) were also present.

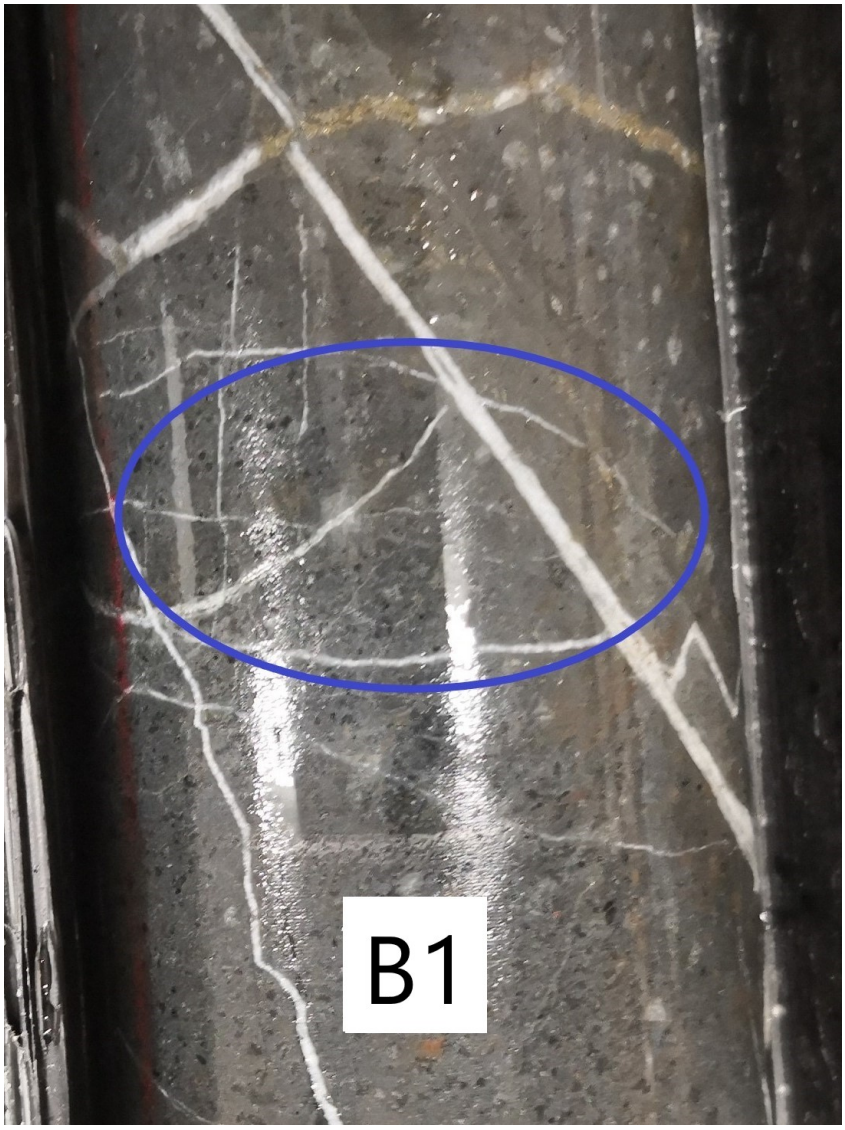

Figure 4.7: Figure showing B1 facies. Blue circle demonstrates irregular nature of quartz stringer styled veining present in the facies.

Facies B2 (Trachy-andesite)

Facies B2 was porphyritic with 15 – 20% phenocrysts present in a greyish white groundmass. ≈ 10% sub angular – sub-rounded feldspar phenocrysts were present. Some (5 – 10%) mafic phenocrysts were also present. Few 1 – 2 mm stringer veins present, highlighted by the blue circle in fig 4.8.

Figure 4.8: Figure showing B2 facies. Blue circle is an example of quartz veining present in the facies.

4.6 Breccia related facies

The breccia facies consisted of facies that were partially or completely brecciated. They were defined using the criteria discussed in section 4.2. The facies labelled breccia were all given the letter C and separated into their respective facies in numerical order to produce facies C1, C2 and C3. The brecciated facies C1, C2, and C3 are described further below. Note, facies C3 was separated into four separate sub-facies associations – C3a, C3b, C3c and C3d – to be able to best distinguish the repetitive nature of what was observed during core logging.

Facies C1 (Black breccia)

Facies C1 comprised clasts that were porphyritic with 40% feldspar phenocrysts that appeared to be brecciated and disseminated generously as 2–10 mm clasts inside the matrix. Clasts appeared shattered and sub–angular – angular and were supported within a visibly dark brown / charcoal black matrix. Individual breccia clasts ranged in size from very fine <1 mm to clasts > 100 mm. There was an observably low hardness compared to more coherent rock facies such as those encountered in facies A or B. Logged sections of C1 appeared flaky in various sections and the rock easily crumbled. Occasional thick bands (10 mm) of calcite veining were present (fig 4.9).

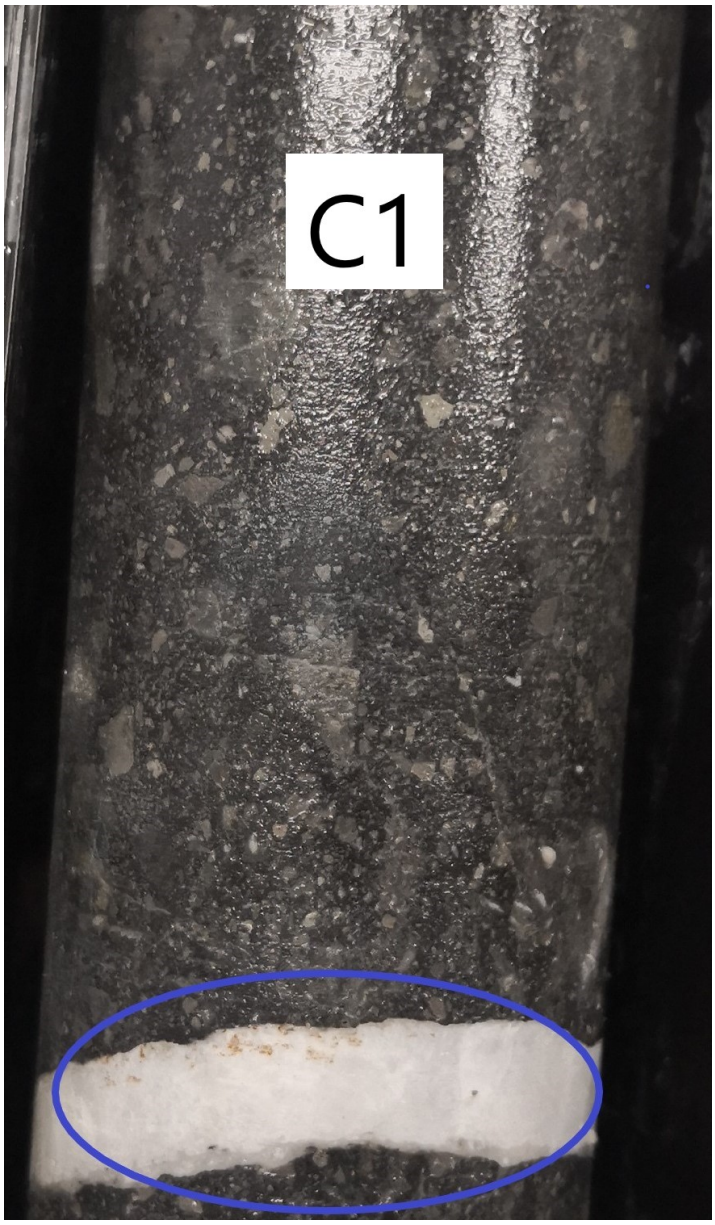

Figure 4.9: Figure showing C1 facies. Blue circle demonstrates 10 mm thick calcite vein.

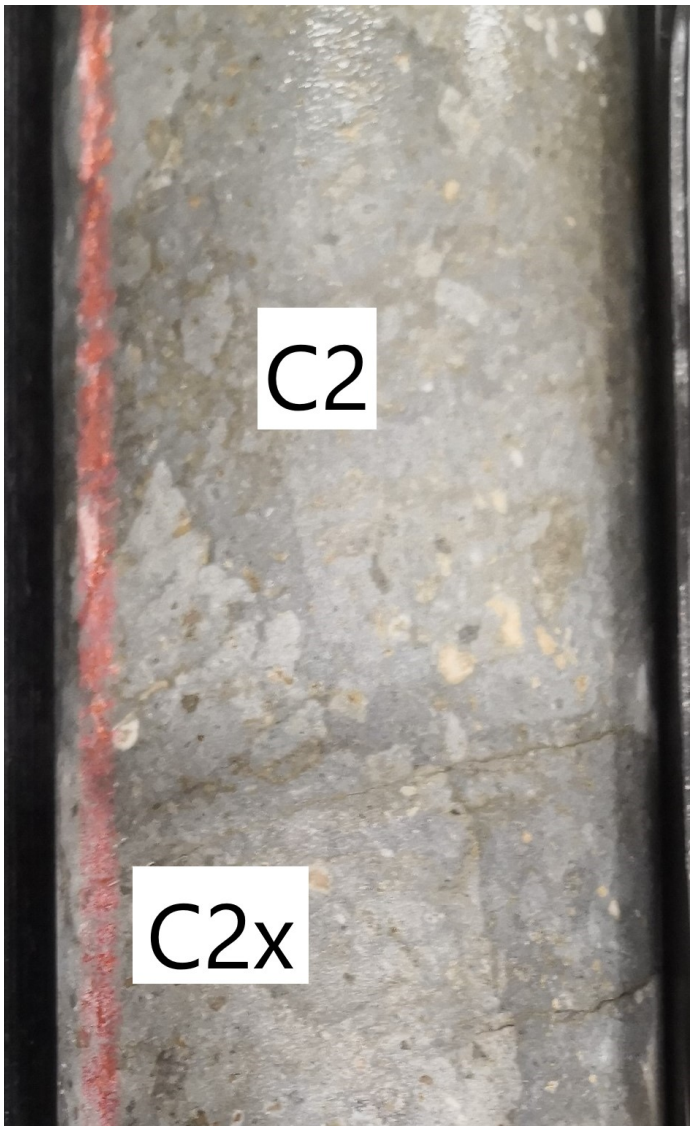

Figure 4.10: Figure showing C2 facies.

Facies C2 (Partial – complete brecciated coherent rock)

Facies C2 comprises porphyritic clasts with 25% subhedral feldspar phenocrysts in a grey matrix (fig 4.10). Some subhedral mafic phenocrysts 5—10% of the rock. In contrast to C1, facies C2 contained an observable increase in hardness, no apparent flakiness/tendency to crumble and a lighter matrix colour. Internally, some clasts appear partially brecciated. Clast sizes range from 2–80 mm with an average size of 5 mm. Quartz seemed to occur as disseminations within the matrix.

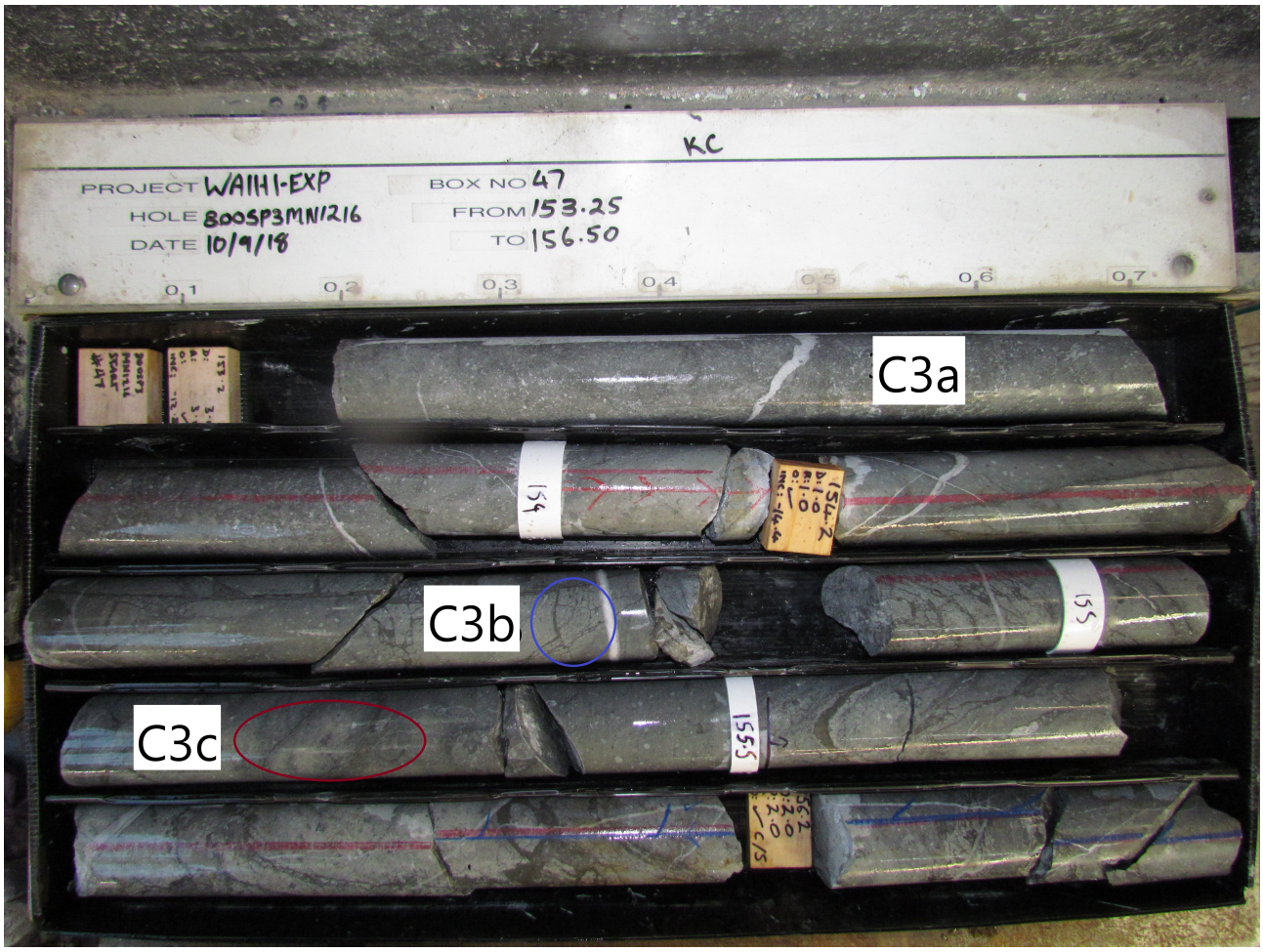

Figure 4.11: Figure showing facies C3a, C3b and C3c. Blue circle demonstrates crackle texture used to distinguish C3b. Red circle shows the flow–boundary texture used to distinguish C3c.

Facies C3a (patchy large feldspar variant)

Facies C3a was porphyritic with a patchy texture. Facies C3a consisted of 5 – 50 mm sized breccia clasts containing ≈ 10% phenocrysts. These phenocrysts were 8% sub–angular feldspar phenocrysts ≈ 1.5 mm in size and 2% mafic phenocrysts ≈ 1 mm in size. C3a had a grey coloured matrix with smaller feldspar and mafic phenocrysts than what was contained within the clasts. C3a was different from other C3 facies by the lack of a crackle or flow texture, abundant feldspar phenocrysts and quartz disseminations (fig 4.11).

Facies C3b (crackle texture variant)

Facies C3b was porphyritic with 5 – 50 mm sized breccia clasts containing ≈ 20% feldspar and mafic phenocrysts. 15% were subhedral feldspar phenocrysts ≈ 2mm in size and 5% were euhedral mafic phenocrysts. The clasts were supported in a dark grey matrix. In contrast to other C3 facies it formed a prominent crackle texture (fig 4.11).

Facies C3c (patchy boundary variant)

Facies 3Dc comprised porphyritic, breccia clasts containing 15% sub–angular phenocrysts of which 5% were feldspars ≈ 1 mm thick and 10% mafic ≈ 1.5 m in size in a greyish white groundmass. These clasts were held within a dark grey matrix that appeared as a flow texture around clast boundaries (fig 4.11). C3c was separated from other C3 facies primarily by the presence of a flow texture.

Facies C3d (thick calcite vein variant)

Facies C3d comprises porphyritic, 100 mm-sized breccia clasts containing 15 – 20 % phenocrysts. Of these phenocrysts, 17% were subhedral feldspar phenocrysts and 3% subhedral mafic phenocrysts in a grey groundmass. The matrix was a dark grey colour. Separated from other C3 facies by the prominent calcite disseminations and >≈ 5 mm thick calcite veins(fig 4.12).

Figure 4.12: Figure showing facies C3d. Red circle shows the often abundant calcite veining used to disguish this facie. Blue circle shows a quartz vein terminating against the calcite veins.

4.7 Drill hole descriptions and facies distribution

Detailed below are the summary descriptions for all the drill hole data logged. Facies distribution is provided as a description for how each facies fits together within each of the logged cores. Identified facies relationships such as facies appearances, boundaries and their repeatability within core logs are discussed below.

4.7.1 Drill hole 1842 [EMP16RG1842]

Drill core data for hole 1842 was logged at depths of 100.9 m – 117.4 m (box 31 – 35) and 134.1 m – 137.2 m (box 41). The identified facies for this hole were; A1, A2, A3, A3, A4, B1, A5 C1 and C2. Facies A1 was logged from 101 – 101.5 m. Facies A1 graded into A2 at ≈ 101.5 m. Facies A2 was a prominent facies from 101.5 – 104.1 m (3.6 m) where it was terminated along the contact boundary of A4. A sharp boundary was observed at 106.5 m where A2 was terminated against A4. A3 was logged as a short (0.15 m) interstitial facies occurring between and overlying A2 at 104.2 – 104.35 m. A3 was also logged at 104.9 – 105.05 m. Facies A4 was logged at 106.5 – 107 m (0.5 m). Another sharp boundary was observed at 107 m where A4 terminated against C1. C1 was logged at 107 - 109.5 m (2.5 m). A sharp boundary was observed at 109.5 – 109.55 m (0.05mm) where two sets of C1 and C2 contacts were superimposed on each other and eventually phased into C2 at 109.55 mm. Facies C2 was logged from 109.5 – 111.6m (2.1 m), 111.95 – 113 m (1.05 m), 114.05 – 114.4 (0.35 m) and 115.2 – 117.6 m (2.4 m). A sharp contact was observed at 111.6 m where C2 transitioned into A3 between 111.6 - 111.95 m (0.35 m). Another sharp contact was logged at 111.95 where A3 transitioned back to C2. A gradational contact was observed at 112.02 m whereby, C2 transitioned in to A5. Facies A5 was present from 112.02 – 112.4 m (0.38 m) and 113 – 114.05 m (1.05 m) and 114.6 – 115.2 m (0.6 m) in between facies C2 as a sort of interstitial weakly altered coherent section in between the brecciation. Facies B1 was the weakly altered facies that closely resembled the original andesitic texture. Facies B1 was only logged at greater depths of 134.1 – 137.4 m (box 41) within this hole.

4.7.2 Drill hole [800SP3MN1216]

Drill core data for hole 1216 was logged at depths of 56.5 m – 63 m (box 18 – 19) and 153.2 m – 169.3 m (box 47 – 51). Facies C2 was logged in this hole from 56.5 – 60.2 m and 62.4 – 63.2 m. At 60.2 m, facies C2 is in contact with facies C3c where brecciation intensity lessens and is replaced by a flow–like or patchy texture. Facies C3c ceases at 62.4 m. For boxes 47 – 51, a new facies (C3) and associations (C3a, C3b, C3c and C3d) are introduced. Facies C3a was observed from 153.2 – 154 m where it graded into C3b. C3a was also observed at 163.6 – 164 m where it became intensely brecciated to create the 'flow–like' texture characteristic of C3c. C3b was logged at 154 – 155 m, 161.2 - 161.4 m, 161.6 m – 162.8 m, 163.4 – 163.6 m, 166.4 –167.4 m and 168.2 – 169.6 m. Facies C3b logged at 154 – 154 m and 161.6 – 162.8 m, gradually transitioning into C3c – evident by the brecciated crackle texture. Between 167.4 m – 168.2 mm, facies C1 (black breccia) was logged in between two sets of C3b. C3c was logged at 155 – 156.5 m where it contacted C3b above and C3d below. C3c logged at 158.6 – 159.4 m was in between two sets of C3d. C3c was also logged between two sets of C3b facies at 161.4 – 161.6 m and 162.8 – 163.4 m. C3d was logged at 156.4 m – 158.6 m and 159.8 – 161.2 m. Both the overlying and underlying facies contacts around C3d are C3c except for at 161.2 m where it transitioned into C3b.

4.7.3 Drill hole [920SP2MN1164]

Drill core data for hole 1164 was logged at depths of 145 - 165.2 m (box 44 – 52) and 193.6 – 218.4 m (box 58 – 65). Core data logged from 145 - 165.2 m, displayed only 2 facies: A2 and A3. A2 showed a close alternating relationship with A3 whereby, these alternating facies (A2 and A3), would be present for 0.2 – 2 m before gradually transitioning into the other facies. In some areas where A2 was present (such as, 158.8 m), facies A3 was still present as a sort of dissemination. A2 had a higher feldspar phenocryst concentration and in contrast to A3, appeared more altered. Any veining present between 148 – 165.2 m was only in the form of stringer veins.

Core data logged from 193.6 – 218.4 m (box 57 – 65) displayed the following facie: A2, A3, A4, A5, C1 and C3c. A2 was logged from 193.6 – 195.6, 197.4 – 198.2 m, 190.4 – 201.5 m, A3 was logged at 202 – 202.8m, 205.2 – 214 m and 216.1 – 216.2 m. A4 was logged at 188.7 – 189.6 m, 190 – 190.4 m and 195.9 – 197.4 m where it was terminated by a sharp contact with A2 every time. A4 logged at 202.8 – 204.5 and formed a gradational contact with B1. A4 at 201.6 – 202 m formed a gradational contact with the overlying and underlying A3 facies. A4 was logged at 205 – 205.2 m with a gradational contact with the overlying B1 facies and a transition into the underlying altered A3 facies. A5 was only logged 195.7 – 195.9 m where it contacted the overlying A2 and gradually transitioned from patches of A5 in the overlying A2 facies into A5. Where the A5 facies contacted A4 at 195.9 m, a gradational contact was observed. C1 was logged at 213.05 m – 216.1 m where it formed sharp contacts with both the overlying and underlying A3 facies facies. C3c was logged at 216.3 m – 218.4 m where it transitioned from the overlying A3.

Chapter 5

Petrography and geochemistry

5.1 Thin section preparation

Sections of interest within the core log were taken to a rock saw to create 28 small rectangle blocks 3–4 cm by 2 cm. Thin section glass was frosted on one side using a grinder. Both the cut blocks of rock and glass were cleaned under cold water. These blocks of rock were then mounted onto the frosted glass using a Hillquist resin for block mounting to create the thin section. A respective mixing ratio of 7:3 (Hillquist part A : Hillquist part B) was used to create this resin. The blocks were left to dry overnight on a hot plate set at 80 °C. When the resin had set, the thin section was placed on to a rock saw, where the overhanging block of rock was cut down to < 1 mm thick. Each thin section was then placed on to a grinder rock were taken down to thicknesses ranging from 10 µm – 18 µm. The remaining surface of each thin section was then sanded using 400 and 1200 grit sand paper, until the visible feldspar phenocryst were white–grey to straw yellow in birefringence colour under cross polarised light [XPL]. Finally the thin sections were polished for ≈ 20 minutes each, until the grinding marks (visible under reflective light) had been polished out.

5.2 Microscope petrography

Thin section microscopy was carried out using a Nikon Eclipse, LV100 P0 and thin section images were taken using an Olympus SC50 camera. Transmitted [TL] and reflective light [RL] microscopy was performed on a total of 28 thin sections using different objective lenses which ranged from: 1x, 4x, 10x, 20x and 40x and an ocular lens at 10x. The first thin section observation was whether an observable groundmass or matrix was present. Primary textures were recorded, which first gave a descriptive term for the relationship of crystal sizes with other crystals and groundmass / matrix (e.g. porphyritic). Primary textures also involved describing the types of crystals present within the thin sections and their average abundances, shapes, colour, size and other noteable features were recorded. Next, alteration features were recorded, with a descriptive term denoted for the degrees of alteration, whereby: 0% = unaltered, 1-25% = weakly altered, 26 - 50% = altered, 51 - 75% very altered, 76 - 100% = extremely altered. Additional percentages were given for the degree of alteration of individual grains (e.g. % of calcite alteration within existing plagioclase crystals). Alteration features that were unidentifiable under thin section microscopy were given a temporary identifier (e.g. alteration 1) and their appearance, size and general locale were recorded. Lastly, the groundmass or matrix was recorded as an overall percentage of the whole rock. Each unique mineral responsible for making up a portion of the groundmass / matrix was given a percentage of total space in the thin section it occupied. The mineral name, shape, size and additional features were recorded. Data entry was input into 3 separate tables to record thin section primary textures, groundmass and matrix and alteration. It should be noted that minerals observed under the microscope were only representative of a very small area within the facies. Facies with multiple thin sections reflected some differences in the observed

abundance or presence of minerals. When generating graphs for facies that were studied using multiple thin sections, an average value was generated for phenocryst abundance, size and groundmass/matrix mineral percentages. Furthermore, thin section features that may have only been observed once across multiple thin sections from the same facies, were recorded but not included in the averages. Alteration features that were devised, (such as G.A.P, R.G.B and P.M.G.B) were only created in an attempt to generalise re–occurring alteration textures.

Quartz

Quartz under the microscope was colourless under plain polarised light [PPL] and white or grey under cross polarised light [XPL]. These phenocrysts were easily identified by their lack of alteration and tendency to form embayments and fracture textures (fig. 5.1(a)). Being a relatively hard mineral, quartz can sometimes be more resistant to the thin section sanding and polishing process. Therefore, under XPL some quartz may not have been white and instead other low 1st order birefringence colours such as orange or straw yellow. Quartz veins tended to show a mosaic collage of low 1st order birefringence colours. Quartz within the thin sections were often subhedral – anhedral in shape and found as larger individual phenocrysts or within the groundmass or matrix as disseminations.

Plagioclase

Plagioclase was colourless under PPL and white or grey under XPL. Diagnostic features displayed by plagioclase included twinning or zonation which was used to identify these minerals. Fig. 5.1(b), displays an identified phenocryst of plagioclase. In contrast to quartz, plagioclase phenocrysts responded well to the sanding and polishing process and were all subsequently grey or white under XPL. All of the plagioclase phenocrysts observed under the microscope were partially or entirely altered to secondary alteration minerals. Plagioclase phenocrysts were mostly subhedral shaped and typically around $\approx$ 1.5 mm. Plagioclase identified within the groundmass or matrix in some thin sections as very fine microlites – often partially or almost entirely altered into secondary minerals such as calcite.

Orthopyroxene [Opx]

For the purpose of this study, individual orthopyroxene minerals (e.g. enstatite, bronzite) were not distinguished. Instead, based on a few diagnostic features (such as extinction angle and birefringence colour), only the percentages, shapes and sizes of Opxs collectively were recorded. Opxs were typically light olive green – olive green pleochroic under PPL. Opx under XPL displayed an array of low 1st order birefringence colours in the range of low straw yellow – blue (fig. 5.1(b)). Opxs were subhedral – anhedral and observed primarily as phenocrysts. Opx sizes varied among the different thin sections and were typically between <0.25 mm to 2 mm. Opx was prone to alteration evident by secondary mineral disseminations obscuring the phenocryst area and boundary. Opxs that were partially altered were still able to be recognised by their characteristic parallel extinction following the presence of Opx being established within the thin section.

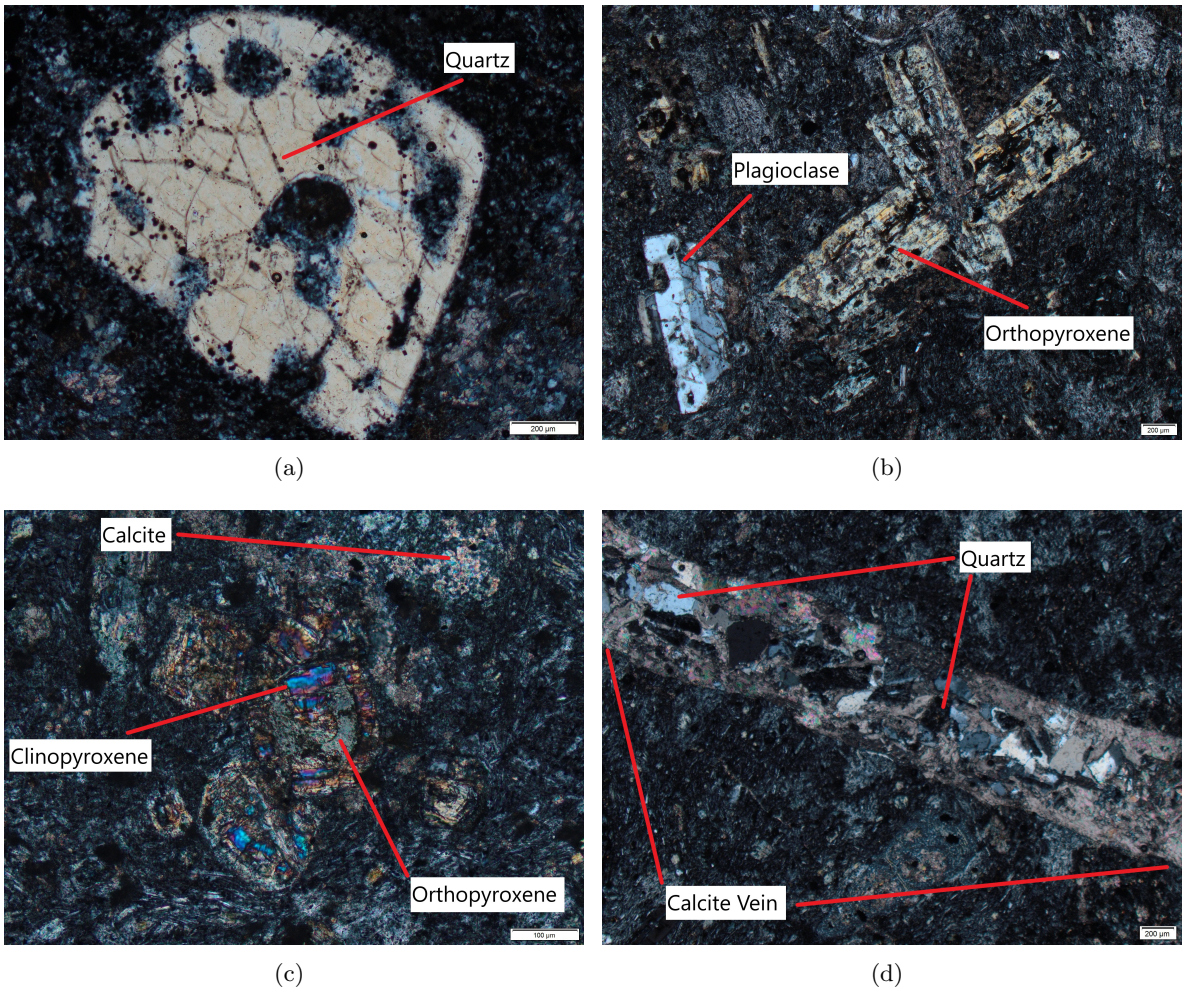

(a) (b)

(c) (d)

Figure 5.1: The above photomicrographs represent: (a) quartz with fractures and embayments, (b) orthopyroxene and plagioclase, (c) calcite, Cpx and Opx and (d) angular quartz fragments in a calcite vein. The photomicrographs were taken under the following thin sections with XPL; (a) was taken under thin section TZ 2 (facies A2); (b), (c), and (d) were taken under TZ 1 (facies B1).

Clinopyroxene [Cpx]

For the purpose of this study, individual clinopyroxene minerals (e.g. aegerine, jadeite) were not distinguished. Instead, based on a few diagnostic features (such as extinction angles and birefringence colour), only the percentages, shapes and sizes of Cpxs collectively were recorded. Not a lot of Cpxs were identified. Only two thin sections were recorded includingCpxs with an average abundance of only 1 – 2 %. These Cpxs were subhedral – anhedral, only 0.1 mm and displayed a characteristic inclined extinction (fig. 5.1(c)).

Opaque minerals

'Opaque minerals' is an overarching term for any mineral that was black under both PPL and XPL Reflective light microscopy [RL] and was useful to separate and identify individual minerals that were opaque under transmitted light [TL] (PPL and XPL). Opaque minerals tended to occur within the thin sections as sulphides or metals. The most common opaque mineral identified was pyrite, localised

either as clusters or disseminations within the groundmass. Diagnostic features for pyrite are its light yellow colour under RL (fig. 5.2(d)) and its relatively higher hardness and higher relief than the surrounding minerals. Occasionally, pyrite would retain some of the grinding marks generated by the thin section creation process. Other opaque minerals identified within thin sections were chalcopyrite, galena and sphalerite. In contrast to pyrite, chalcopyrite was more yellow under RL and had a lower relief. Galena had a silver – light grey colour with low relief (fig. 5.2(c)). In some larger phenocrysts, galena tended to form triangular pits – a product of crystals being plucked out during the polishing process. Sphalerite was classed as an opaque mineral but was not truly opaque under XPL and PPL. Where sphalerite was present, it was identified as a dark murky–brown patch. Although harder to observe, after crossing the polars in TL, sphalerite tended to form a glowing gold–orange–yellow effect, which was a product of its internal reflections.

Calcite

Calcite was a secondary mineral that was commonly observed to be altering plagioclase crystals. A diagnostic feature of calcite was a collage of high birefringence colours that displayed an oil–slick like appearance (fig. 5.1(d)).

Grey amorphous patches [G.A.P]

This amorphous material formed grey patched under PPL and XPL. It was found within thin sections as thick (almost opaque) patches disseminated through the groundmass or altering surrounding boundary edges of larger phenocrysts (fig 5.2(b) and 5.2(a)).

Radial golden brown [R.G.B]

This alteration mineral was dark golden brown under both PPL and XPL (fig. 5.2(b)). Diagnostic features that separated this mineral from other secondary minerals were its colour and fibrous appearance, which produced radial streaks of low first order orange and yellow under XPL. Streaks of orange yellow under XPL tended to radiate from an internal centre point toward the crystal boundary edge.

Pervasive murky grey–brown matrix fill [P.M.G.B]

Fig. 5.2(b) shows a pervasive amorphous murky grey – orange-–brown mineral in PPL and XPL. Dirt–like texture found as the matrix in–fill of C1 (black breccia). The grain sizes of this alteration texture were unable to be distinguished using 40x lens.

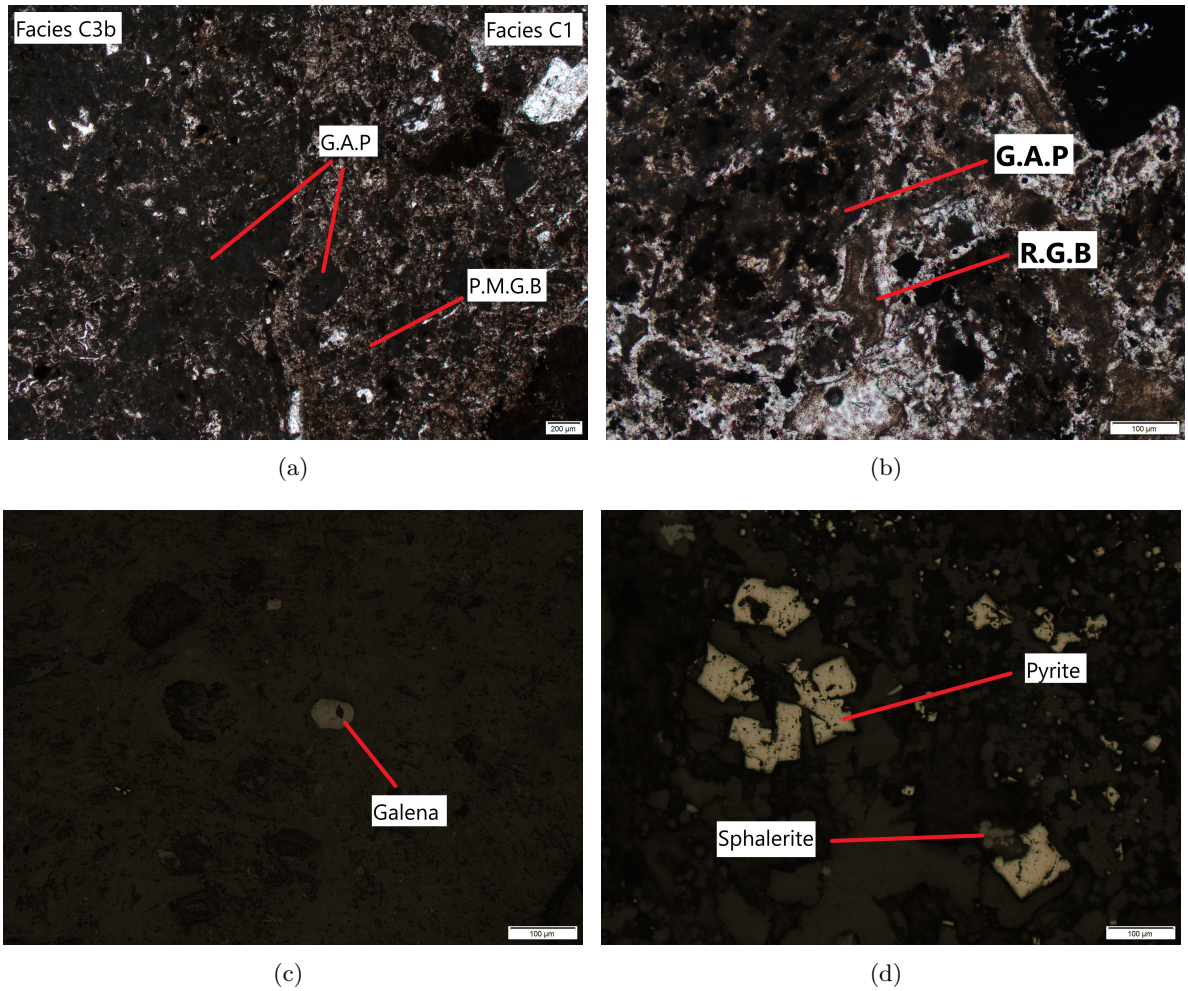

Figure 5.2: The photomicrographs represent: (a) grey amorphous patches alteration [G.A.P] and pervassive murky grey brown alteration [P.M.G.B], (b) G.A.P and radial golden brown alteration [R.G.B], (c) small galena mineral $\approx$ 100μm and (d) pyrite and sphalerite minerals 100 μm. The photomicrographs were taken under the following thin sections with PPL and RL; (a) and (b) were both taken under PPL using thin sections TX 8 (facies C2) and TX 9 (facies C2x) respectively. (c) and (d) were taken using RL under thin sections TZ 1 (facies A2) and TZ 2 (facies A2). (a) displays a brecciated contact between facies C3b and facies C1 (black breccia).

5.2.1 Highly altered facies

The heavily altered facies (see Chapter 4) encapsulates five separate facies (A1, A2, A3, A4 and A5), which were investigated under the microscope using 13 different thin sections. Each facies displayed similarities and differences in the primary volcanics, groundmass and alteration textures present. Fig. 5.3 simplifies the raw data from petrography tables in the appendix.

Facies A1 (Greyish white feldspar rich)

Facies A1 was identified and investigated using one thin section. The thin section was from drill hole 1842 at 101.2 m. Primary volcanic minerals for facies A1 was quartz and Opx (fig 5.3). The percentage of quartz phenocrysts were $\approx$ 5% which were on average 1.5 mm. The Opx phenocryst percentages

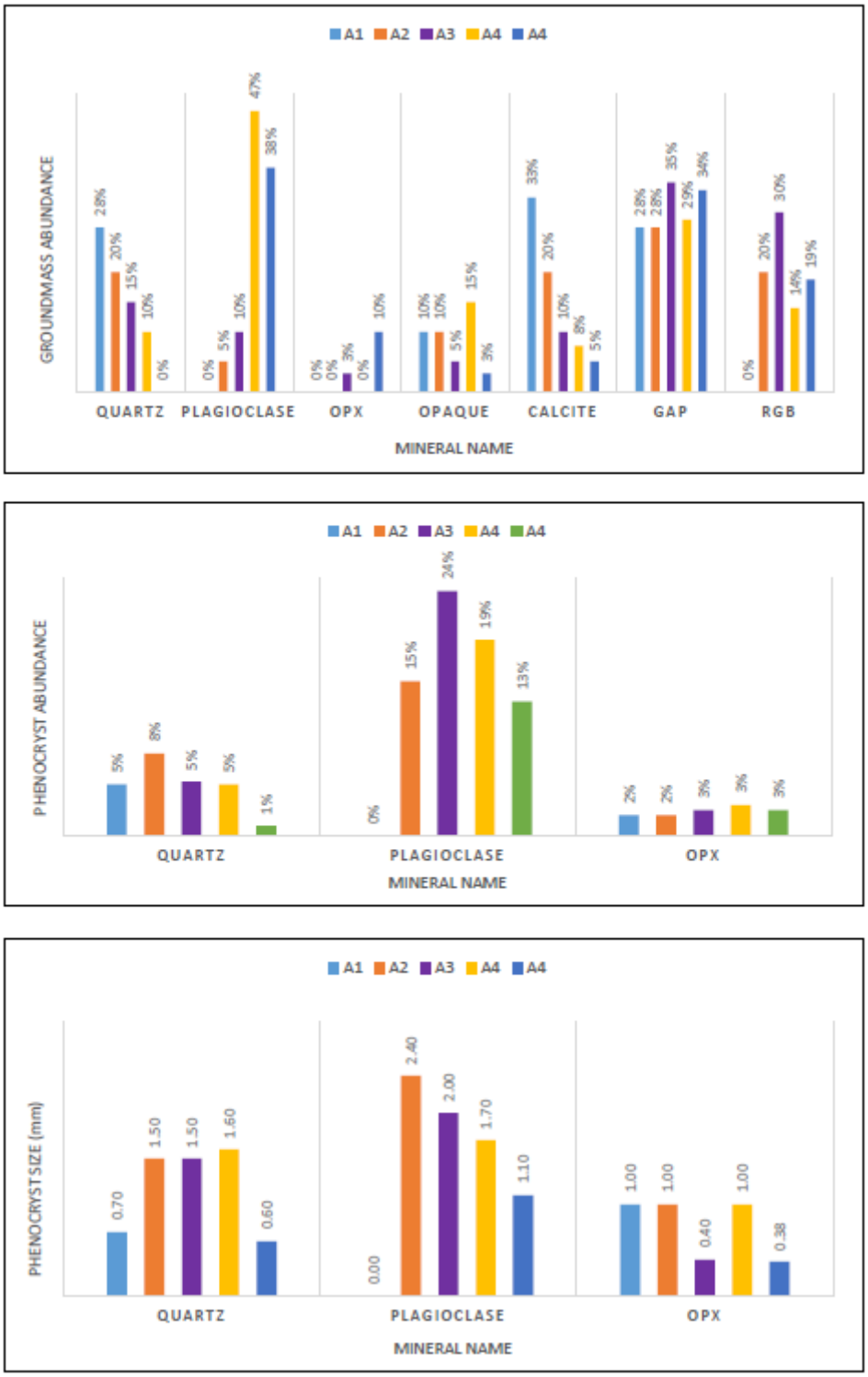

Figure 5.3: Figure showing petrography data for facies identified as heavily altered coherent. Each graph displays groundmass, phenocryst abundance or size data for each heavily altered facies, which is plotted against a mineral name.

were < 2% and were 1 mm in size. Opx phenocrysts appeared to be quite heavily altered to a clay sized, grey amorphous fill (G.A.P). The groundmass consisted of 28% quartz, 10% opaque minerals, 33% calcite and 28% G.A.P. The minerals identified within the groundmass were somewhat consistent with the larger phenocryst minerals identified. Opaque minerals consisted of euhedral – subhedral 0.4 mm phenocrysts of pyrite. Other opaque minerals also included some galena and magnetite < 1 % with an average size of 0.5 mm and < 1 %, 0.1 mm sphalerite. This thin section was considered extremely altered.

Facies A2 (Feldspar rich in dark grey)

Facies A2 was identified and investigated using one thin section. The thin section was from drill hole 1842 at 102.4 m. Primary volcanic minerals for facies A2 were quartz, plagioclase and Opx (fig 5.3). The percentage of quartz phenocrysts were ≈ 8% which were on average 1.5 mm. Plagioclase phenocrysts were ≈ 15% which were on average 2.4 mm. The Opx phenocryst percentages were < 2% and were 1 mm in size. Opaque minerals were < 2% and consisted of predominantly < 0.01 mm pyrite disseminations. The groundmass consisted of 20% quartz, 5% plagioclase, 10% opaque minerals, 20% calcite, 28% G.A.P and 20% R.G.B. Facies A2 was considered very altered. Facies A2x was a breccia clast hosted by facies A2. Facies A2x consisted of only < 4% plagioclase with > 90% of plagioclase having been altered into calcite. 50 – 55% G.A.P made up the groundmass of this thin section. Facies A2x was labelled extremely altered.

Facies A3 (White alteration patches)

Facies A3 was identified and investigated using four separate thin sections. One thin section was from drill hole 1842 at 104.2 m and three thin sections were from drill hole 1164 at 205.8, 205.9 and 206.1 m. Primary volcanic minerals for facies A3 were quartz, plagioclase and Opx (fig 5.3). The percentage of quartz phenocrysts were ≈ 5% which were on average 1.5 mm. Plagioclase phenocrysts were ≈ 24% which were on average 2 mm. Larger plagioclase phenocrysts were commonly fractured and G.A.P and R.G.B alteration surrounded crystal boundaries and occupied fractures. The Opx phenocryst percentages were 3% and were 0.4 mm in size. The groundmass consisted of 15% quartz, 10% plagioclase, 3% Opx, 5% opaque minerals, 10% calcite, 35% G.A.P and 30% R.G.B. Petrography data for primary volcanics and groundmass minerals such as presence, abundance, and size, were mostly consistent across all four thin sections with the exception of no Opx being found within one thin section (TX 12). Facies A3 was labelled as altered – very altered across the four different thin sections. Some thin sections (TZ 7) displayed barren 2.5 and 9 mm quartz veining. Opaque minerals were mostly pyrite with some chalcopyrite, galena and sphalerite also recorded.

Facies A4 (Dark grey, quartz disseminated)

Facies A4 was identified and investigated using four separate thin sections. One thin section was from drill hole 1842 at 106.6 m and the other three thin sections were from drill hole 1164 at 189.3, 192.1 and 203.1 m. Primary volcanic minerals for facies A4 were quartz, plagioclase and Opx (fig 5.3). The percentage of quartz phenocrysts were ≈ 5% which were on average 1.6 mm. The amount of plagioclase phenocrysts within the thin sections were ≈ 19% and on average 1.7 mm. The Opx

phenocryst percentages were 3% and 1 mm in size. The groundmass consisted of 10% quartz, 47% plagioclase, 15% opaque minerals, 8% calcite, 29% G.A.P and 14% R.G.B. Plagioclase within the groundmass consisted of laths that were <0.1 mm in size. Opaque minerals were mostly 0.5 – 2.5 mm pyrite with minor (< 1 %; < 0.01 mm) chalcopyrite ± arsenopyrite and galena. All four thin sections investigated showed similar results for primary volcanic mineral presence, abundance and size. Facies A4 was labelled as an altered thin section. TX 5 displayed a groundmass with a much lower percentage of G.A.P alteration than the other three thin sections. TX 5 groundmass mostly comprised of light brown, translucent mineral, that had low order grey birefringence under XPL (labelled as plagioclase).

Facies A5 (Feldspars in a smoke light grey)

Facies A5 was identified and investigated using two separate thin sections. Both thin sections were from drill hole 1842 at 112.1 and 113.8 m. Primary volcanic minerals for facies A5 was quartz, plagioclase and Opx (fig 5.3). The percentage of quartz phenocrysts were ≈ 1% which were on average 0.6 mm. Plagioclase phenocrysts were ≈ 13% which were on average 1.10 mm. The Opx phenocryst percentages were 3% and were 0.38 mm in size. The groundmass consisted of 38% plagioclase, 10% Opx, 3% opaque minerals, 5% calcite, 34% G.A.P and 19% R.G.B. Both thin sections investigated showed similar results for primary volcanic and groundmass mineral presence, abundance and size. A5 was labelled as a very altered facies.

5.2.2 Weakly altered facies

The weakly altered facies encapsulates two separate facies (B1 and B2), which were investigated under the microscope using two different thin sections. Fig. 5.4 summarises the raw data from petrography tables in the appendix. Thin sections investigated carry identical naming conventions to those described and discussed in Chapter 4.

Facies B1 (Country rock andesite)

Facies B1 was identified and investigated using a thin section from drill hole 1842 at 136.2 m. Primary volcanic minerals for facies B1 was quartz, plagioclase, Opx and Cpx (fig 5.4). The percentage of quartz phenocrysts were ≈ 3% which were on average 0.5 mm. The amount of plagioclase phenocrysts within the thin section were ≈ 20% and on average 2 mm. The percentage of Opx phenocryst was 15% and 1.8 mm in size. Clinopyroxenes were quite rare at only 1% and 0.1 mm in size. The groundmass consisted of 70% plagioclase, 15% Opx, 1% Cpx, 1% opaque minerals and 15% G.A.P. Opaque minerals were < 0.01 mm pyrite ± galena and rare 0.01 mm chalcopyrite. Facies B1 was labelled as a weakly altered thin section with some sulfide bearing (0.04 mm pyrite and 0.01mm chalcopyrite) calcite veins being identified.

Facies B2 (Trachy-andesite)

Facies B2 was identified and investigated using one thin section. The thin section was from drill hole 1842 at 111.7 m. Primary volcanic minerals for facies B2 were quartz, plagioclase and Opx (fig 5.4). The percentage of quartz phenocrysts were ≈ 3% which were on average 2 mm. Plagioclase phenocrysts were ≈ 15% which were on average 2 mm. Larger plagioclase phenocrysts displayed

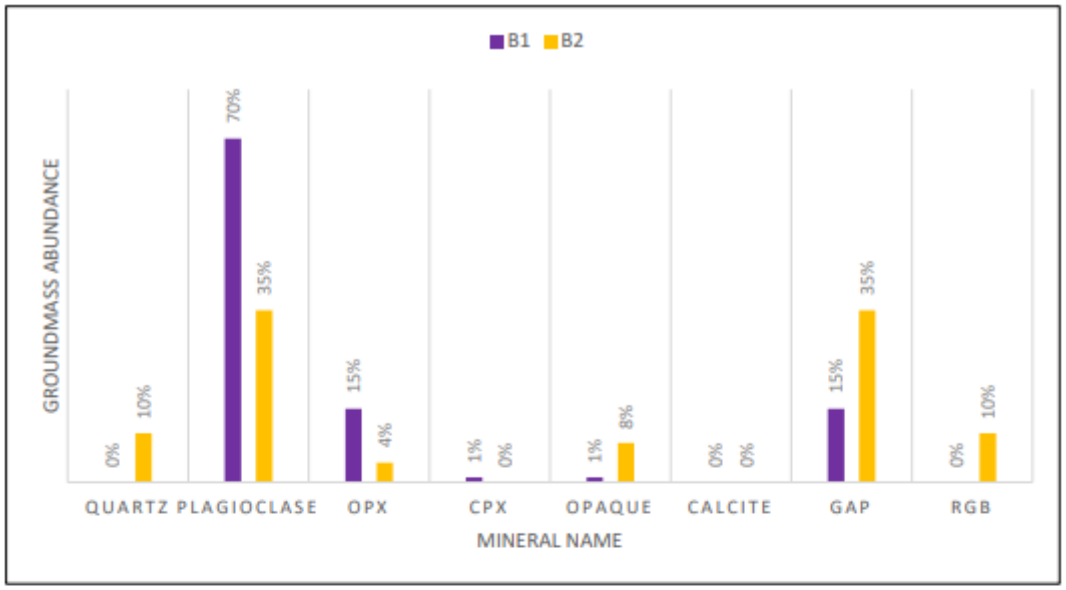

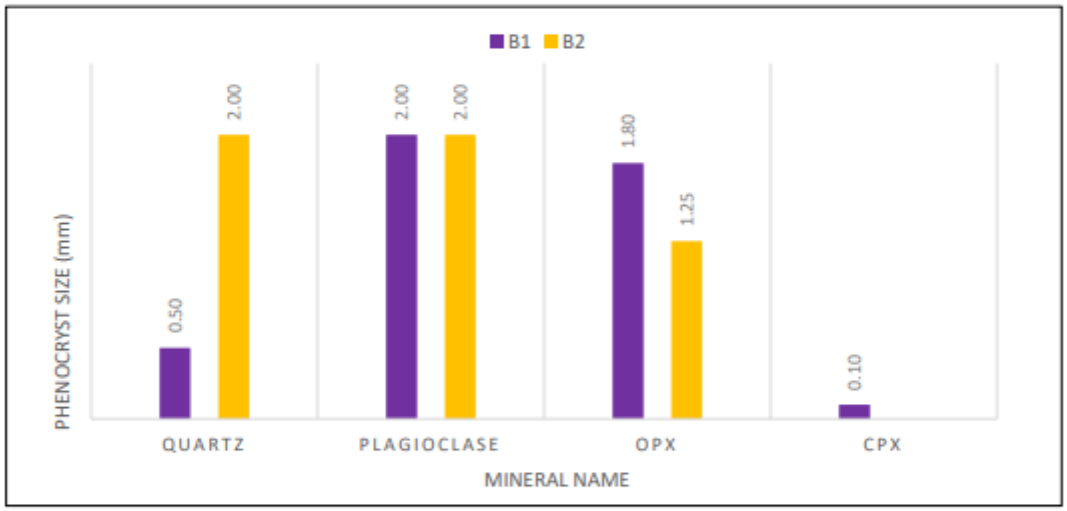

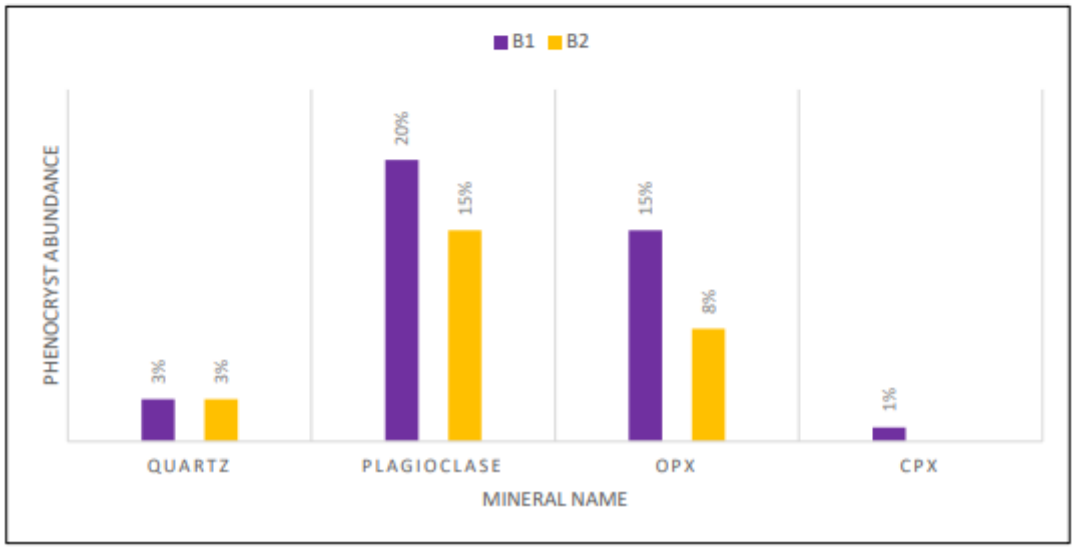

Figure 5.4: Figure showing petrography data for facies identified as weakly altered coherent. Each graph displays groundmass, phenocryst abundance or size data for each weakly altered facies, which is plotted against a mineral name.

concentric rings of G.A.P alteration. The Opx phenocryst percentages were 8% and were 1.25 mm in size. Opaque minerals were $< 2\%$, with a size of < 0.1 mm. Opaque minerals that were observed under RL revealed mostly pyrite phenocrysts with occasional sphalerite. The groundmass consisted of 10% quartz, 35% plagioclase, 4% Opx, 8% opaque minerals, 35% G.A.P and 10% R.G.B. Plagioclase within the groundmass appeared to form as laths which was 0.01 – 0.15 mm. Opx identified in the groundmass were < 0.25 mm. An interesting observation was that facies B2 showed no calcite alteration.

5.2.3 Breccia related facies

The brecciated facies encapsulated three separate facies (C1, C2, C3), which were investigated under the microscope using 15 different thin sections. The graphed units labelled as C1x and C2x refers to the clast portion of the respective facies. In the appendix, tables 7, 8 and 9 show the raw data generated for each facies during microscopy analysis. Fig. 5.5 attempts to simplify the raw data from the petrography tables in the appendix.

Facies C1 (Black breccia)

Facies C1 was identified and investigated using six separate thin sections. One thin section was from drill hole 1842 at 107.4 m, three thin sections were from drill hole 1164 at 213.8, 214 and 214.5 m and two thin sections were from drill hole 1216 at 167.1 and 168 m. Primary matrix crystals for facies C1 were quartz and Opx (fig 5.6). The percentage of quartz within the matrix was $\approx 5\%$ which was on average 1.01 mm. The percentage of Opx in the matrix was 1% and 0.38 mm in size. Alteration minerals within the matrix consisted of 6% calcite, 30% G.A.P, 10% R.G.B and 48% P.M.G.B. Facies C1 ranged from being altered – extremely altered. Partially intact plagioclase phenocryst within the matrix were only observed in thin section TX 13 whilst the other four thin sections displayed 0% plagioclase. Therefore, the findings for the average percentage of plagioclase in the matrix was based on the other four thin sections. The most notable type of alteration feature occurring within the matrix of C1 was a high percentage of P.M.G.B. Thin section TX 8 was created along the brecciated boundary of the black breccia matrix and a larger clast (fig. 5.2(a)). The black breccia clasts were identified and investigated using two thin section. Both thin sections were from drill hole 1216 at 168 m. Primary volcanic minerals identified for the black breccia clasts were quartz, plagioclase and Opx (5.5). The percentage of quartz phenocrysts were $\approx 3\%$ which were on average 0.75 mm. The amount of plagioclase phenocrysts within the thin section was $\approx 26\%$ and on average 1.9 mm. The percentage of Opx phenocrysts was 8% and 0.7 mm in size. The groundmass consisted of 2% quartz, 23% plagioclase, 2% calcite, 55% G.A.P and 21% R.G.B. Similar to the black breccia, the black breccia clasts displayed a low percentage of quartz and calcite. In contrast to the matrix, the clasts contained plagioclase, no P.M.G.B alteration and twice the amount of R.G.B and G.A.P alteration. The clasts ranged from being altered to very altered within the two different thin sections.

Facies C2 (Partial – complete brecciated coherent rock)

Facies C2 was identified and investigated using three thin sections. All thin sections were from drill hole 1842 at 111.37, 112.6 and 114.4 m. Matrix crystals identified for C2 were quartz, plagioclase, Opx and Cpx (fig 5.6). The percentage of quartz crystals in the matrix was $\approx 27\%$ and on average

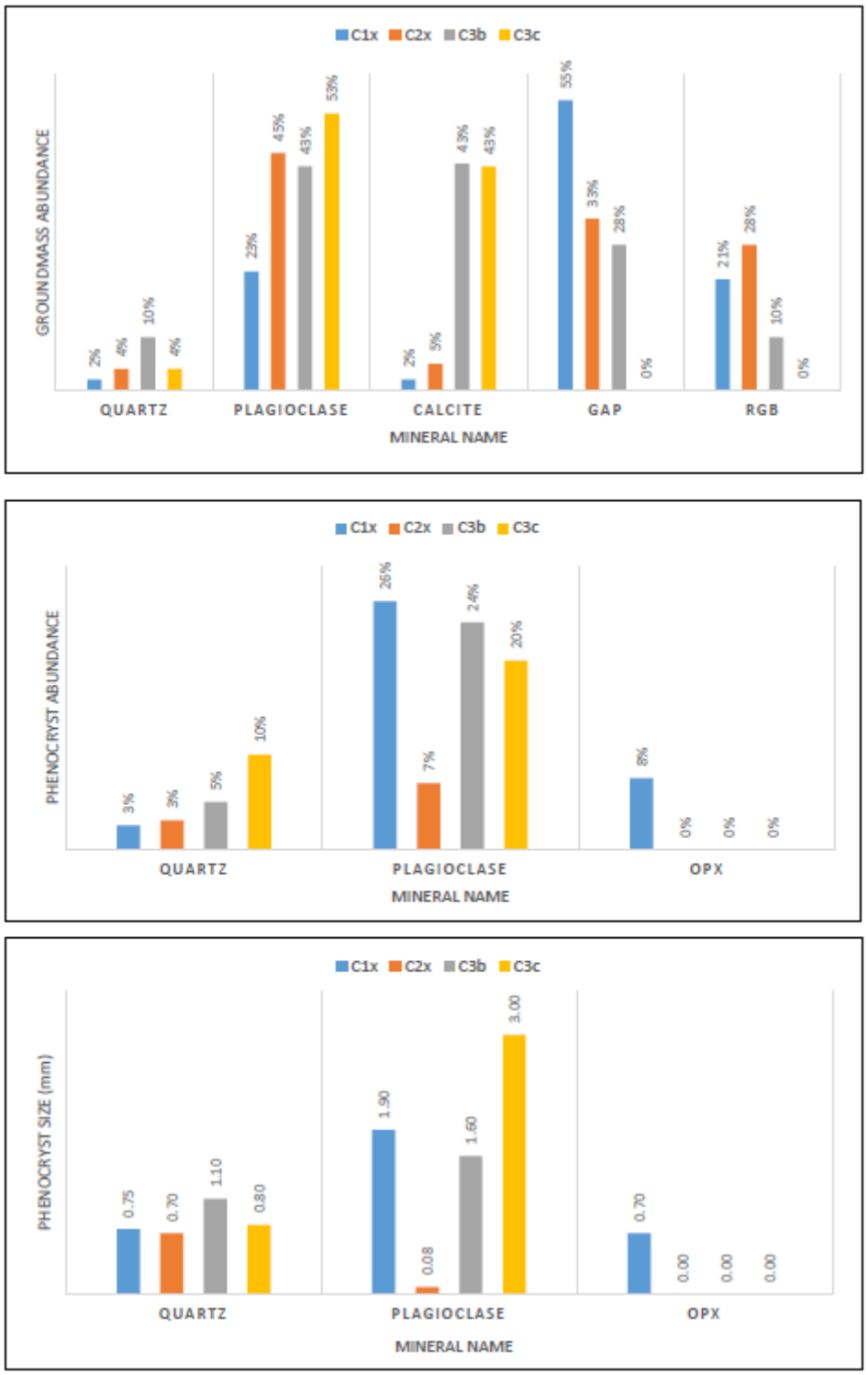

Figure 5.5: Figure showing petrography data for the clast components of related breccia facies. Each graph displays groundmass, phenocryst abundance or size data for each of the clasts which is plotted against a mineral name. Facies C1x and C2x refers to the clast component of facies C1 and C2.

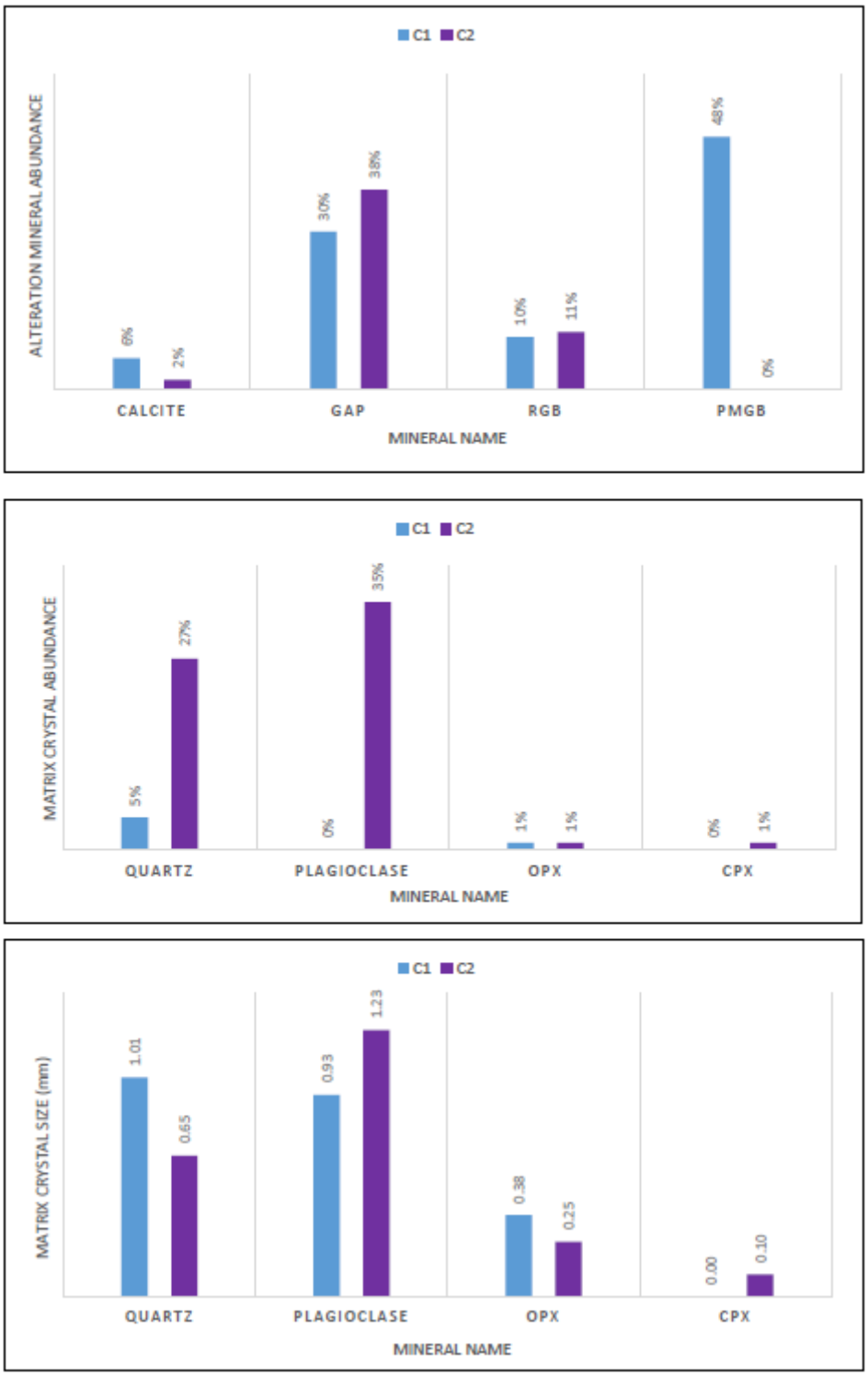

Figure 5.6: Figure showing petrography data for the matrix components of facies identified as being brecciated. The graphs display alteration minerals, matrix crystal abundance or matrix crystal size (mm), which is plotted against a mineral name for the breccia facies C1 and C2.

0.65 mm in size. The amount of plagioclase within the matrix was ≈ 35% and on average 1.23 mm in size. The percentage of Opx in the matrix were 1% and 0.25 mm in size. Clinopyroxenes within the matrix were quite rare at only 1% and 0.1 mm in size. Alteration minerals identified in the matrix were 2% calcite, 38% G.A.P and 11% R.G.B. All three thin sections suggested the matrix of facies C2 was moderately altered. Clasts for facies C2 were identified and investigated using 1 thin section. The thin section was from drill hole 1842 at 111.25 m. Primary volcanic minerals for the clasts of C2 were quartz and plagioclase (5.5). The percentage of quartz phenocrysts were ≈ 3% which were on average 0.7 mm. The amount of plagioclase phenocrysts within the thin section was ≈ 7% and on average 0.08 mm. Alteration minerals identified were 5% calcite, 33% G.A.P and 28% R.G.B. The clasts of C2 appeared moderately altered.

Facies C3b (Grading texture, crackle texture variant)

Facies C3b was identified and investigated using one thin section. The thin section was from drill hole 1216 at 162.2 m. Primary volcanic minerals for facies C3b were quartz and plagioclase (fig 5.5). The percentage of quartz phenocrysts were ≈ 5% which were on average 1.1 mm. The amount of plagioclase phenocrysts within the thin section were ≈ 24% and on average 1.6 mm. The groundmass consisted of 10% quartz, 43% plagioclase, 43% calcite, 28% G.A.P and 10% R.G.B. Both thin sections displayed a groundmass that was translucent and light brown in colour and a grey birefringence with no extinction under XPL. Facies C3b showed a high percentage of groundmass calcite alteration. Facies C3b was altered to very altered.

Facies C3c (Grading texture, patchy boundaries variant)

Facies C3c was identified and investigated using one thin section. The thin section was from drill hole 1216 at 60.2 m. Primary volcanic minerals for facies C1 were quartz and plagioclase (5.5). The percentage of quartz phenocrysts were ≈ 10% which were on average 0.8 mm. The amount of plagioclase phenocrysts within the thin section were ≈ 20% and on average 3 mm. The groundmass consisted of 4% quartz, 53% plagioclase and 43% calcite. C3c was a very altered thin section. Facies C3c showed a high groundmass calcite alteration %. Facies C3c displayed no G.A.P alteration, but rather a groundmass that was translucent light brown and under XPL the birefringence stayed grey with no extinction.

5.3 X-Ray Diffraction [XRD]

Six bulk samples were crushed to fine powder with a tungsten-carbide ring mill and sent away to Auckland University for XRD analyses using a PANalytical Empyrean Alpha-1 X-ray diffractometer with Cuα1 radiation at 45 kV and 40 mA, and scans collected over two theta ranges of 5 - 80 °. Peaks were identified using High Score Plus software. The facies samples for XRD analyses were facies A2, A4, B1, C1, C1x and C2.

5.3.1 Facies A2 (Feldspar rich in dark grey)

A total of seven peaks were generated for analyses for facies A2. The minerals identified by these peaks are limited to only quartz and pyrite. Six out of the seven peaks generated were peaks indicating

quartz. These peaks were at 4.28, 3.36, 3.24, 2.46, 1.82 and 1.54 Å. The other peak was of pyrite at 2.72 Å.

5.3.2 Facies A4 (Dark grey, quartz disseminated)

A total of five peaks were generated during analyses for facies A4. Quartz, orthoclase and pyrite were the minerals identified by these peaks. Two of the peaks were indicating quartz at 4.28 and 3.36 Å. Two peaks indicated orthoclase at 3.80 and 3.24 Å. The last peak was a pyrite peak at 2.71 Å.

5.3.3 Facies B1 (Country rock andesite)

Facies B1 displayed four peaks after analyses. Only quartz and anorthite were the minerals identified by these peaks. Two of these peaks were for quartz at 3.35 and 4.27 Å. The other two peaks indicated anorthite, Na–bearing at 3.21 and 3.19 Å. The rock facies is andesitic not basaltic and more likely reflects fresh plagioclase within the thin section.

5.3.4 Facies C1 (Black breccia)

Four peaks were generated during analyses for facies C1. These peaks were limited to only quartz and orthoclase. Three of these peaks indicated orthoclase at 4.27 (contested with quartz) and 3.24 Å. The other three peaks were quartz peaks at 4.27 (contested with orthoclase), 3.36 and 1.82 Å.

5.3.5 Facies C1x (Black breccia clast)

A total of five peaks were generated during analyses for facies C1x. These peaks indicated quartz, kaolinite and pyrite. Quartz peaks were identified at 4.28 and 3.36 Å. Kaolinite peaks were at 3.57 and 2.56 Å. One pyrite peak was observed at 2.72 Å.

5.3.6 Facies C2 (Partial – complete brecciated coherent rock)

Nine different peaks were identified during analyses for C2. Four peaks out of the nine peaks observed indicated only a single mineral. These single peaks indicated quartz, orthoclase, albite and pyrite and were located at 4.28 Å, 3.30 Å, 3.20 Å and 2.72 Å respectively. Peaks displaying a range of different minerals were observed at the other 5 peaks. At 3.80 Å, a peak indicating orthoclase or albite was observed. The peak at 3.36 Å showed either quartz or albite. The peak at 3.24 Å indicated either orthoclase or albite. At 1.82, there was a peak indicating quartz, orthoclase or albite. A peak at 1.64 Å indicated either pyrite or albite.

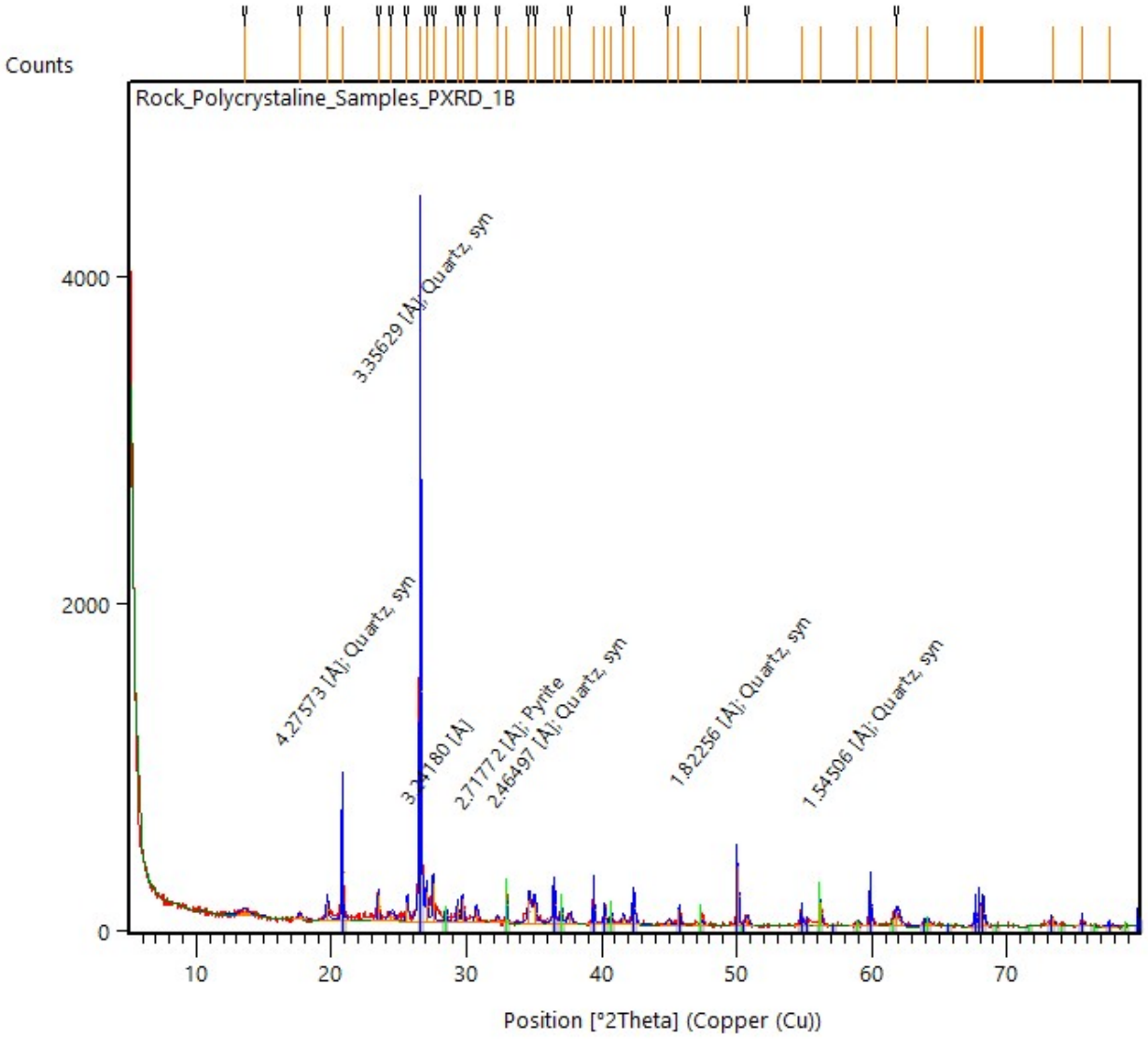

Figure 5.7: XRD peaks for facies A2 indicating quartz and pyrite.

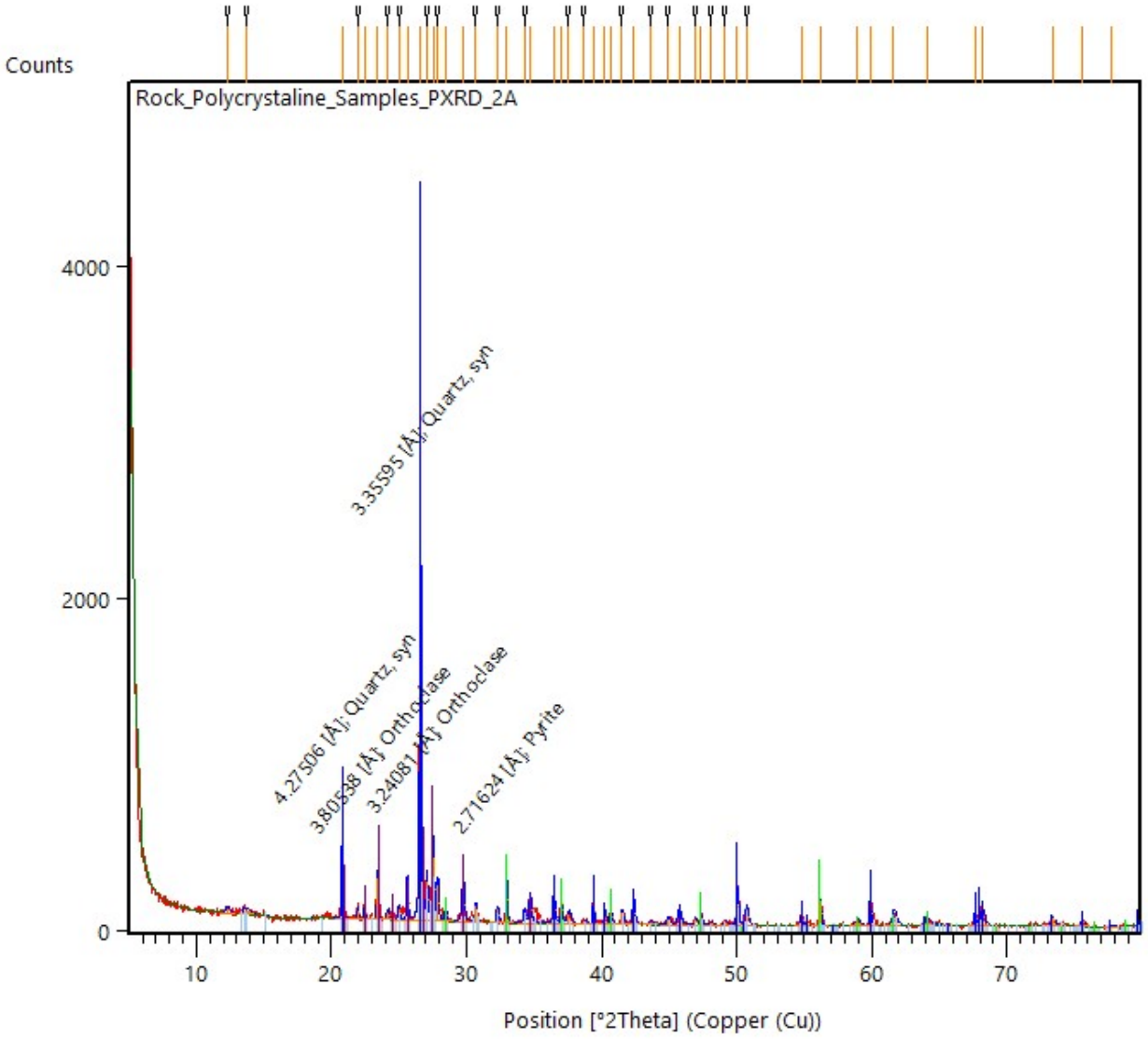

Figure 5.8: XRD peaks for facies A4 indicating quartz, orthoclase and pyrite.

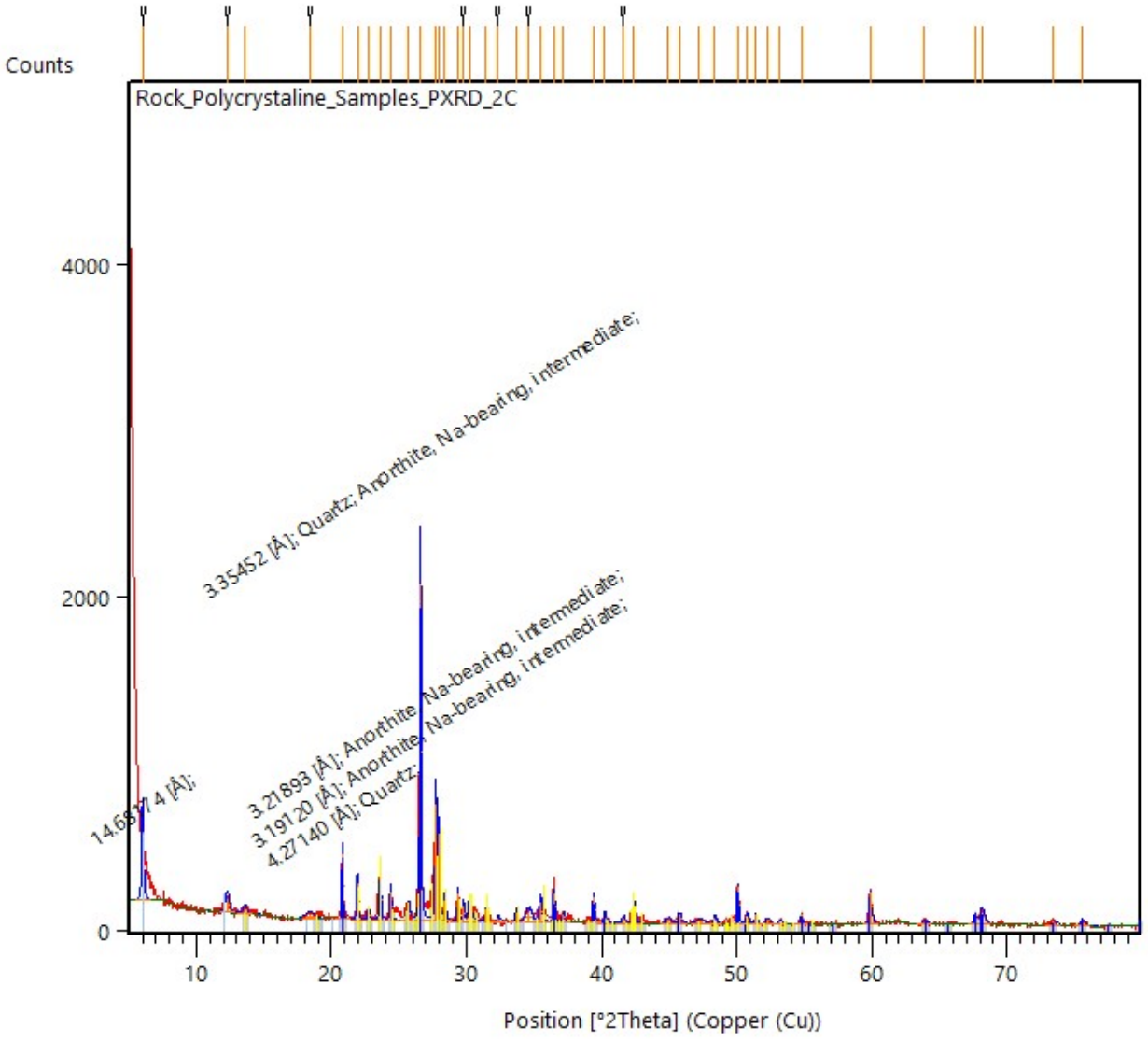

Figure 5.9: XRD peaks for facies B1 indicating quartz and anorthite (plagioclase).

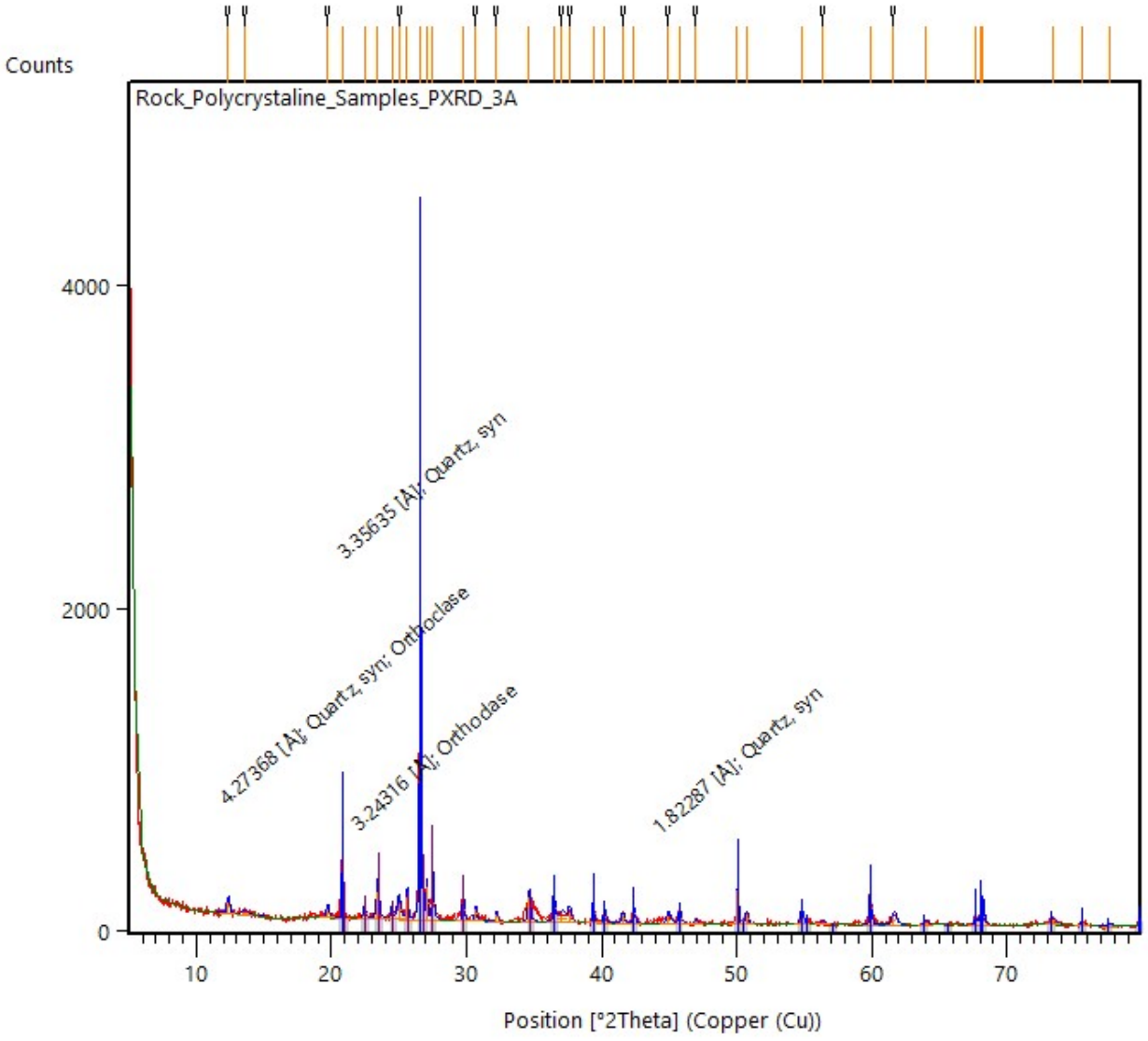

Figure 5.10: XRD peaks for facies C1 indicating quartz and orthoclase.

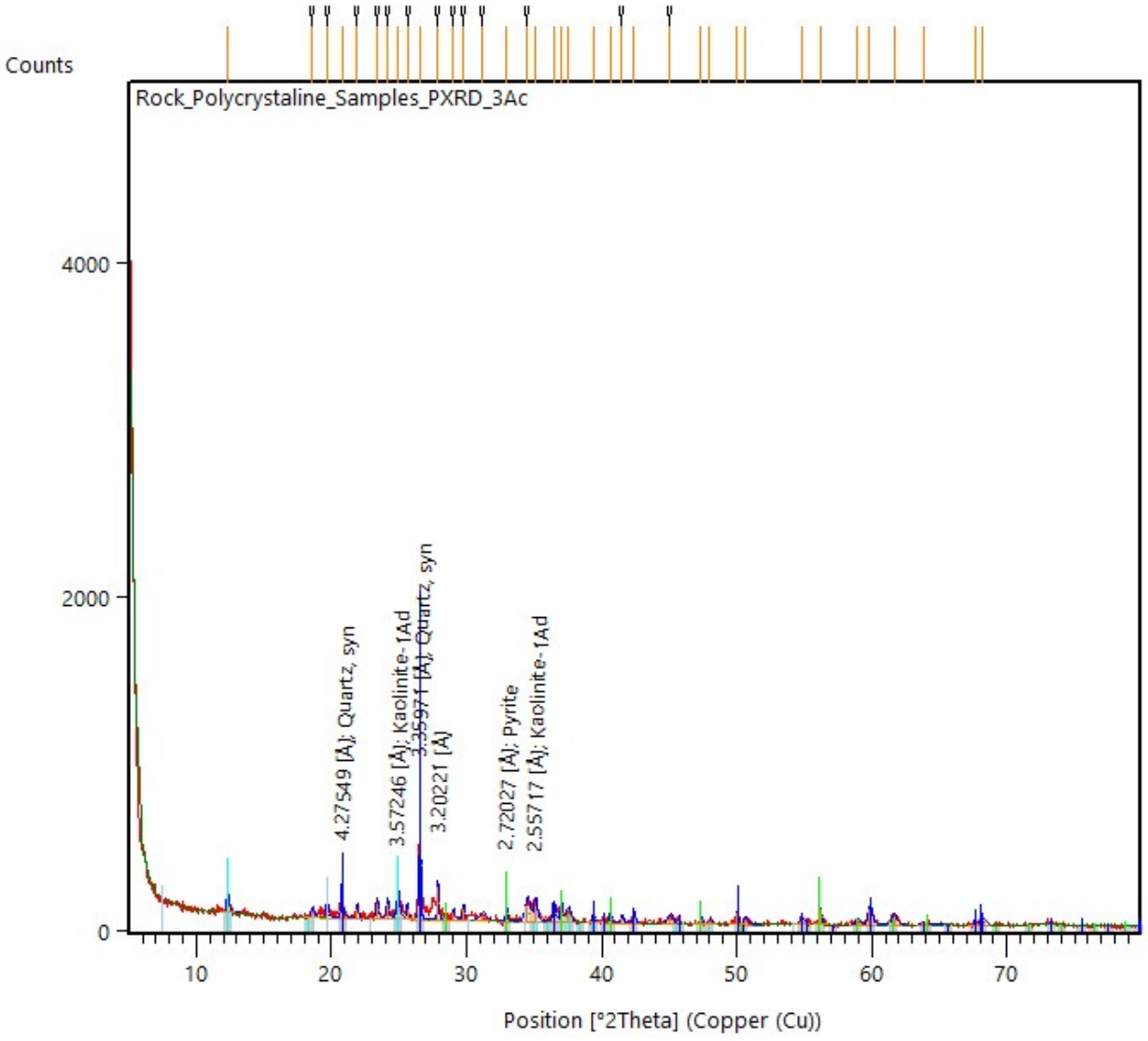

Figure 5.11: XRD peaks for facies C1x indicating quartz, kaolinite and pyrite.

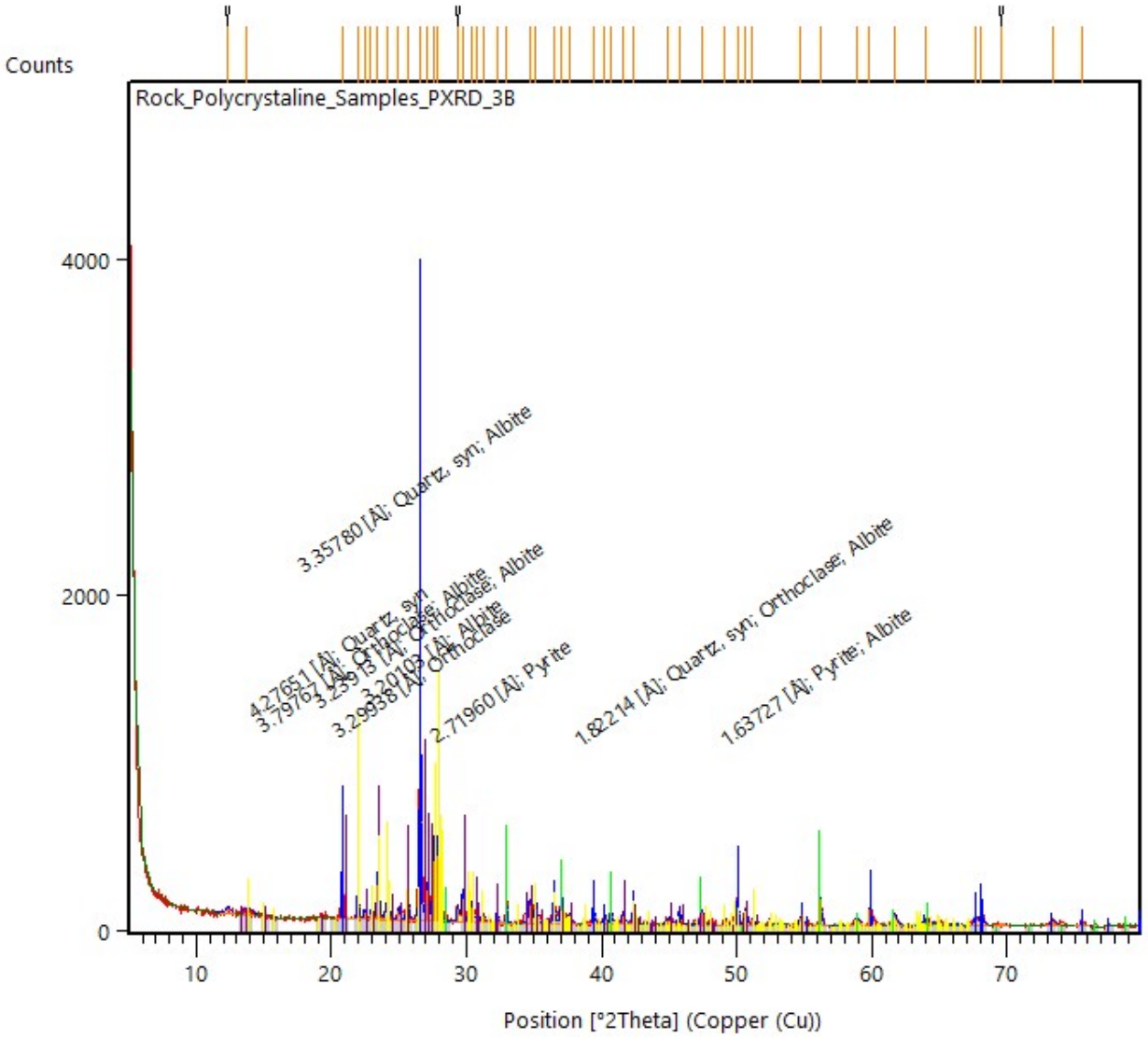

Figure 5.12: XRD peaks for facies C2 indicating quartz, orthoclase, albite and pyrite.

5.4 Portable - X-Ray Flourescence [pXRF] spectrometry

Before XRF was run, samples were tested using a portable X-ray flourescence spectrometer to determine whether samples were safe to be run in the XRF. Fourteen bulk samples were crushed to a fine powder with a tungsten–carbide ring mill. Portable – XRF was used to measure for potential elements that may interfere with the equipment or results. Following a calibration reading, 17 measurements were made on 14 samples. The pXRF instrument was a Delta Olympus Handheld XRF and the powder samples were analysed on "geochem" mode. After samples were analysed using pXRF, samples that resulted in high readings of elements known to cause problems for the XRF instrument (such as copper or sulphur) were not run through XRF. After analysing the XRF data, both facies C1 (black breccia) and C1x (black breccia clasts) were not run on the XRF instrument.

5.5 X-Ray Fluorescence [XRF] spectrometry

1-2 g of samples were weighed out into crucibles and ignited at 1100 °C for 1 hour to calculate the loss on ignition (LOI) by taking the loss in weight as a percentage. Fused beads were made for major oxide element analysis using a flux : sample ratio of 10:1 (8 g flux : 0.8 g sample ± 0.0030). These were fused in the Claisse Neo Fluxer furnace at 1050 °C with 0.1-0.2 g of a releasing agent (NH4I). The flux used was "12:22", lithium tetraborate 35.3% : lithium metaborate 64.7%. Samples were run on the Bruker S8 Tiger at the School of Science, University of Waikato. The resulting totals/sum on 7 out of 9 samples were not great. Ideally, the sum should equal 100% +/- 1, but 7 samples had total sums >101%. Sulphur can have an odd effect on XRF measurements, noticeable by samples (B1 and B2) which contained the least amount of sulphur and subsequently produced the most reliable results. Furthermore, no major relationships between facies for geochemical elements: SiO_2, Al_2O_3, TiO_2, MnO, P_2O_5, SrO and BaO were identified. Regardless, the results of nine facies (and sub-facies) run through the XRF instrument were recorded and graphed on fig. 5.13.

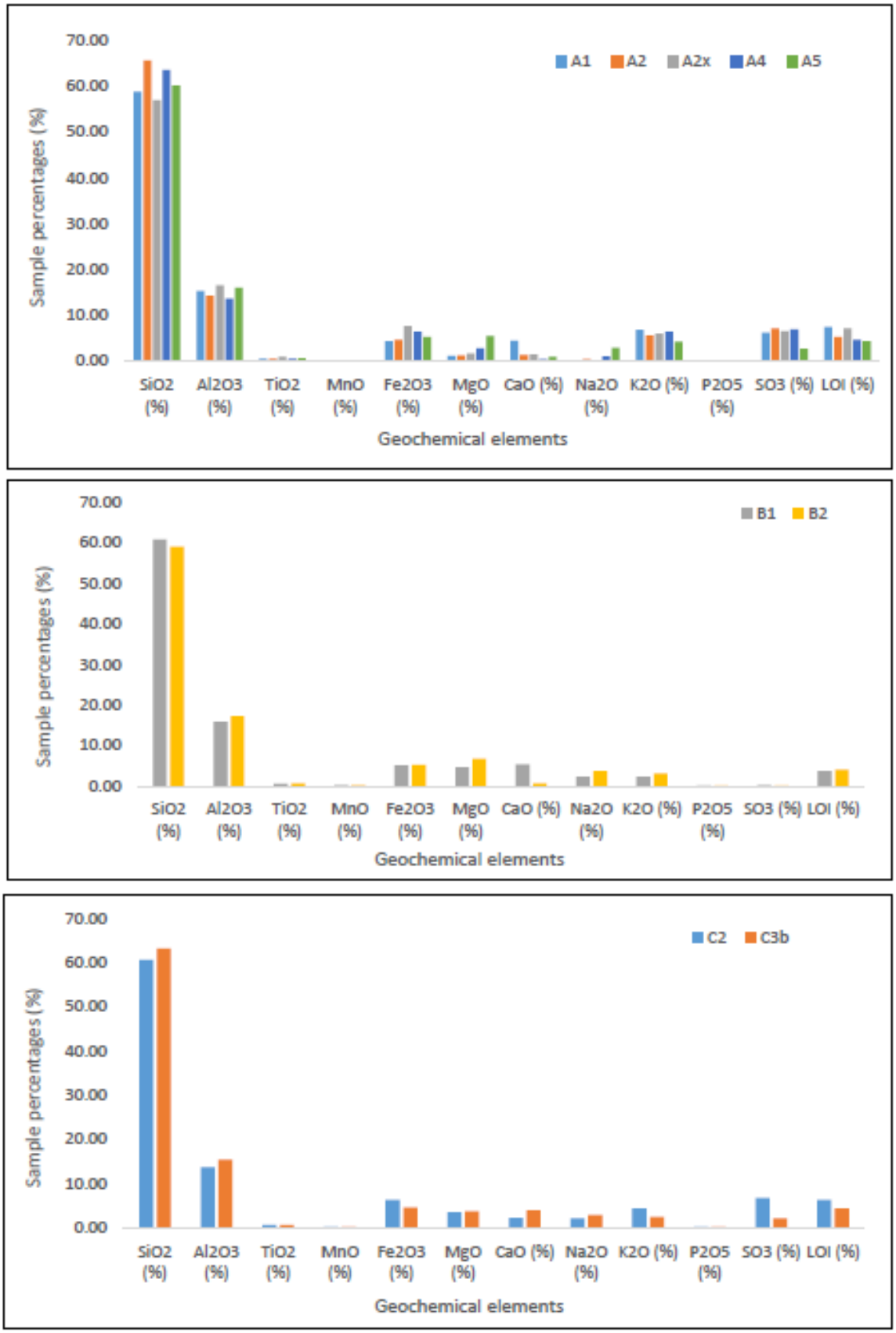

Figure 5.13: Figure showing the XRF data plotted onto three separate graphs. Each graph represents data for either highly altered, weakly altered or brecciated facies.

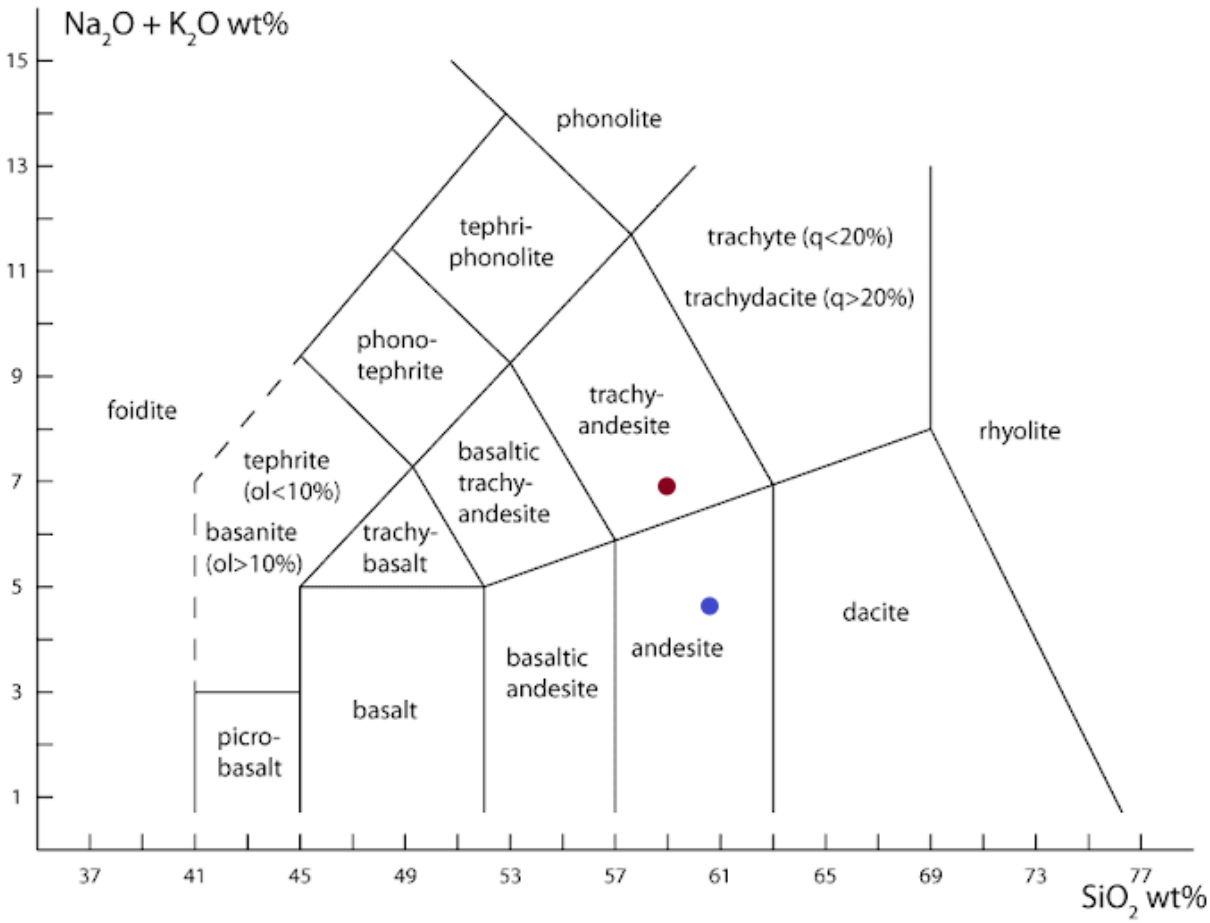

Figure 5.14: Figure showing a total alkali versus silica (TAS) diagram for the weakly altered facies (facies B1 and B2). The blue point within the andesite represents facies B1. The red point within trachy–andesite represents facies B2.

5.5.1 Highly altered facies

XRF data for the highly altered coherent facies encapsulated the results for five different facies. These facies were A1, A2, A2x (Breccia of A2), A4 and A5. The XRF data for all five highly altered facies displayed minor geochemical features for Fe_2O_3, MgO, CaO, Na_2O, SO_3 and LOI. Facies A2x contained the most Fe_2O_3 at 7.63%, closely followed by facies A4 with 6.40 % Fe_2O_3. Facies A1, A2 and A5 all had Fe_2O_3 contents of 4.27, 4.62 and 5.22 %. Facies A5 contained a higher percentage of MgO at 5.45% versus the MgO % of the other four facies which ranged from 1.12 – 2.72%. Facies A1 displayed high amounts of CaO at 4.45%. Facies A2 and A2x displayed much less at 1.28 and 1.37 %, whilst facies A4 and A5 displayed the lowest CaO at 0.41 and 0.89% respectively. Facies A5 also displayed comparatively higher Na_2O at 2.85 % in contrast to facies A1, A2 and A2x which were between 0.08 – 0.39 %. However, facies A4 did display a bit more Na_2O than facies A1, A2 and A2x at 1%. Highly altered facies displayed relatively high SO_3 amounts ranging from 6.14 – 7.15%, except facies A5 which had a SO_3 content of 2.67%. In contrast to the weakly altered coherent and breccia facies, the highly altered facies showed on average higher K_2O % ranging from 4.21 – 6.85%. Additionally, the LOI and SO_3 for facies A1, A2, A2x, A4 and A5 tended to be higher than the observed weakly altered coherent and breccia facies.

5.5.2 Weakly altered facies

XRF data for the weakly altered coherent facies encapsulated the results of two different facies. These facies were facies B1 and B2 and displayed very similar values for Fe_2O_3 SO_3 and LOI. The XRF data for weakly altered facies displayed geochemical differences for MgO, CaO, Na_2O. Facies B2 contained a higher percentage of MgO at 6.78% versus the MgO % of B1 which was 4.68%. These MgO values were considered relatively high compared to the other measured facies (excluding facies A5). Facies B2 displayed the lowest amounts of CaO out of the weakly altered facies and all other facies at 0.66% whilst facies B1 had the highest CaO percentage out of all other facies at 5.32 %. Facies B2 displayed comparatively higher Na_2O at 3.64 % in contrast to facies B1 at 2.23 %. Further differences between weakly altered facies and other facies include K_2O, SO_3 and LOI %. Both B1 and B2 displayed K_2O percentages that were lowest among all measured facies at 2.31 and 3.12% respectively. Additionally, B1 and B2 facies held very rare – almost negligible amounts of SO_3 percentages at 0.23 and 0.15% and a low LOI% of 3.68 and 4.04 % respectively. Through addition of Na_2O and K_2O wt% plotted against SiO_2, these facies were able to be plotted on a TAS diagram shown in fig. 5.14.

5.5.3 Breccia related facies

XRF data for the breccia facies was for two different breccia facies (C2 and C3b), which only displayed similar values for MgO. The rest of the XRF data for these breccia facies displayed geochemical differences for Fe_2O_3. CaO, Na_2O, K_2O, SO_3 and LOI. Facies C2 contained a higher percentage of Fe_2O_3 at 6.22% versus C3b which was 4.48 %. Facies C2 displayed the lower amount of CaO out of the breccia facies at 2.17% whilst facies C3b had the highest CaO percentage out of all other facies at 3.87 %. Facies C2 had a lower Na_2O at 1.99 % in contrast to facies C3b at 2.76 %. Facies C2 had a higher K_2O percentage at 4.30 % versus C3b which was 2.36 %. The SO_3 of C2 was higher at 6.64 % whilst C3b only consisted of 2.07 %. LOI values were slightly different between the two facies, with C2 being higher at 6.24 % versus C3b at 4.24 %. Further differences between the breccia facies and other facies were not identified.

5.6 Scanning Electron Microscopy [SEM]

SEM focussed on the black breccia facies (facies C1). First, polished thin sections were mounted on to a steel block mount, built to hold thin sections within the SEM. Colloidal graphite was applied to the 4 corners of the thin section for conductivity. The mounted thin section was then placed inside a 70 °C oven for 1 minute, to dry the carbon paint. The mounted thin section was then placed inside the Quarum Q 150V ES plus, ion spotter coater - to spot the surface of the thin section with platinum. Samples were then placed inside the Regulus 8230 SEM, and analysed using Aztex A-Z technology for nanoanalysis OXFORD instruments. Both backscattered and secondary electron images were taken to examine the variety of microtextures of the black breccia matrix. Back scattered electron images were taken using an improved back scattered electron detector of the YAG type [YAGBSE]. Images that were taken at high magnifications, e.g. x90,000, are written as x90.0k. Energy dispersive X-ray spectroscopy [EDS] was used for elemental analysis both as spots on individual minerals and geochemical maps across fields of view. The results for these analyses were automatically generated in a report format within Microsoft Word. Thin sections (TZ 11 and TX 8) that were run under the

instrument were sections pertaining to the black breccia bearing facies – C1. Images and subsequent reports generated were taken at three different locations across the two separate thin sections. The same site was used for taking images at 20.0kV 14.7 mm x6.0k and x90.0k on thin section TZ 11. Different sites were used for taking images at 20.0kV 14.7 mm x250, and x80.0k on thin sections TX 8 and TZ 11 respectively. These results are discussed further below.

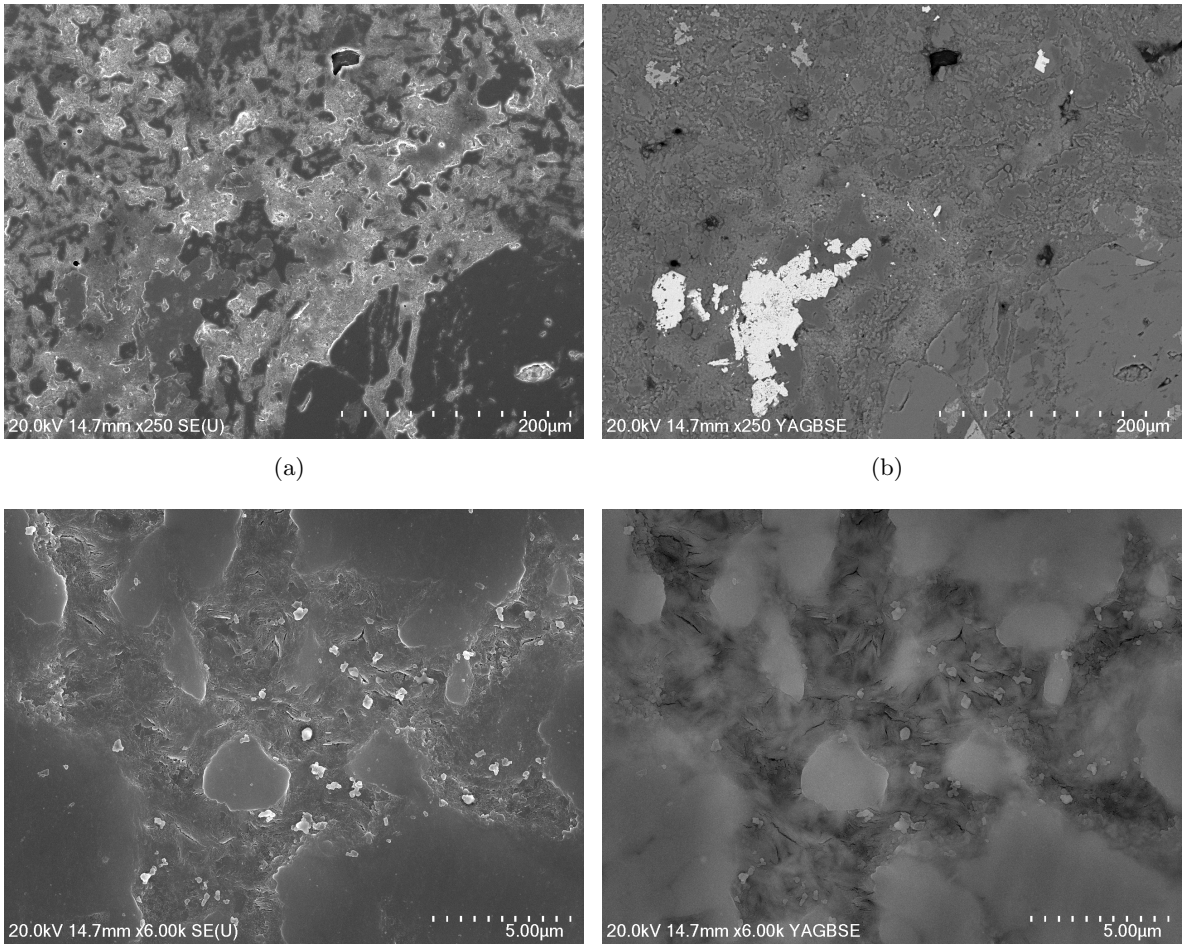

Figure 5.15: Figure showing both secondary electron [SE] and back–scattered electron using the YAG detector type [YAGBSE] images for site 1 and site 2. The four images displayed are; (a) a SE image of site 1 at x250 magnification, (b) YAGBSE image of site 1 at 250 magnification, (c) SE image of site 2 at x6.0k magnification and (d) YAGBSE image of site 2 at x6.0k magnification.

5.6.1 SEM Texture descriptions

The SEM texture descriptions are provided for fig 5.15. In the low magnification images (fig 5.15(a) and 5.15(b)) there appears to be two intergrown components: (i) fine discrete crystal grains (light grey shade) surrounded by a (ii) near-amorphous material (darker grey shade). The two components are almost at a 50:50 proportion. In the higher magnification images (fig 5.15(c) and 5.15(d)) the size of the larger discrete grains become more apparent. Additionally, the interstitial amorphous material appears to comprise of very small (submicron) platy/prismatic mineral grains.

5.6.2 Element mapping

Element mapping was carried out on two sites (site 1 and site 2). The main elements discovered during element mapping were oxygen [O], sodium [Na], magnesium [Mg], aluminium [Al], silicon [Si], sulphur [S], potassium [K], calcium [Ca], titanium [Ti] and iron [Fe].

Site 1 – Lowest magnification [x250]

Oxygen was abundant throughout the mapped area, except for a section which instead was occupied by sulphur and iron. There is an observable relationship between Na and K which occupied mutual spaces. Likewise, Fe and Mg displayed a similar relationship. In areas where Na and K were observed quite strongly, Fe and Mg was rare. Furthermore, this held true for Si and Al, whereby areas rich in Si and Al contained rare/trace amounts of Mg and Fe. Ca occupied only small, pocket areas that did not contain any other elements. Similarly, Ti also occupied very small areas that were barren of other elements (fig 5.16 and 5.17).

site 2 – Moderate magnification [x6.0k]

Like site 1, oxygen was abundant throughout the mapped area. Again, a relationship between Fe – Mg was observed. Fe – Mg occupied mutual space in areas where Si and K were not as strongly present. Within this section, K appeared more abundant in areas that did not contain Si. Furthermore, a slight decrease in the presence of O was observed where the presence of K increased. The area where K appeared more abundant was within the finer matrix material between larger clasts / minerals. The appearance of Al at this site was relatively abundant, except for spaces occupied by Si. Al was strongest in areas containing K and was moderately present in areas of Mg and Fe (fig 5.18 and 5.19).

5.6.3 Spot analyses

Spot analyses was done on one site (site 3) at magnifications greater than the element mapping. The spot analysis was labelled as spectrum 17 for site 3 (fig 5.21). Primary peaks for elements measured were O, Si and Al at 52.6, 21.6 and 19.8 % respectively. Minor Fe, Mg and K were also observed respectively at 1.8, 1.8 and 2.1 %.

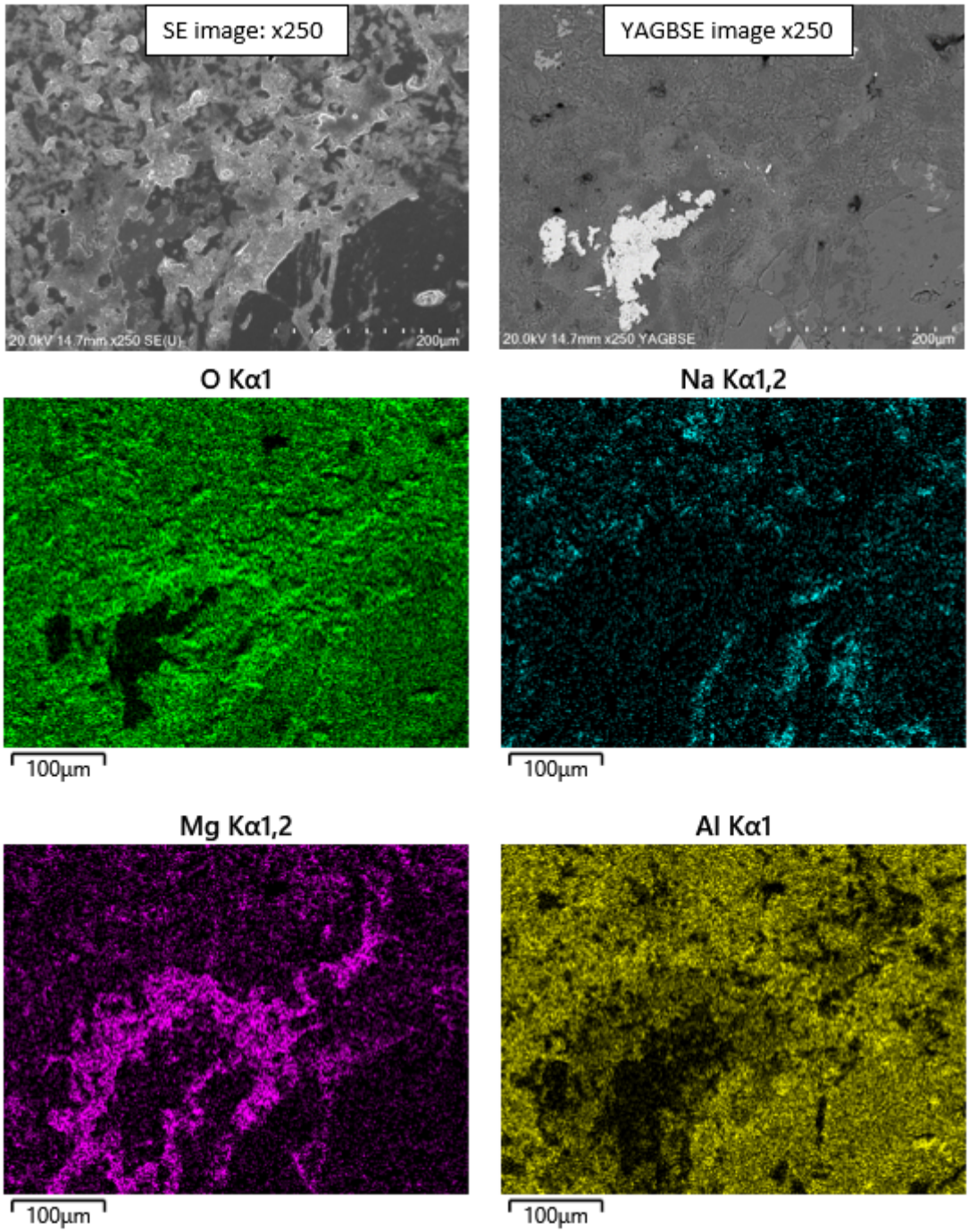

Figure 5.16: Figure showing the generated element map for facies C1 (black breccia) at site 1 using thin section TX3 at x250 magnification. The SE image and YAGBSE for site 1 are located in the top left to top right respectively. Under these two images are the mapped elements: oxygen, sodium, magnesium and aluminium. (Image 1/2).

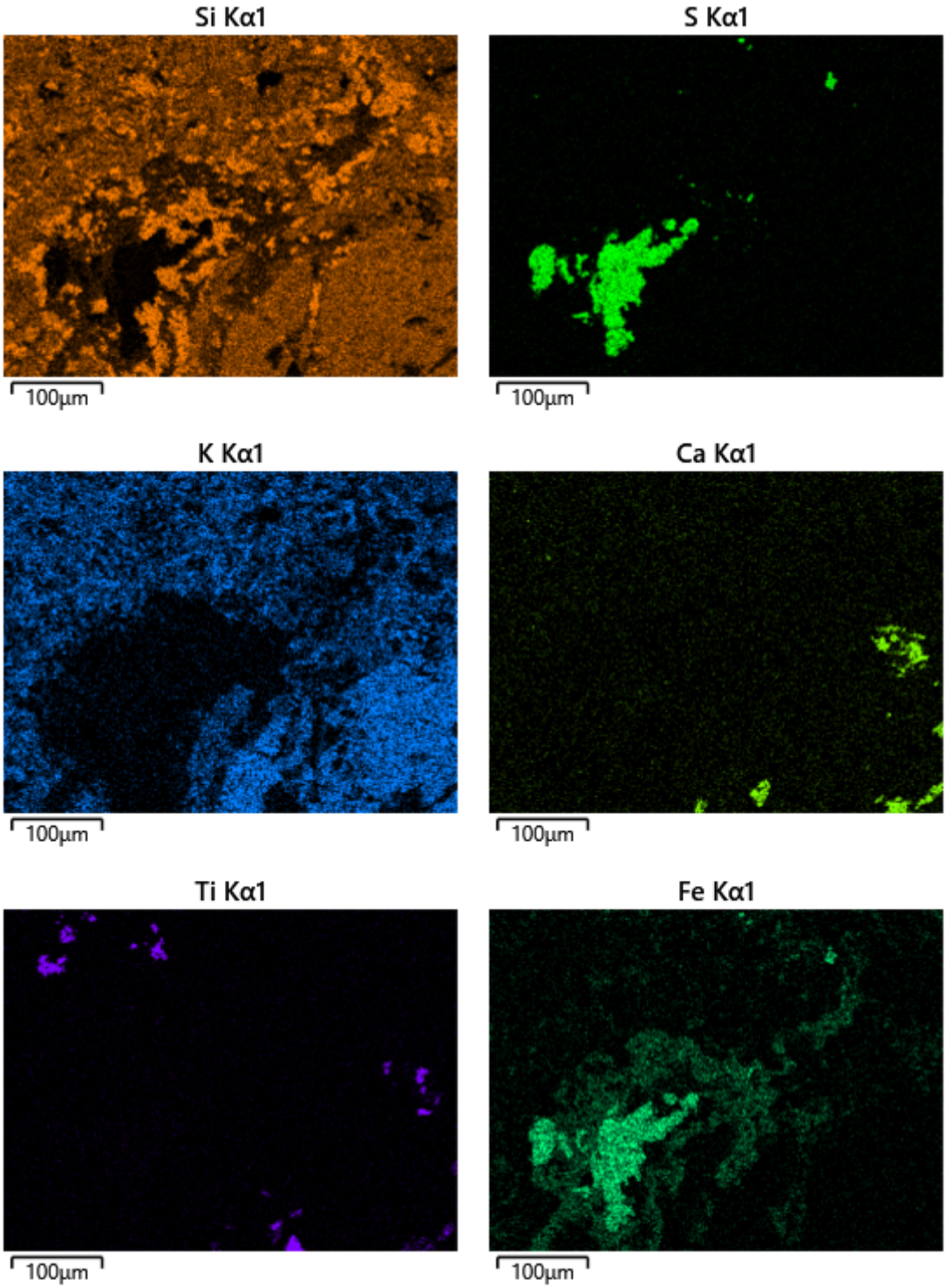

Figure 5.17: Figure showing the generated element map for facies C1 (black breccia) at site 1 using thin section TX3 at x250 magnification. Mapped elements from left to right are: silica, sulphur potassium, calcium, titanium and iron. (Image 2/2)

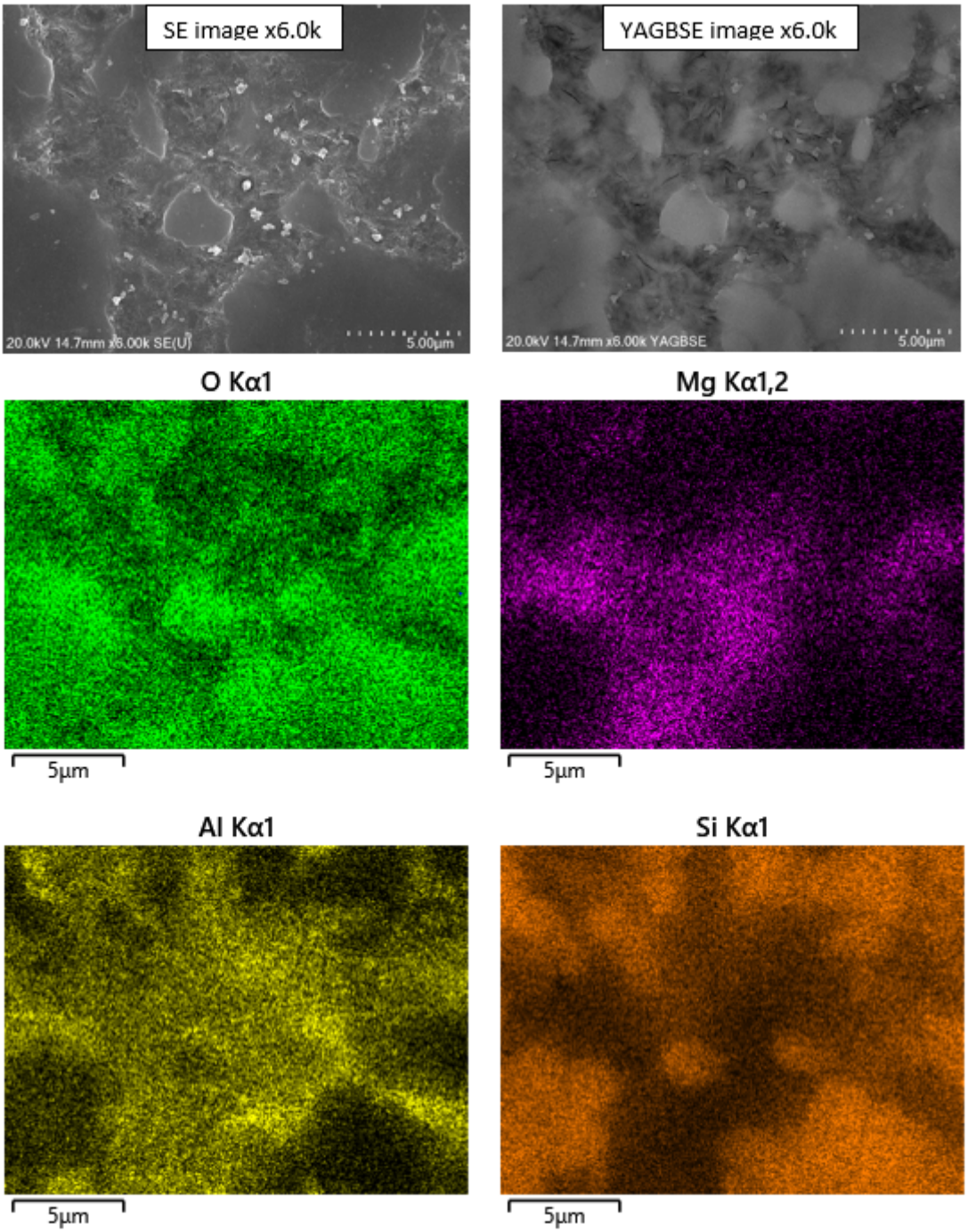

Figure 5.18: Figure showing the generated element map for facies C1 (black breccia) at site 2 using thin section TZ 11 at x6.0k magnification. The SE image and YAGBSE for site 2 are located in the top left to top right respectively. Under these two images are the mapped elements: oxygen, magnesium aluminium and silica. (Image 1/2).

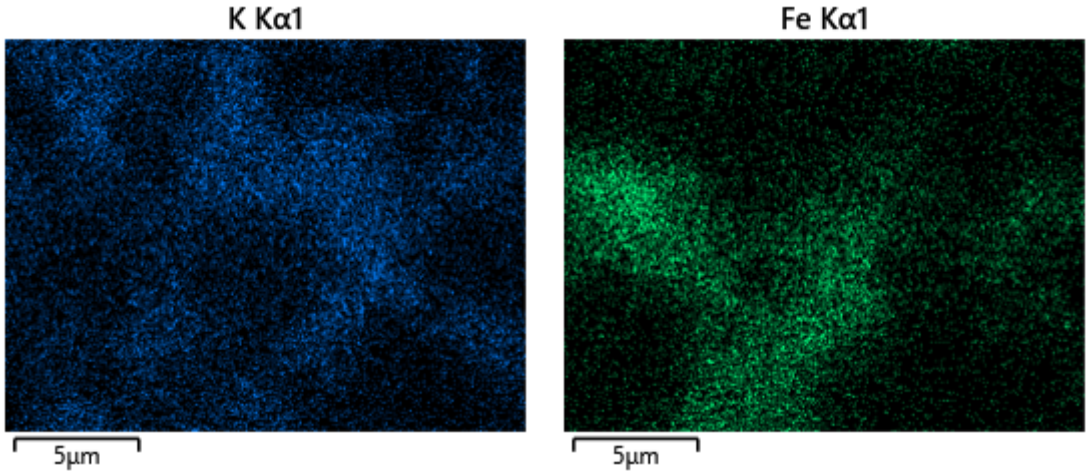

Figure 5.19: Figure showing the generated element map for facies C1 (black breccia) at site 2 using thin section TZ 11 at x6.0k magnification. Mapped elements from left to right are: potassium and iron. (Image 2/2)

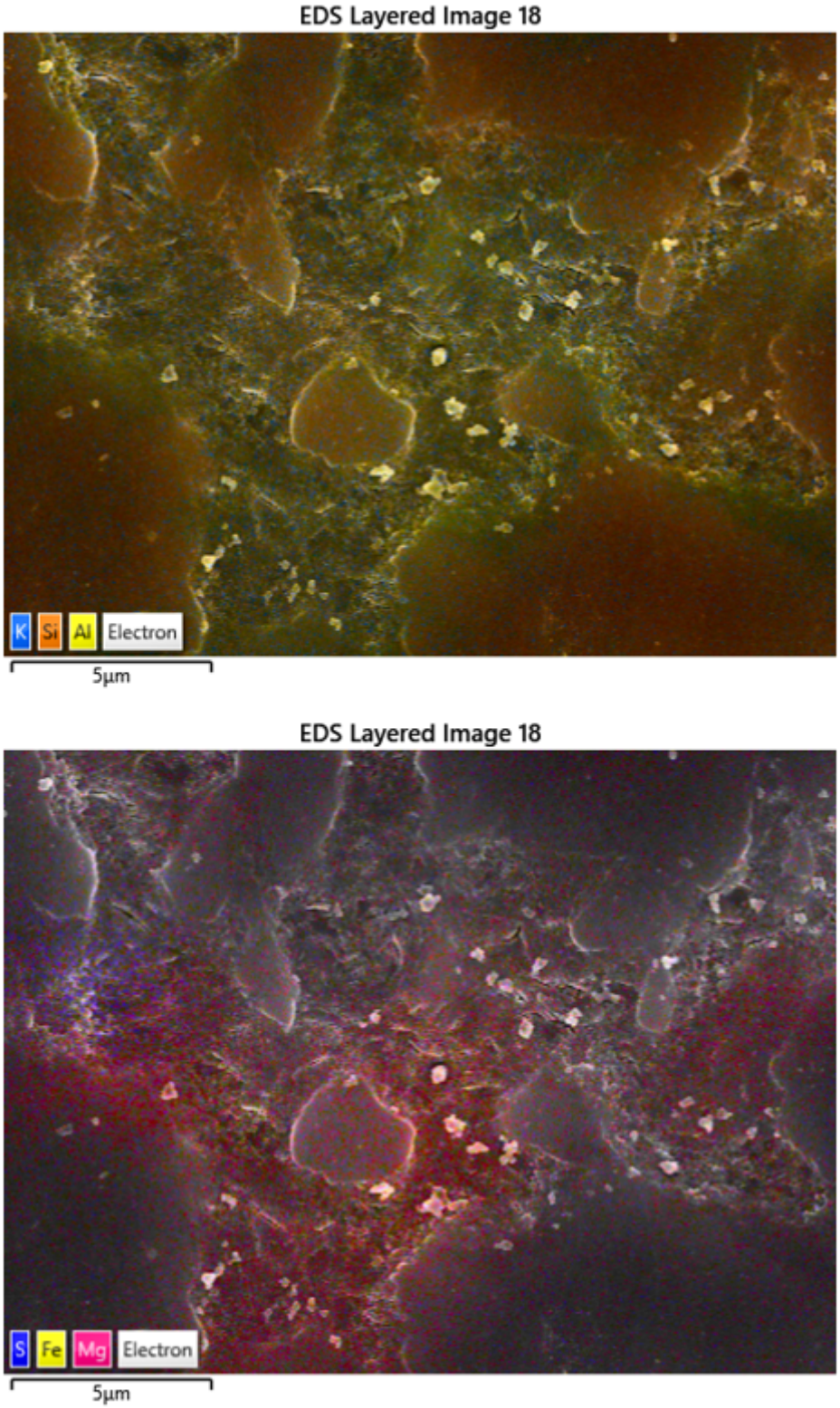

Figure 5.20: Figure showing two EDS layered images generated for facies C1 (black breccia) at site 2 using thin section TZ 11 at 6.0k magnification. The upper image shows potassium, silica and aluminium. The lower image shows sulphur, iron and magnesium occurring in mutual areas.

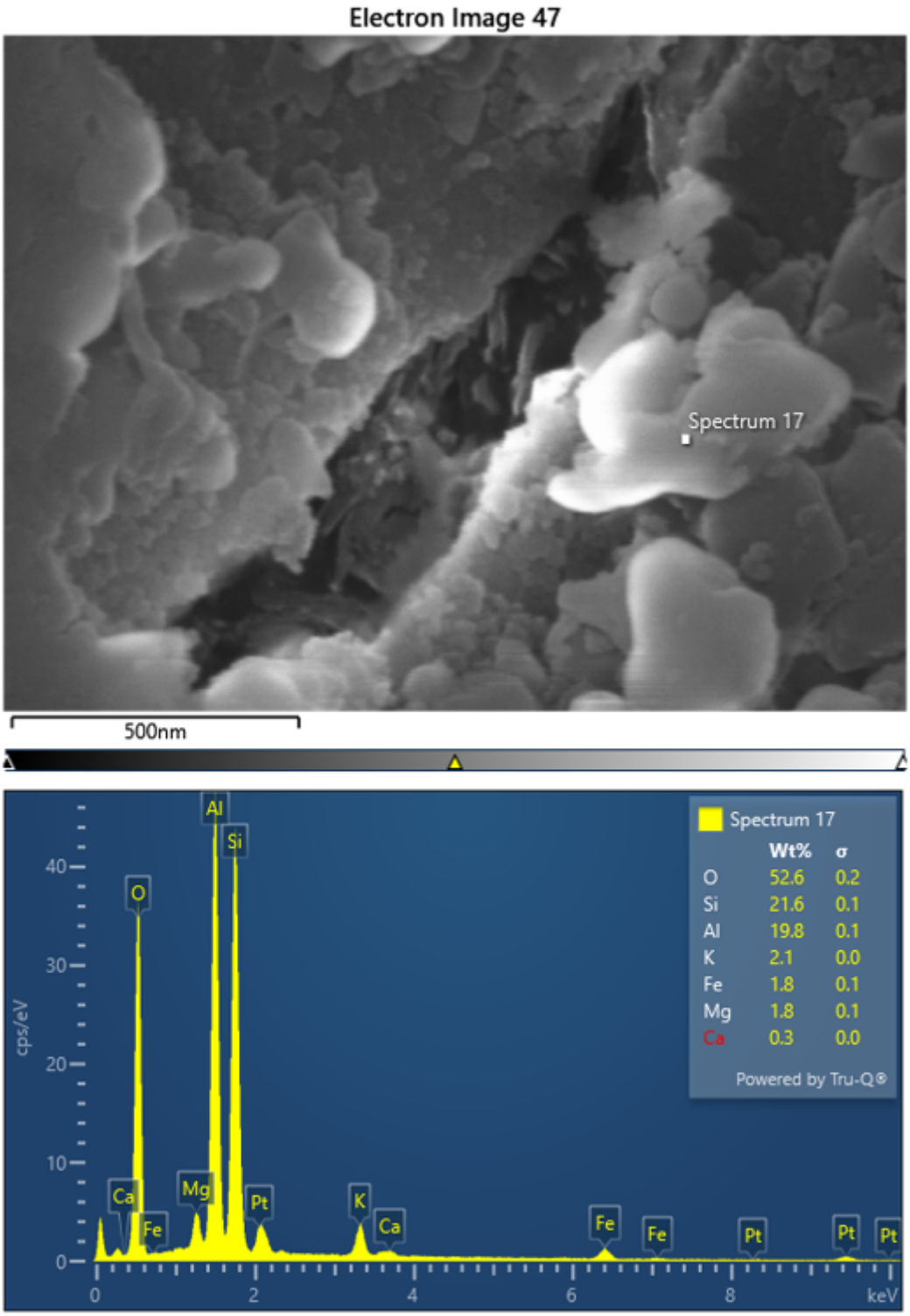

Figure 5.21: Figure showing facies C1 (black breccia) spot analyses for spectrum 17 at site 3 using thin section TZ 11 at 80.0k magnification.

Chapter 6

Discussion

Results from Chapters 4 and 5 for the weakly altered, highly altered and breccia facies will be discussed here. First, a reflection on the implications for alteration based on core logging, petrographical and geochemical data will be discussed. Following this will be the respective sections pertaining to the origins of the weakly altered, highly altered and breccia related facies. Finally, the characteristics of the black breccia described ion Chapters 4 and 5 are discussed and similarities between breccias found in other literature are made. Different theories for the origin of the black breccia and its significance within the hydrothermal environment are discussed.

6.1 Facies perspective of volcanism

Traditionally, the application of facies for studying geology has been utilised by sedimentologists. However, such an approach can be used for separating and detailing the differences in geology occurring within core log to provide a useful perspective on the nature and style of volcanism as well as the nature of hydrothermal alteration. The generation of facies is simply the sum total of features that reflect the specific environmental conditions under which a given rock was formed or deposited. Further development of this definition is through facies association, which represents a group of 'facies' used to define a particular geological environment (Gibbard, 1991). When applying a facies model to my research, an attempt to subdivide different sections within core logs was made based on hard or gradational contacts where features within the observed rock tended to change subtly or excessively over a few metres. The study of this research was focussed on the black breccia, however, an attempt to generate and discuss neighbouring facies proved useful for understanding the origin and significance of black breccia in the epithermal environment. The generated facies were separated into weakly altered, highly altered and breccia related facies.

6.2 Petrographical and geochemical indicators of alteration

As discussed in Chapter 2, where alteration is observed, there are observable mineralogical, chemical and textural changes within host rocks the cause a change in primary volcanic minerals altering in to other secondary minerals. These observable changes in the country rock andesite are brought on by fluid interactions between the paleo–hydrothermal fluid and the host rock. Typically, alteration zones are discussed in literature through the presence or absence of clay minerals. However, XRD analysis on clay separates was unavailable during the course of this study, hence these zones of alteration could not be identified with respect to the facies defined here. Instead, the elements and minerals listed below identified during analyses in Chapters 4 and 5, were used as hydrothermal alteration indicators for how the paleo–hydrothermal fluid impacted the original andesite host rock.

6.2.1 Feldspar

Feldspars that were present during my research were plagioclase and potassium feldspars. The plagioclase feldspars series spans from albite ($NaAlSi_3O_8$) to anorthite ($CaAl_2Si_2O_8$) and were most indicative of weakly altered facies. Anorthite is a mineral associated with mafic to ultramafic volcanics. Anorthite that was identified during XRD analyses simply reflected the presence of plagioclase and not the plagioclase feldspar end member. Alkali feldspars include minerals such as orthoclase, sanidine, microcline and anorthoclase. Within the Tauhara geothermal field of New Zealand, plagioclase was commonly observed to be altering to calcite, chlorite, as well as adularia (Mielke et al., 2015). As the site for this study was situated in an andesitic environment, X-ray diffraction peaks that were recognised as orthoclase by the Highscore software (typically associated with granites) most likely reflected K–feldspar forming as a secondary mineral from the hydrothermal alteration (e.g. adularia). X-ray fluorescence was a great tool for observing alteration intensity and overall supporting the separation of facies through the presence of K_2O. A higher percentage of K_2O typically reflected the formation of such secondary K-feldspar minerals and was indicative of more highly altered facies.

6.2.2 Carbonates

Rabone (1975) found that plagioclase altering in moderate to strongly altered zones were partly ($<$ 50%) replaced by cabonates, clay minerals, minor sericite and rare epidote. Additionally, in areas where carbonate activity was low and plagioclase was at least as sodic as An_{50}, rare rims or crack fillings of albitic plagioclase formed. Carbonate minerals in the middle stages of both phenocryst pseudomorphs may inherit the fibrous or vermiform texture of replacement calcite (Rabone, 1975). The alteration mineral described as radial golden brown [R.G.B] was always found as subtle disseminations among the groundmass or matrix. This alteration mineral may indicate either a percentage of chlorite or carbonate minerals that were in the middle stages of plagioclase and carbonate pseudomorphing. The most easily identifiable (and most abundant) carbonate mineral observed during microscopy was calcite.

Calcite

Calcite is a common carbonate alteration mineral present at varying temperatures and stable in zones representing: smectite–kaolinite, mixed layer illite–smectite, propylitic and propylitic–potassic zones. Whilst the presence of calcite does not reflect the zone of alteration very well, the abundance of calcite observed in thin sections was a great indicator for alteration under the microscope. During thin section microscopy, when considering a descriptive name for the degree of facies alteration, the percentage of calcite pseudomorphs and remaining plagioclase phenocrysts was taken in to account. Calcite, that may have been tied in with XRF data for CaO % was not the greatest indicator for alteration. Facies B1 consisted of a relatively high CaO % whilst it was considered a weakly altered facies. Likewise, facies A1 also had a high % of CaO, was highly altered and riddled with calcite pseudomorphs in thin section and core logging. It's likely both of these CaO % originated from separate sources. Given the appearance of facies A1 in core logging and the observed calcite pseudomorphs in thin section, the high percentage of CaO from facies A1 was likely the result of secondary alteration from orthopyroxen [Opx] and plagioclase in to calcite. Although XRF data for facies B1 displayed an even greater CaO

reading, an abundance of calcite was not observed in core logging, thin section or XRD data. The CaO % for facies B1 is likely tied to other minerals that are a part of the original volcanics. XRF data for CaO for other facies was trivial and did not show an increasing trend or any noticeable relationship for facies labelled as highly altered versus facies that were weakly altered.

6.2.3 Pyroxenes

The abundance of orthopyroxenes ((Mg, Fe^{2+}+)Si_2O_6) identified during thin section analyses was most prevalent in thin sections representing the weakly altered facies and facies A5 from the highly altered facies. This presence of orthopyroxenes is further supported by XRF data for both the weakly altered facies and facies A5 as the Fe_2O_3 + MgO percentage are reasonably balanced and abundant. Rabone (1975) found that orthopyroxene and clinopyroxenes are susceptible to alteration. The presence of these minerals in greater abundances, reflects units that are not as strongly altered. Typically, orthopyroxenes are seen altering to chlorite. Clinopyroxenes [CPX] in moderately to strongly altered facies are almost completely replaced by carbonates (Rabone, 1975). Facies that displayed higher levels of alteration had a lower percentage of observable Opx in thin sections and a low MgO % relative to a high % of Fe_2O_3.

6.2.4 Sulphur

The accumulation of sulphur is another great indicator for the presence of alteration. Sulphur, amongst other volatiles and metals, is circulated through the original country rock andesite by a paleo-hydrothermal fluid that has interacted with a sub–surface magmatic source. Therefore, the original andesite host rock is expected to have negligible amounts of sulphur. The sulphides present within thin section samples were mostly in the form of pyrite ± chalcopyrite and sphalerite. X-ray diffraction peaks revealing pyrite supported the presence of sulphur within facies. An observable trend within XRF data was that facies that contained relatively higher percentages of SO_3 tended to be those labelled as highly altered. Facies labelled as weakly altered had negligible SO_3 percentages.

6.2.5 Quartz

Quartz phenocrysts are resistant to alteration and therefore not the greatest indicator for alteration. However, quartz phenocrysts can hint at processes within original magma. The presence of quartz embayments and holes imply disequilibrium during quartz formation due to magma mingling. Thin sections for the highly altered facies A1, A2 and A3 all contained quartz phenocrysts with embayments. Hydrothermal quartz can occur in the andesite groundmass, breccia matrix and veins due to hydrothermal alteration and could be caused by release of silica by chloritisation of pyroxenes as well as replacment of chlorite carbonates (Rabone, 1975). Hydrothermal quartz can also form through overprinting events. Calcite that is initially saturated during first boiling may be replaced by silica following boiling propogation and resulting in quartz deposition. Typically, hydrothermal quartz is angular and does not form embayments. No observable trends for alteration intensity between facies were observed in XRF data for SiO_2 %.

6.3 Origin of the weakly altered facies

The weakly altered facies showed the least amount of hydrothermal alteration during core logging, petrography and geoochemical analyses. Geochemical analyses for facies B1 (country rock andesite) and B2 (trachy–andesite) involved XRF for geochemical majors. In contrast to all the other facies, the XRF data for both weakly altered facies (B1 and B2) displayed very low K_2O, LOI and sulphur percentages. This data reveals that alteration in to K – feldspars such as adularia as well as the introduction of sulphur due to the hydrothermal fluid was minimal for these two facies. There were many implications that supported facies B1 closely resembling the original andesite formation. According to Rabone (1975), zones deemed unaltered to weakly altered typically displayed OPX (one of the most susceptible minerals to becoming altered) that may be partially or completely altered into chlorite minerals. Facies B1 representing the country rock andesite displayed abundant OPX, some of which had been partially altered. Furthermore, fresh plagioclase was observed under the microscope, which was only minimally altered to other secondary minerals (e.g. calcite). XRD observed multiple peaks at quartz and anorthite (indicative of fresh plagioclase). After plotting facies B1 on a TAS diagram, (through addition of Na_2O and K_2O plotted against Si_2O), facies B1 was revealed to be andesite consistent with the original andesite lavas of the Waipupu Formation. The origin of facies B2 – trachy–andesite may be slightly more complex. Plagioclase laths were observed under the microscope, which had a preferential alignment forming crude trachytic fabric – indicating movement of magma after at least partial crystallization. Plagioclase within the groundmass was ≈ 50 % altered. However, none of this alteration displayed preferential alteration in to calcite. Furthermore, XRF data revealed facies B2 had the lowest CaO % out of all other facies, further supporting that the presence of a hydrothermal fluid was limited. Facies B2 was only observed once in drill hole 1842 occupyingd a minimal area during core logging (0.35 m) with sharp contacts with the breccia facies C2 – partial to completely brecciated coherent rock. Based on the rarity of this facies within drill core and the sharp boundaries it formed with a brecciated facies, I suspect the origin of facies B2 to be a larger, foreign clast incorporated in to facies C2, which was deposited during the emplacement of breccia facies C2.

6.4 Origin of the highly altered facies

The highly altered facies represents a stronger hydrothermal overprint on the andesite facies B1. Rabone (1975) found that in zones deemed weak to moderately altered, orthopyroxenes were completely altered to chlorite, which then became replaced by carbonates. Furthermore, quartz became abundant within the groundmass due to a release of silica by chloritisation of pyroxenes and from replacement of chlorite by carbonate. Zones deemed moderate to strongly altered consisted of complete replacement of CPX by carbonates whilst plagioclase was partly replaced by carbonates, clay minerals, minor sericite and rare epidote. In the later stages of zones of moderate to strong alteration, secondary quartz can be observed replacing carbonates (Rabone, 1975). Facies that were identified in this study as being highly altered were at least weak to strongly altered in accordance to the findings of Rabone (1975). Some of these indicators of alteration were uncovered during initial core logging (discussed in Chapter 4) and/or petrographical and geochemical data (discussed in Chapter 5). Ultimately, the observable physical characteristics and the presence or absence of minerals and elements were the primary indicators for whether a facies was deemed highly altered. Primary observations for

petrographical analyses for microscopy of the highly altered facies was that facies A1, A2 and A3 were in the later stages of moderate to strong alteration, evident by the apparent low percentage of plagioclase within the groundmass. Facies A4 and A5 contained higher plagioclase percentages within the groundmass than the other highly altered facies and could subsequently be deemed moderately altered in accordance to Rabone (1975). However, microscopy data can be highly subjective as far as average percentages are considered and XRD and XRF data may be more useful for generating quantitative data indicating alteration. An important observation during XRF analyses for the highly altered facies was that Fe_2O_3 was comparitively more abundant than MgO. This is linked to the alteration of orthopyroxenes (Mg + Fe_2O_3) in to other secondary alteration minerals such as pyrite (Fe_2S). XRF identified that there was an observable CaO difference between facies A1 containing over four time more calcium versus other highly altered facies. XRF data for facies A5 (feldspars in a smoke light grey), displayed geochemical data indicative of weak to moderate alteration. Additionally, facies A5 showed K_2O and SO_3 percentages that were noticably lower than other highly altered facies whilst the MgO % was more than double. However, overall the highly altered facies contained higher percentages of SO_3, K_2O and LOI percentages compared to weakly altered facies. The origin of these facies is simply related to hydrothermal activity and affected by a combination of country rock rheology and lithology affecting the migrating fluid pathways such as faults, fault splays and overall permeability of adjacent rock facies.

6.5 Origin of the breccia related facies – excluding black breccia

The final criteria for distinguishing facies was the presence of brecciation. Breccia facies identified are either related to the original volcanic processes and occur as autobreccia around the edges of lava flows or they are the product of hydrothermal brecciation (Jébrak, 1997). Typically when considering both styles of breccia, more fluidal shaped clasts resemble autobreccias of lava whilst angular clasts are more likely related to hydrothermal brecciation. Facies C2 represented the partial – completely brecciated facies with a mosaic texture. It was polymict, whereby, multiple different clasts were incorporated in to the breccia. Clasts sizes were highly variable, ranging from 2 – 80 mm, with some clasts appearing internally brecciated/fractured. One of the measured clasts consisted of mostly plagioclase with minor quartz and an abundance of secondary mineral alteration. Quartz veins were only present as a form of dissemination within the matrix and surrounding clasts. Facies C2 was originally an autobreccia deposited during the emplacement event of the country rock andesite (Waipupu formation). Following hydrothermal activity, this facies become altered, evident by XRD data indicating quartz, orthoclase (adularia), albite and pyrite, which are typical products of hydrothermal alteration. Despite the characteristics for alteration depicted by the XRD data, an identified clast for facies C2 (facies B2 – trachy andesite) still displayed weak alteration and a geochemical composition resembling a trachy–andesite. Facies C3 was a breccia facies only described in drill hole 1216. Facies C3 was further separated into four separate facies (facies C3a, C3b, C3c, C3d) that showed repeating association and gradational contacts with one another over several metres of core log. Facies C3a – patchy large feldspar variant was only described during core logging in Chapter 4. The main separator of C3a from other C3 facies was that it did not form a patchy boundary texture, crackle texture or calcite veining and instead contained quartz disseminations and large feldspar phenocrysts. Facies C3b – crackle texture variant was identified in core logging where C3a had begun to grade into something

else and become brecciated to form a crackle texture. Brecciation appeared to be clast supported and consist of angular, monomict, clasts that had very limited rotation and a low percentage of matrix fill. The clasts for facies C3b were analysed during microscopy to show quartz and plagioclase. The groundmass for these clasts of facies C3b showed predominantly plagioclase, some quartz and a very high percentage of alteration minerals such as calcite, grey amorphous patches (G.A.P) and the radial golden brown mineral (R.G.B). Geochemical analyses revealed this facies contained a comparatively minor percentage of SO_3 to other breccia and highly altered facies. K_2O % was also minimal whilst consisting of moderately higher CaO and Na_2O % than other highly altered and breccia related facies. Facies C3c – patchy boundary variant was observed in core logging and microscope petrography. It formed a gradational boundary with facies C3b and was comprised of circular boundary patches. This facies was observed using microscopy to discover that the primary volcanic minerals were quartz and plagioclase. The groundmass was predominantly plagioclase and calcite with no G.A.P alteration being observed. Instead a translucent light brown colouration was present that went grey with no extinction under XPL. Facies C3d was the thick calcite vein variant and the last variant identified for C3. It was only discussed within core logging in Chapter 4 and separated from other C3 variants by the presence of thick pervasive $\approx 5 - >5$ mm calcite veins that caused some quartz veins to terminate against it. The earliest origin of facies C3 is related to the initial emplacement of andesite lavas which were then subjected to hydrothermal alteration and subsequent hydrothermal brecciation. Jébrak (1997) discusses eight different processes for brecciation in hydrothermal deposits, one of which is fluid assisted pulse brecciation or hydraulic fracturing (fig. 6.1). Hydraulic fluid assisted brecciation is the result of uniform (mainly tensile) stress due to pressure buildup in the hydrothermal environment. Facies C3b reflected hydraulic brecciation evident by its crackle texture and lack of clast rotation observed during core logging. Another important observation was the sheer nature of facies C3d – calcite veining variant identified during core logging. Facies C3d displayed some minor quartz veining, which terminated against thicker calcite veins, perpendicular to the quartz veins. The deposition of this comb quartz vein can be attributed to slower cooling rates of hydrothermal fluids (Corbett & Leach, 1998). The termination of this quartz vein against thick calcite vein signifies the introduction of carbonate rich hydrothermal fluid overprinting earlier alteration and is likely attributed to hydraulic fracturing in the sub–surface permitting fluid flow.

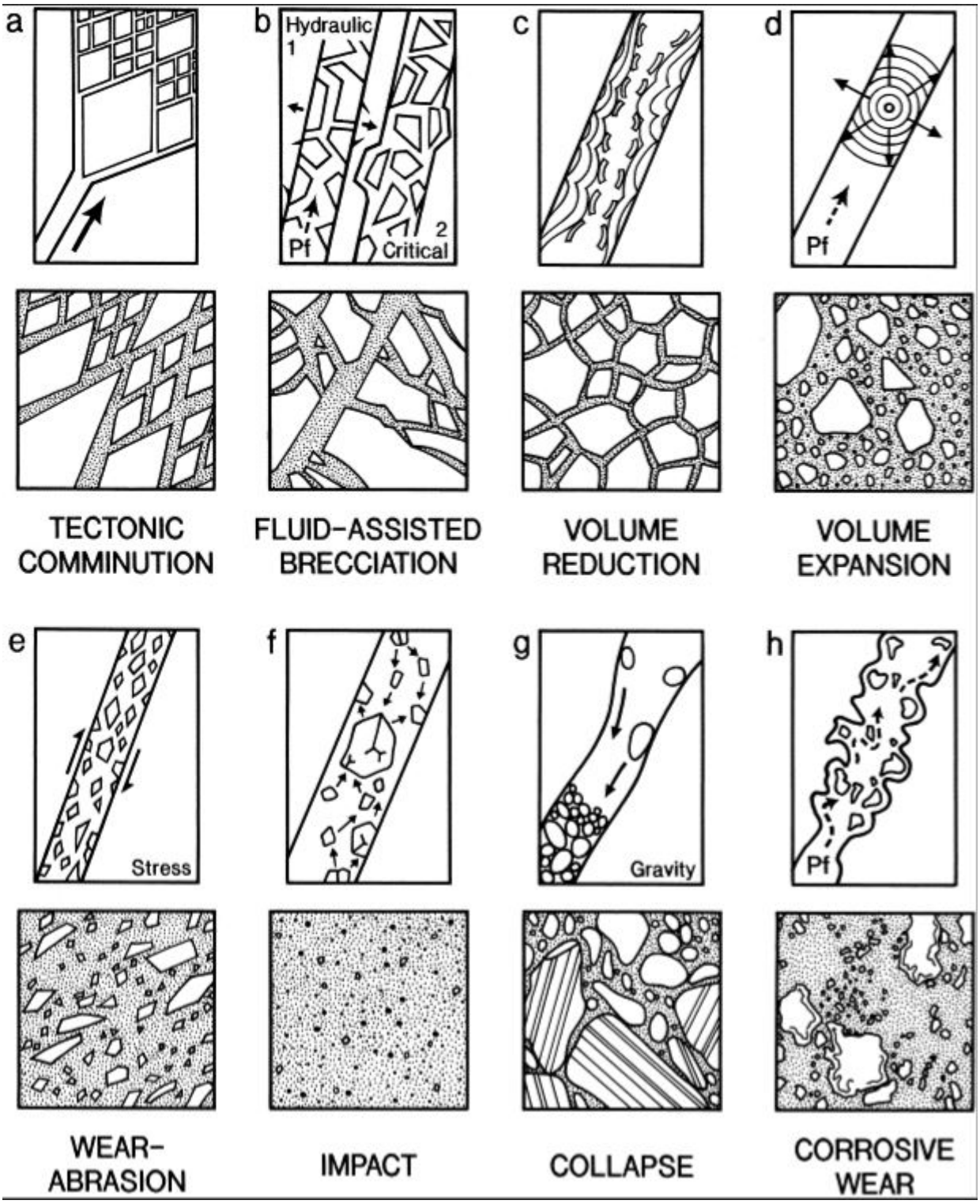

Figure 6.1: Figure showing the eight mechanisms and subsequent textures for hydrothermal brecciation. Large arrow (tectonic comminution) indicates fault propogation direction whilst smaller arrows indicate displacement of the wall or fragments. Pf is fluid pressure. (from Jébrak, 1997)

6.6 Origin of the black breccia

There are similarities between the observed black breccia and breccia facies originating from hydrothermal eruptions identified in other works (Browne & Lawless, 2001; Cerpa et al., 2013; Davies et al., 2008; Hedenquist & Henley, 1985). Based on similar works where hydrothermal breccias were observed, I propose two theories for black breccia origin and diatreme formation at Martha Hill. Both theories are related to diatreme formation and are largely dependent on whether an intruding dike encountered the water table and generated a phreatomagmatic eruption at depth or whether hydrothermal eruptions occurred due to depressurisation. Below I discuss the findings of other studies and relate them to results observed in Chapters 4 and 5.

6.6.1 Diatreme formation

Hydrothermal eruptions can last from seconds to hours with crater production spanning from a few meters to several hundred meters and are mostly dependent on host rock composition and lithology (Browne & Lawless, 2001). Their deposits are generally low volume ($<10^5$ m^3; very–poorly sorted, matrix support and bearing hydrothermally altered clasts from the geothermal reservoir (Browne & Lawless, 2001). The crater deposits generated from hydrothermal eruptions are referred to as diatreme deposits. Diatreme deposits consist of infilling of brecciated rock, sediments and other foreign deposits and are typically subvertical upwards–flaring in shape (Browne & Lawless, 2001). Volume expansion is the brecciation process associated with diatreme formation (fig. 6.1). It is a non–renewable process of brecciation, which is also described as milled, explosive, decompressive or a pushup process (Jébrak, 1997). Hydrothermal eruptions and diatreme formation are the result of rapid increases in temperature and/or a decrease in pressure. The increase in temperature may be caused by injection of magma or magmatic gases such as in the Mt. Ontake eruption (Kato et al., 2015), whilst pressure reductions are the result of a removal of overburden from a geothermal area.

6.6.2 Increase in temperature

In a study by Davies et al. (2008), hydrothermal breccia in a high sulphidation zone was interpreted to be tectonic or phreatomagmatic in origin, associated with an intruding volcanic dike. Davies et al. (2008) devised a six–part schematic model for the formation of diatremes at Kelian gold mine, Kalimantan Indonesia. Initial downfaulting caused fault–bounded blocks to become sheared and techtonically brecciated. Additionally, an andesitic intrusion was present before the formation of carbonaceous matrix–rich breccia. Next, multiple intruding rhyolite dikes percolated along fault lines and encountered groundwater. Volume expansion occurred due to rapid conversion of groundwater to steam causing phreatomagmatic eruption. Two subsequent facies were produced which were either massive, unstratified, polymicit, carbonaceous and matrix–rich in the subsurface or related to wet pyroclastic base–surges and fallout deposits. Continued phreatomagmatic explosions widened the diatreme, increased its depth and produced multiple crosscutting breccias. At Martha hill, the implications for the origin of the black breccia being associated with volume expansion and diatreme formation are likely. Angular clasts present within the black breccia matrix were monomict and comprised of smaller fragments of adjacent facies. Similarily, the summary of breccia facies by Davies et al. (2008) for facies A1, monomict carbonaceous breccia, fits the internal organisation of the black breccia facies

in this study. In Chapter 4, the logged drill holes encountered, transitioned in to the black breccia facies only once. Each transition was characterised by a strictly bounded breccia contact with the same highly altered facies overlying and underlying the black breccia. Black breccia that was logged at drill hole 1842 was 2.5 m in thickness at 107 – 109.5 m. Black breccia at drill hole 1216 was 0.8 m thick and logged at depths of 167.4 – 168.2 m. Black breccia logged in drill hole 1164 was 1.05 m thick and logged at 215.05 – 216.1 m. Whilst 3D modelling data and drill hole orientation were unavailable, in order to be in agreement with black breccia being associated with diatreme formation, the observed trend for the appearance of black breccia should thin laterally and telescope outwards from the sub–surface to the near–surface environment. However, intrusive rhyolite dikes along fault lines at Martha hill required for generating a similar phreatomagmatic eruption to Davies et al. (2008), were not observed within drill core data nor well documented in literature. Additionally, the nature of low sulphidation epithermal environment that the black breccia is hosted in, is at much greater distance from an inferred magmatic source than at Kelian. Therefore, the possibility that diatreme formation is the result of phreatomagmatism at Martha Hill is inconclusive.

6.6.3 Depressurisation

A study by Montanaro et al. (2016) discusses hydrothermal explosions based on the 2013 Gengissig lake events. Unlike the injection of magma as observed in Davies et al. (2008), hydrothermal explosion and diatreme formation at Gengissig was the product of depressurisation. The lake level was dropped by approximately 30 m, decreasing the pressure on the lake bed and triggering several hydrothermal explosions. Hedenquist and Henley (1985) devised two models for brecciation based on the Waiotapu geothermal system. The models suggest that hydrothermal explosions in geothermal settings may occur where local accumulations of gas form due to local silica sealing of near–surface fractures. Explosions may be initiated by hydraulic fracturing when gas pressures exceed lithostatic presures or by seismicity. During an explosion scenario for a shallow hydrothermal reservoir (temperatures of $\approx 195^{\circ}C$ and 200 m depth), the hydrodynamic flow follows fracture systems and a pressure–balance eruption occurs. This diatreme formation scenario fits well for the origin of black breccia. As the hydrothermal fluid ascended in the paleo–environment, its temperature was constrained by the boiling point for a given pressure. Local silica sealing within the sub–surface environment from the paleo-hydrothermal fluid contributed to sufficient pressures from gas build up to generate the explosivity required for a hydrothermal explosion event.

Extent

The extent of breccia deposits caused by hydrothermal eruptions varies and is largely dependent on the magnitude, nearby topography, vent geometry, nature of ejected material, whether the eruption occurred through water and post depositional history of breccia. However, even the largest hydrothermal eruptions produce deposits that are several orders of magnitude smaller in volume than those from typical silicic pyroclastic eruptions (Browne & Lawless, 2001). The lateral and vertical extent of the black breccia was inconclusive when determining its origin due to a lack of exposure.

Textural

Deposits from hydrothermal eruptions are very poorly sorted and invariably matrix supported (implying rapid settling velocities with little opportunity for settling). Unlike base surge deposits, bedding forms are rare and deposits that were wet during deposition would show vesicular texture and accretionary lapilli in the matrix . Indeed, the black breccia was very poorly sorted and matrix supported with no clear bedding formations being observed in the limited core log data.

Lithology and alteration of clasts

Clasts identified in hydrothermal eruptions are hydrothermally altered. These clasts differ from clasts in debris or lahars of volcanic origin, which are altered differently (if at all). For example, it is unlikely that clasts in a lahar of volcanic origin would contain alteration minerals such as epidote or adularia (formed at near–neutral pH waters at moderate temperatures) (Browne & Lawless, 2001). According to Browne and Lawless (2001), clasts identified for hydrothermal diatreme breccias indicated kaolin and alunite. When considering XRD data for the clasts of black breccia, peaks were in fact observed for kaolinite.

Products such as vein quartz and platy calcite are recognised in hydrothermal eruption breccias and are indicative of shallow two phase conditions in a convective reservoir. When considering XRD data from Chapter 5 for the black breccia, some areas of the logged black breccia contained occasional thick (10 mm) bands of calcite veining. The presence of these bands indicates that a paleo–hydrothermal fluid was present during or after the emplacement of the breccia. Furthermore, angular quartz was observed within thin section microscopy which can be inferred to be hydrothermal in origin as it lacked the rounded and embayed nature sometimes observed in volcanic quartz.

One of the textures observed in the matrix of the black breccia under the SEM, revealed larger grey grains that were exclusively silica and oxygen on the element map and likely represent quartz/silica in the matrix. Another texture observed was fine interstitial platy grains which were supported by high potassium, aluminium, silica and oxygen within the element map. These interstitial platy grains could indicate adularia, however, they could equally be a nanocrystalline clay mineral. Petrography data for the matrix of the black breccia confirmed the presence of adularia as orthoclase. Orthoclase (adularia) is a secondary mineral formed at near–neutral pH waters at moderate temperatures. According to White and Hedenquist (1990) the presence of adularia is indicative that boiling has occurred and caused an increase in pH. This further supports that a paleo–hydrothermal fluid was present during and/or after the emplacement of the black breccia. Typical temperatures for the occurrence of adularia are 180 to 350°C, which indicates that this was the temperature range of the hydrothermal fluid during/after the formation of the black breccia (Corbett & Leach, 1998).

Other characteristics of the black breccia identified during core logging include an observably low hardness compared to more coherent rock units such as those encountered in the coherent highly and weakly altered facies. Furthermore, some logged sections of black breccia appeared flaky in areas where it was also present as a breccia crumble. These observations are likely the product of clasts being matrix supported by a high percentage of clays and secondary minerals such as adularia. However, clay separation XRD was unavailable during analyses, which meant the specific clay components of the black breccia were unable to be determined.

Top down model

For hydrothermal eruptions to occur, a field wide cap or cover is required to allow for reservoir pressures to exceed lithostatic pressure or tensile strength of rock. However, more commonly, most natural hydrothermal eruptions start at the ground surface and penetrate downwards into the reservoir. Conditions are that boiling water exists at or close to the surface and is underlain by water at boiling point for depth temperature gradient (Browne & Lawless, 2001, and references therein). The reason this is more commonly observed in nature is because the ability to lift a cone shaped mass of overburden at great depths within a geothermal reservoir, requires a tremendous amount of energy. The top down model can be separated into a six step process for a common hydrothermal eruption (fig. 6.2 and 6.3).

1. Initial steam bursts eject the covering materials along with entrained water and mud.
2. This eruptive phase reduces pressures further within the reservoir and produces more steam from any residual meteoric or thermal water present.
3. Additional fragmentation and brecciation of rock is initiated by the increased steam.
4. A progressively downward migrating flashing front and brecciation surface within the reservoir, followed by the eruption front.
5. Eruptions occur for hours to days and cease when steam supply rate is insufficent to further brecciate and lift rock fragments.
6. Piezometric surface ascends to its former level and hydrothermal alteration restarts.

The top down model discussed in Browne and Lawless (2001) aligns well with the origin of the black breccia at the paleo–geothermal field of Waihi. Whilst a scale is not presented within figures 6.2 and 6.3, typical vertical distances for the top down model may span over vertical distances of 5 – 300 m. Assuming drill hole orientations for the logged black breccia were near vertical, the maximum depth of the logged black breccia was 216.1 m in drill hole 1164, suggesting that brecciation through the top down model seems plausible. Following the brecciation discussed in step five of the top down model, it is likely that there was a fine matrix (as is normal in a diatreme deposit), which was altered in to other secondary minerals to form the different fine grained matrix components – such as adularia. Clasts that were altered differently to the matrix may indicate that the pre-existing country rock was already partly altered by the pre-existing hydrothermal system. Indeed following the brecciation event, the new hydrothermal system had a greater influence on the alteration of the new matrix between the clasts.

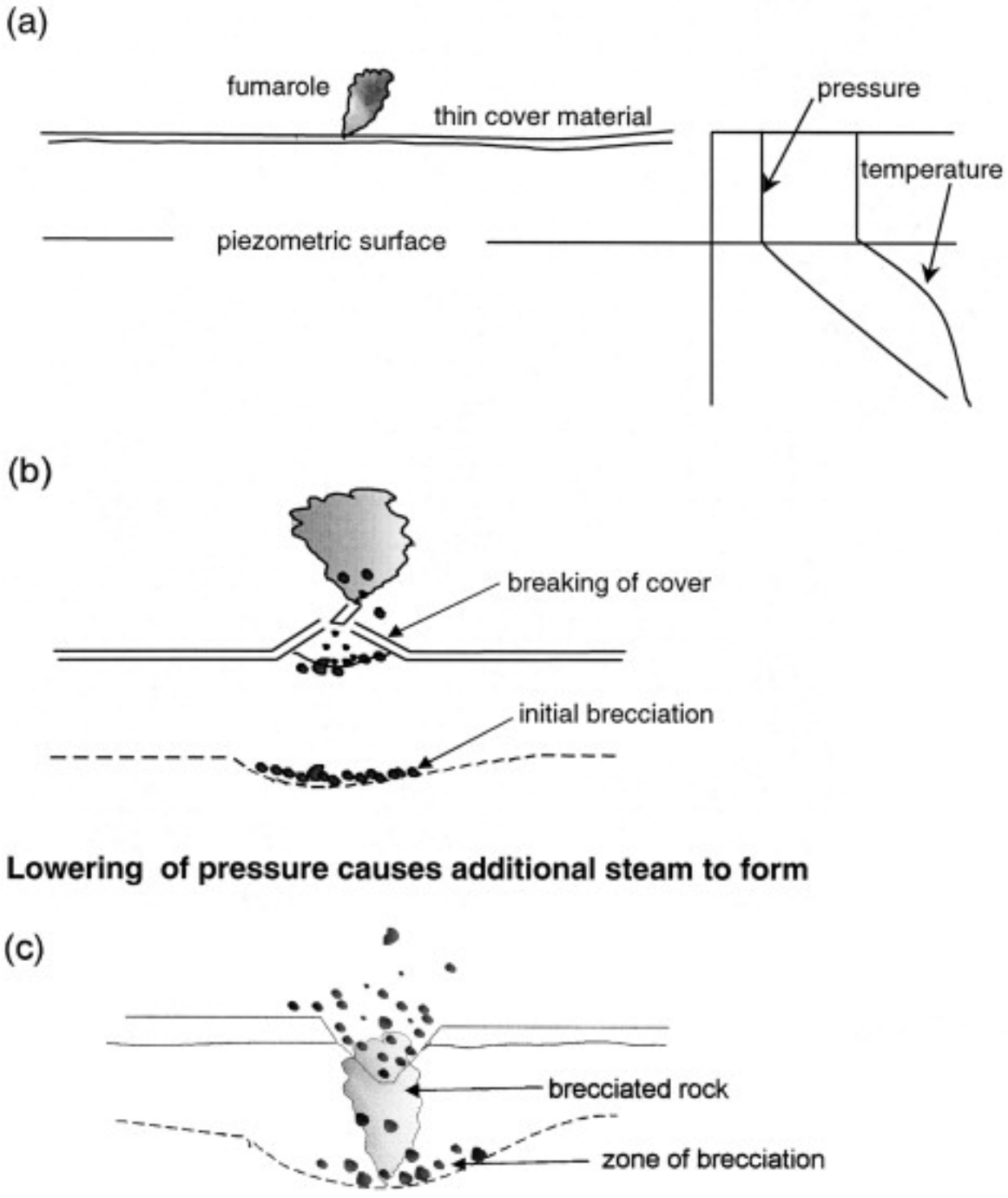

Figure 6.2: The first three steps involved in the development of a hydrothermal eruption. (a) Initial steam bursts in an environment where boiling water exists at or close to the surface and is underlain by water at a boiling point for depth temperature gradient. (b) Steam bursts ejects covering materials together with entrained water and mud and reduces pressures further within the reservoir producing more steam from any residual meteoric or thermal water present. (c) Additional fragmentation and brecciation of rock initiated by the increased steam and a downward migrating zone of brecciation. (from Browne & Lawless, 2001)

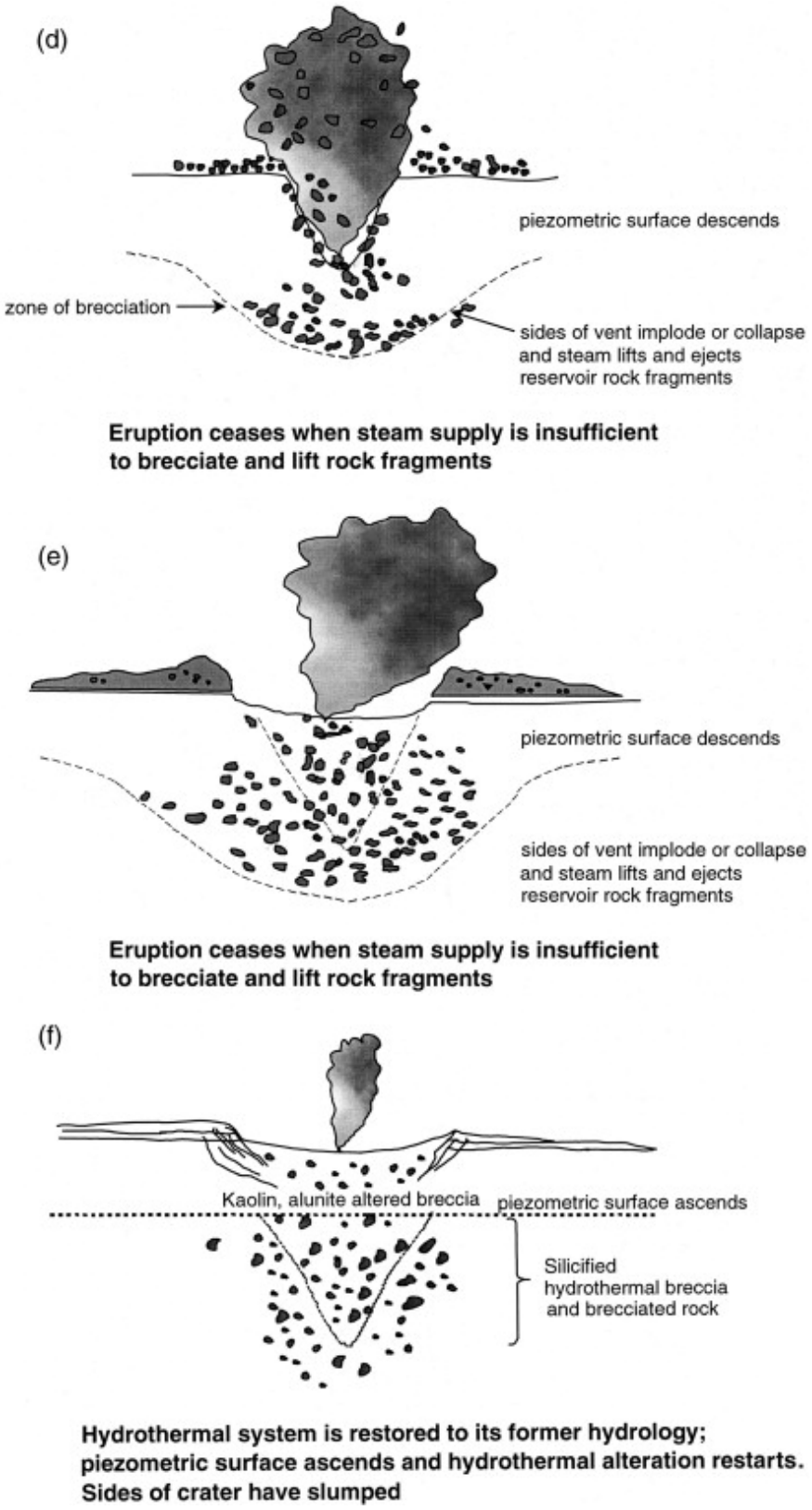

Figure 6.3: The final three steps involved in the development of a hydrothermal eruption. (d) and (e) A progressively downward migrating flashing front, brecciation surface and eruption front within the reservoir. Eruptions occur for hours to days and cease when steam supply rate is insufficent to further brecciate and lift rock fragments. (f) Piezometric surface ascends to its former level and hydrothermal alteration restarts (from Browne & Lawless, 2001).

Chapter 7
Summary and conclusions

7.1 Key findings

The Martha hill deposit is an epithermal adularia–sericite gold deposit situated in the township of Waihi, New Zealand. This study involved the analyses and interpretation of sections of core log for three separate drill core from the Martha Hill deposit provided by OceanaGold. The primary focus of the study was on the black breccia. However, analyses and interpretation of adjacent facies was generated to better determine the significance and origin of the black breccia facies. These facies were subdivided in to weakly altered, highly altered and breccia facies. Initial attempts during core logging were made to broadly subdivide sections of core in to their respective facies. Further petrographical and geochemical data assisted in determining the degree of facies alteration based on the appearance or disappearance of minerals or elements within the sampled facies. Weakly altered facies encapsulated two facies that were analysed in hand sample (core logging) and petrographically and geochemically. The origin of the weakly altered facies B1 – country rock andesite, was determined to be the facies resembling the original andesite Waipupu Formation that displayed a minor degree of alteration. The other weakly altered facies (facies B2 – trachy–andesite) was present as a larger clast within the polymict breccia facies of C2. The highly altered facies involved five separate facies that were more than weakly altered with some facies displaying a high degree of alteration. All five facies were directly related to hydrothermal alteration by the paleo–hydrothermal fluid. Facies that displayed the highest degrees of alteration, were influenced more by the hydrothermal fluid and involved multiple overprinting events through the propogating hydrothermal fluid. Likely, the overall hydrothermal fluid pathway was responsible for generating the different highly altered facies. Where the hydrothermal fluid was influenced more by lithology and various minor structures to allow for better permeability throughout the andesite, it resulted in facies that were more highly altered. The final facies recognised in my study were facies that were hydrothermally brecciated or brecciated as a result of original lava processes (autobreccia). The breccia facies included three separate facies, one of which contained four separate sub-facies. The breccia facies C2 (partial – completely brecciated) was polymict and contained a mixture of clasts, some of which were weakly altered. This facies was interpreted to be initially an autobreccia that was deposited during the emplacement of the country rock andesite that was then later weakly to moderately altered. Facies C3 was separated in to four sub-facies: C3a – patchy large feldspars, C3b – crackle texture, C3c – patchy boundary and C3d – thick calcite veins. Sub-facies for C3 were due to both the gradational contacts and repetitive nature of the facies observed during core logging. I infer that C3 originates from the original andesite emplacement process that was hydrothermally altered and later hydraulically fractured (brecciated) in the sub-surface. This was made evident by the crackle texture and calcite veining overprinting pre–existing quartz veins. The black breccia was interpreted to be associated with diatreme formation as a result of phreatomagmatism or hydrothermal eruptions. Carbonate veins ($\approx$ 10 mm) present within the black breccia indicate that a paleo–hydrothermal fluid was present during or after the emplacement

of the black breccia. Additionally, the occurrence of adularia detected by XRD analyses indicates that black breccia emplacement temperatures were 180 to 350°C. It is possible that the black breccia is the product of phreatomagmatism and diatreme formation due to interactions by a sub–surface feeder. Indeed, additional drill data may reveal a feeder dike at depth below the Martha Hill deposit which supports this claim. However, based on the data available and analyses generated during my study, the presence of black breccia in core log is more likely the result of hydrothermal eruptions due to depressurisation. Depressurisation of overburden was commonly associated with hydrothermal eruptions and diatreme formation in other studies (Browne & Lawless, 2001; Hedenquist & Henley, 1985; Montanaro et al., 2016). Browne and Lawless (2001) suggest that most natural hydrothermal eruptions start at the ground surface and penetrate downwards. I infer that the devised top down model in Browne and Lawless (2001) is the most logical explanation for the occurrence of black breccia in core log at the Martha Hill mine. Conditions of the paleo–geothermal field was boiling water at or close to the surface that was underlain by water at boiling point for depth temperature gradient (Browne & Lawless, 2001). As fragmentation and brecciation was initated by steam, depressurisation from the release of overburden caused boiling in the subsurface and a progressively downward migrating flashing front, brecciation surface and eruption front. These eruptions would have occurred for hours to days and ceased when steam supply rate was insufficient. Furthermore, local silica build up in the near–surface described by Hedenquist and Henley (1985), likely assisted in capping fluid pathways and further increasing pressures in the sub–surface to levels capable of generating continued hydrothermal eruptions.

7.2 Further work

Clay separation XRD would allow for a more typical approach to modelling zones of alteration utilised in other literature by identifying the dominant clay minerals present (e.g. alunite–kaolin, illite–smectite). Diatreme modelling and root zone identification may be possible with 3D data (e.g. Leapfrog 3D data) and drill hole orientations. Unfortunately, Leapfrog 3D data that was provided toward the beginning of my research had corrupted and became unavailable to be used within the timeframe of this project to generate a mock diatreme model for the black breccia. Additional drill holes that encounter an intrusive feeder dike or outcropping sections of black breccia may influence the proposed theory of hydrothermal eruptions causing diatreme formation.

References

Adams, C., Graham, I., Seward, D., Skinner, D., Adams, C., Skinner, D., & Moore, P. (1994). Geochronological and geochemical evolution of late cenozoic volcanism in the coromandel peninsula, new zealand. *New Zealand journal of geology and geophysics*, *37*(3), 359–379.

Arribas, A., Hedenquist, J., & Gonzalez-Urien, E. (2000). Exploration for epithermal deposits.

Bodger, B. (2015). *Andesite volcanic facies and hydrothermal alteration in the subsurface peripheral to existing waihi mine workings* (Doctoral dissertation). University of Waikato.

Brathwaite, R. L., & Skinner, D. N. B. (1997). The Coromandel epithermal gold-silver province: A result of collision of the Northland and Colville volcanic arcs in northern New Zealand. *1997 New Zealand Minerals and Mining Conference*, 111–118.

Brathwaite, R. (1989). Geology and exploration of the karangahake gold-silver deposit. *Mineral Deposits of New Zealand, Australasian Institute of Mining and Metallurgy, Monograph*, *13*, 73–78.

Brathwaite, R., & Christie, A. (1996). Geology of the waihi area, scale 1:50 000. institute of geological map 21. 1 sheet + 64p.

Brathwaite, R., & Faure, K. (2002). The waihi epithermal gold-silver-base metal sulfide-quartz vein system, new zealand: Temperature and salinity controls on electrum and sulfide deposition. *Economic Geology*, *97*(2), 269–290.

Brathwaite, R., Torckler, L., Jones, P., & Christie, A. B. (2006). *The martha hill epithermal au-ag deposit, waihi–geology and mining history* (Vol. 25). Australasian Institute of Mining; Metallurgy Monograph.

Briggs, R., Houghton, B., McWilliams, M., & Wilson, C. (2005). 40ar/39ar ages of silicic volcanic rocks in the tauranga-kaimai area, new zealand: Dating the transition between volcanism in the coromandel arc and the taupo volcanic zone. *New Zealand Journal of Geology and Geophysics*, *48*(3), 459–469.

Brown, K. L. (1986). Gold deposition from geothermal discharges in new zealand. *Economic Geology*, *81*(4), 979–983.

Browne, P. (1978). Hydrothermal alteration in active geothermal fields. *Annual review of earth and planetary sciences*, *6*, 229–250.

Browne, P., & Lawless, J. (2001). Characteristics of hydrothermal eruptions, with examples from new zealand and elsewhere. *Earth-Science Reviews*, *52*(4), 299–331. https://doi.org/https://doi.org/10.1016/S0012-8252(00)00030-1

Cargill, H. (1994). *Aspects of the structural geology of the martha hill epithermal au-ag deposit, waihi, new zealand* (Doctoral dissertation). University of Auckland.

Cathles, L. (1983). An analysis of the hydrothermal system responsible for massive sulfide deposition in the hokuroku basin of japan.

Cerpa, L. M., Bissig, T., Kyser, K., McEwan, C., Macassi, A., & Rios, H. W. (2013). Lithologic controls on mineralization at the lagunas norte high-sulfidation epithermal gold deposit, northern peru. *Mineralium Deposita*, *48*(5), 653–673.

Christie, A., & Brathwaite, R. (1997). New zealand's geological framework. *Windows on New Zealand: Proceedings*, *1*, 3.

Christie, A., Simpson, M., Brathwaite, R., Mauk, J., & Simmons, S. (2007). Epithermal au-ag and related deposits of the hauraki goldfield, coromandel volcanic zone, new zealand. *Economic Geology*, *102*(5), 785–816.

Corbett, G., Hunt, S., Cook, A., Tamaduk, P., & Leach, T. (2001). Geology of the ladolam gold deposit, lihir island, from exposures in the minifie open pit. *PNG Geology, Exploration and Mining Conference June*, 69–77.

Corbett, G. J. (2002). Epithermal gold for explorationists. *AIG News*, *67*, 1–8.

Corbett, G. J., & Leach, T. M. (1998). *Southwest pacific rim gold-copper systems: Structure, alteration, and mineralization* (Vol. 6). Society of Economic Geologists Littleton, Colorado.

Davey, F., Henrys, S., & Lodolo, E. (1995). Asymmetric rifting in a continental back-arc environment, north island, new zealand. *Journal of volcanology and geothermal research*, *68*(1-3), 209–238.

Davies, A. G., Cooke, D. R., Gemmell, J. B., & Simpson, K. A. (2008). Diatreme breccias at the kelian gold mine, kalimantan, indonesia: Precursors to epithermal gold mineralization. *Economic Geology*, *103*(4), 689–716.

Dix, G. R., & Nelson, C. S. (2004). The role of tectonism in sequence development and facies distribution of upper oligocene cool-water carbonates: Coromandel peninsula, new zealand. *Sedimentology*, *51*(2), 231–251.

Gibbard, P. (1991). The concise oxford dictionary of earth sciences. a. allaby and m. allaby. publisher oxford university press 1990 £20.00 isbn 0 19 866146 0. *Journal of Quaternary Science*, *6*(1), 79–80. https://doi.org/https://doi.org/10.1002/jqs.3390060109

Giggenbach, W. (1986). The use of gas chemistry in delineating the origin of fluids discharged over the taupo volcanic zone. *Proceedings of Symposium 5, Int. Volc. Congress, Auckland*, 47–50.

Hayward, B. W., Grenfell, H. R., Mauk, J. L., Moore, P. R., & Mildenhall, D. (2006). The west-flowing "clevedon river," auckland. *Geological Society of New Zealand Newsletter*, *141*, 24–29.

Hedenquist, J. W. (1986). Geothermal systems in the taupo volcanic zone: Their characteristics and relation to volcanism and mineralisation. *Late Cenozoic Volcanism in New Zealand.*, *23*, 134–168.

Hedenquist, J. W. (1987). Volcanic-related hydrothermal systems in the circum-pacific basin and their potential for mineralisation. *Mining Geology*, *37*(205), 347–364.

Hedenquist, J. W., Arribas, A., & Gonzalez-Urien, E. (2000). Exploration for epithermal gold deposits.

Hedenquist, J. W., & Henley, R. W. (1985). Hydrothermal eruptions in the Waiotapu geothermal system, New Zealand; their origin, associated breccias, and relation to precious metal mineralization. *Economic Geology*, *80*(6), 1640–1668. https://doi.org/10.2113/gsecongeo.80.6.1640

Hochstein, M., & Ballance, P. (1993). Hauraki rift: A young, active, intra-continental rift in a back-arc setting. *South Pacific sedimentary basins, sedimentary basins of the world*, *2*, 295–305.

Houghton, B., & Cuthbertson, A. (1989). Kaimai, geological map of new zealand 1: 50000, t14bd, 35. *Department of Scientific and Industrial Research, Wellington, New Zealand.*

Jébrak, M. (1997). Hydrothermal breccias in vein-type ore deposits: A review of mechanisms, morphology and size distribution. *Ore Geology Reviews*, *12*(3), 111–134. https://doi.org/https://doi.org/10.1016/S0169-1368(97)00009-7

John, D. A. (2011). Epithermal Gold-Silver Deposits of the Hauraki Goldfield, New Zealand: An Introduction. *Economic Geology*, *106*(6), 915–919. https://doi.org/10.2113/econgeo.106.6.915

Julian, H. A. (2016). *Volcanology of the owharoa and waikino ignimbrites, waihi, coromandel volcanic zone* (Doctoral dissertation). University of Waikato.

Kato, A., Terakawa, T., Yamanaka, Y., Maeda, Y., Horikawa, S., Matsuhiro, K., & Okuda, T. (2015). Preparatory and precursory processes leading up to the 2014 phreatic eruption of mount ontake, japan. *Earth, Planets and Space*, *67*(1), 1–11.

King, P. R. (2000). Tectonic reconstructions of new zealand: 40 ma to the present. *New Zealand Journal of Geology and Geophysics*, *43*(4), 611–638.

Laird, M. (1996). Mid and early late cretaceous break-up basins of the south island, new zealand. *GEOLOGICAL SOCIETY OF AUSTRALIA ABSTRACTS*, *43*, 329–336.

Lindgren, W. (1933). Chapter xxiv: Epithermal deposits–metalliferous deposits formed near the surface by ascending thermal waters and in genetic connection with igneous rocks, mineral deposits. *Mineral Deposits, fourth edition. McGraw-Hill Book Company, Inc., New York and London*, 444–513.

Mauk, J. L., Hall, C. M., Chesley, J. T., & Barra, F. (2011). Punctuated Evolution of a Large Epithermal Province: The Hauraki Goldfield, New Zealand*. *Economic Geology*, *106*(6), 921–943. https://doi.org/10.2113/econgeo.106.6.921

Mielke, P., Prieto, A., Bignall, G., & Sass, I. (2015). Effect of hydrothermal alteration on rock properties in the tauhara geothermal field, new zealand. *Proc World Geothermal Congress*.

Montanaro, C., Scheu, B., Gudmundsson, M. T., Vogfjörd, K., Reynolds, H. I., Dürig, T., Strehlow, K., Rott, S., Reuschlé, T., & Dingwell, D. B. (2016). Multidisciplinary constraints of hydrothermal explosions based on the 2013 gengissig lake events, kverkfjöll volcano, iceland. *Earth and Planetary Science Letters*, *434*, 308–319. https://doi.org/https://doi.org/10.1016/j.epsl.2015.11.043

Nicholson, K., Black, P., Hoskin, P., & Smith, I. (2004). Silicic volcanism and back-arc extension related to migration of the late cainozoic australian–pacific plate boundary. *Journal of Volcanology and Geothermal Research*, *131*(3), 295–306. https://doi.org/https://doi.org/10.1016/S0377-0273(03)00382-2

Panther, C., Mauk, J., Arehart, G., St George, J., et al. (1995). A petrographic and oxygen isotope study of banded epithermal veins from the martha hill au-ag mine, waihi, new zealand. *Proceedings of the 1995 PACRIM Congress, Australasian Institute of Mining and Metallurgy, Carlton, Australia*, 447–452.

Pirajno, F. (2009). Hydrothermal processes and wall rock alteration. *Hydrothermal processes and mineral systems* (pp. 73–164). Springer.

Rabone, S. (1975). Petrography and hydrothermal alteration of tertiary andesite-rhyolite volcanics in the waitekauri valley, ohinemuri, new zealand. *New Zealand Journal of Geology and Geophysics*, *18*(2), 239–258.

Rytuba, J. (1981). Relation of calderas to ore deposits in the western united states. *Relations of tectonics to ore deposits in the southern Cordillera: Arizona Geological Society Digest*, *14*, 22.

Schofield, J. (1959). Whitianga group.

Shannon, R., & Lorrance, T. (2022). *The influence of host rocks on epithermal veining in the waihi area of new zealand* [16th SGA BIENNIAL MEETING]. https://az659834.vo.msecnd.net/eventsairseasiaprod/production-confer-public/92374758d1c84f2ba418d33ba360fbf8

Sillitoe, R. H. (1994). Erosion and collapse of volcanoes: Causes of telescoping in intrusion-centered ore deposits. *Geology*, *22*(10), 945–948. https://doi.org/10.1130/0091-7613(1994)022⟨0945:EACOVC⟩2.3.CO;2

Sillitoe, R. H. (2000). Styles of high-sulphidation gold, silver and copper mineralisation in porphyry and epithermal environments. *Proceedings of the Australasian Institute of Mining and Metallurgy*, *305*(1), 19–34.

Simmons, S., & Browne, P. (1997). Understanding epithermal ore deposits from new zealand geothermal systems. *Windows on New Zealand: Proceedings*, *1*, 71.

Simmons, S., White, N., & John, D. (2005). Geological characteristics of epithermal precious and base metal deposits.

Singh, R. S. (2015). *Identifying mineralogical and geochemical vectors towards the epithermal au-ag correnso mine, waihi* (Doctoral dissertation). University of Waikato.

Skinner, D. N. B. (1972). Subdivision and petrology of the mesozoic rocks of coromandel (manaia hill group). *New Zealand Journal of Geology and Geophysics*, *15*(2), 203–227. https://doi.org/10.1080/00288306.1972.10421955

Skinner, D. N. (1993). *Geology of the coromandel harbour area: Sheets s11 bd & t11 ac, scale 1: 50000*. Institute of Geological & Nuclear Sciences.

Skinner, D. (1976). Sheet n40 and parts n35, n36, n39–northern coromandel. geological map of new zealand 1: 63 360.

Skinner, D. (1986). Neogene volcanism of the hauraki volcanic region. *Royal society of New Zealand bulletin*, *23*, 21–47.

Spörli, K., Begbie, M., Irwin, M., & Rowland, J. (2006). Structural processes and tectonic controls on the epithermal au-ag deposits of the hauraki goldfield. *Geology and exploration of New Zealand mineral deposits: Australasian Institute of Mining and Metallurgy*, 85–94.

Spörli, K., & Cargill, H. (2011). Structural Evolution of a World-Class Epithermal Orebody: The Martha Hill Deposit, Waihi, New Zealand. *Economic Geology*, *106*(6), 975–998. https://doi.org/10.2113/econgeo.106.6.975

Stevens, M. T. (2010). Miocene and pliocene silicic coromandel volcanic zone tephras from odp site 1124-c: Petrogenetic applications and temporal evolution.

Weissberg, B. (1969). Gold-silver ore-grade precipitates from new zealand thermal waters. *Econ. Geol.;(United States)*, *64*.

White, N. C., & Hedenquist, J. W. (1990). Epithermal environments and styles of mineralization: Variations and their causes, and guidelines for exploration. *Journal of Geochemical Exploration*, *36*(1), 445–474. https://doi.org/https://doi.org/10.1016/0375-6742(90)90063-G

White, N. C., & Hedenquist, J. W. (1995). Epithermal gold deposits: Styles, characteristics and exploration. *SEG Discovery*, (23), 1–13.

Appendix

New Facies	Old Facies	Thin Sectio	Drill Hole	Depth
A1	1A	TZ:5	1842	101.2
A2	1B	TZ:2	1842	102
A2x	1Bb	TZ:4	1842	102.3
A3	1C	TX:4	1164	205.8
A3	1C	TX:12	1164	205.9
A3	1C	TX:6	1164	206.1
A3	1C	TZ:7	1842	104.2
A4	2A	TX:11	1164	189.3
A4	2A	TX:14	1164	192.1
A4	2A	TX:5	1164	203.1
A4	2A	TZ:3	1842	106.6
A5	2B	TZ:15	1842	113.8
A5	2Bx	TZ:10	1842	112.1
B1	2C	TZ:1	1842	136.2
B2	1D	TZ:14	1842	111.7
C1x	3Ac	TX:8	1216	168
C1	3A	TX:13	1216	168
C1	3A	TX:2	1164	213.8
C1	3A	TX:7	1164	214
C1	3A	TX:16	1164	214.5
C1	3A	TZ:11	1842	107.4
C1	3A	TX:3	1216	167.1
C1x	3A(c)	TX:15	1216	168
C1x	3A(c)	TX 18	1216	167.7
C2	3B	TZ:6	1842	111.37
C2	3Bx	TZ:13	1842	112.6
C2	3C	TZ:8	1842	114.4
C2x	3Bb	TZ:9	1842	111.25
C3b	3Db	TX:9	1216	162.2
C3c	3Dc	TX:1	1216	60.2

Figure 1: Figure showing the generated new facies names, old facies names, thin section IDs, drill hole IDs and drill hole depth.

16/07/22 12:20pm Sun & some cloud cover

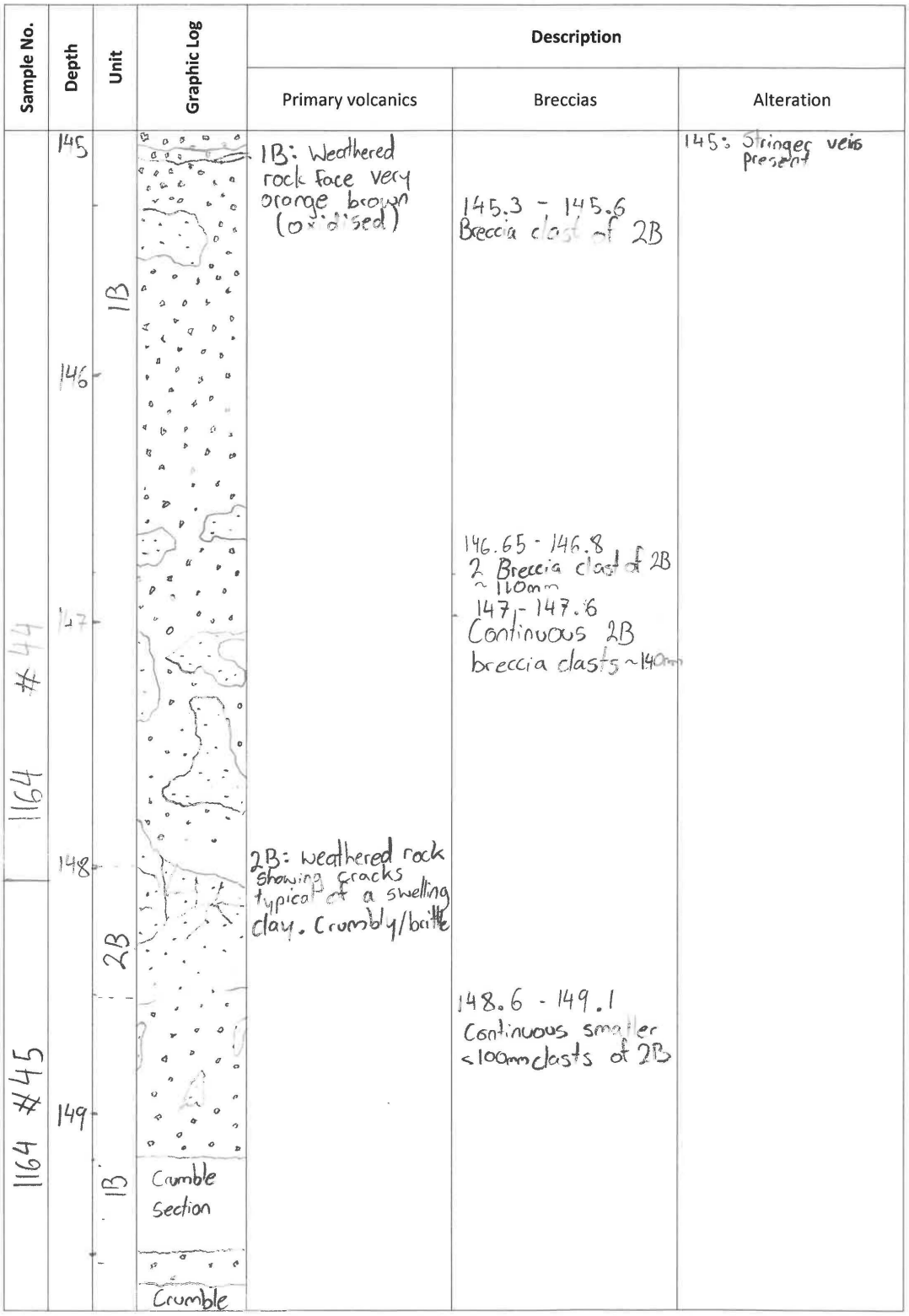

Figure 2: Figure showing core log for drill hole 1164 (1)

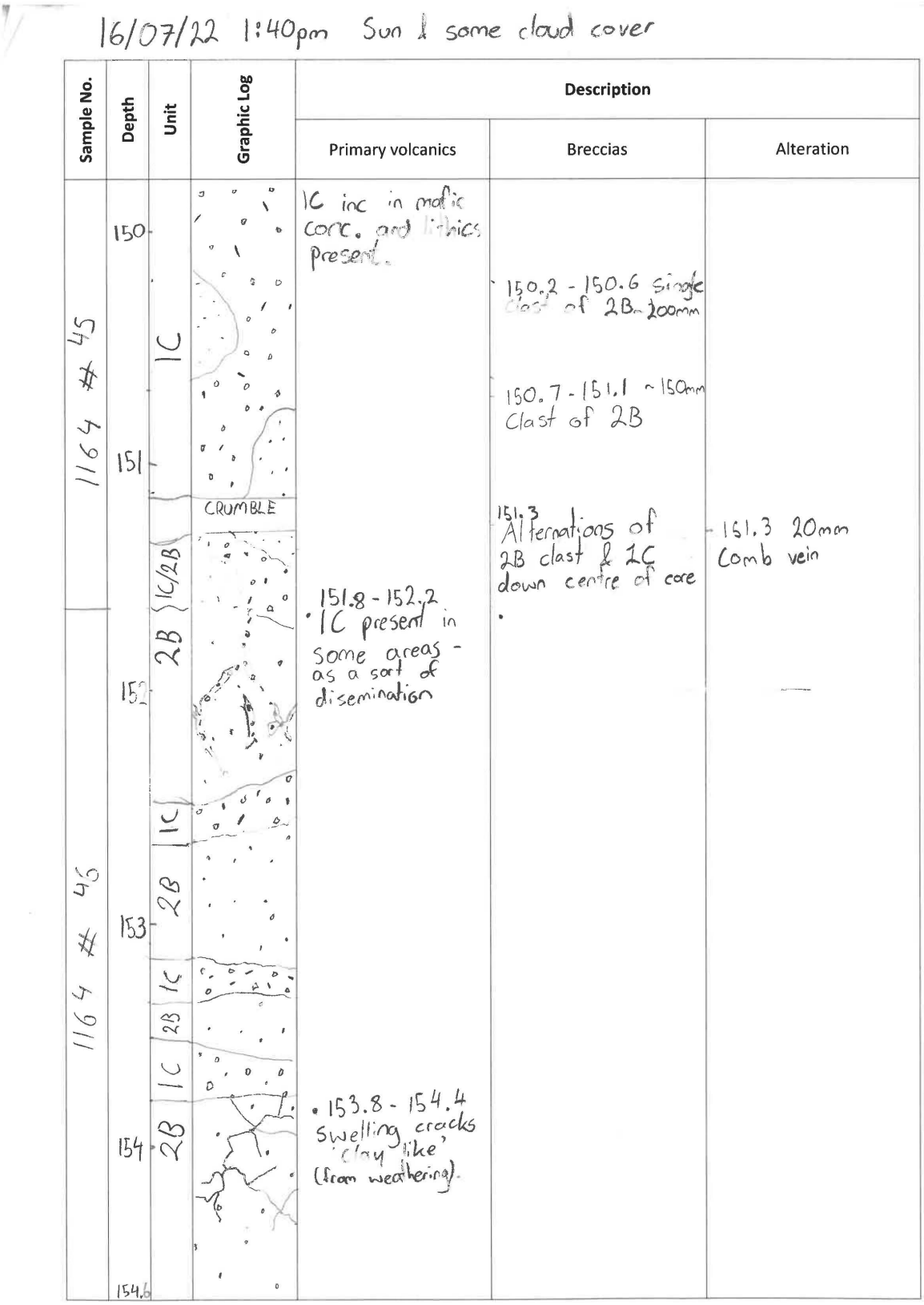

Figure 3: Figure showing core log for drill hole 1164 (2)

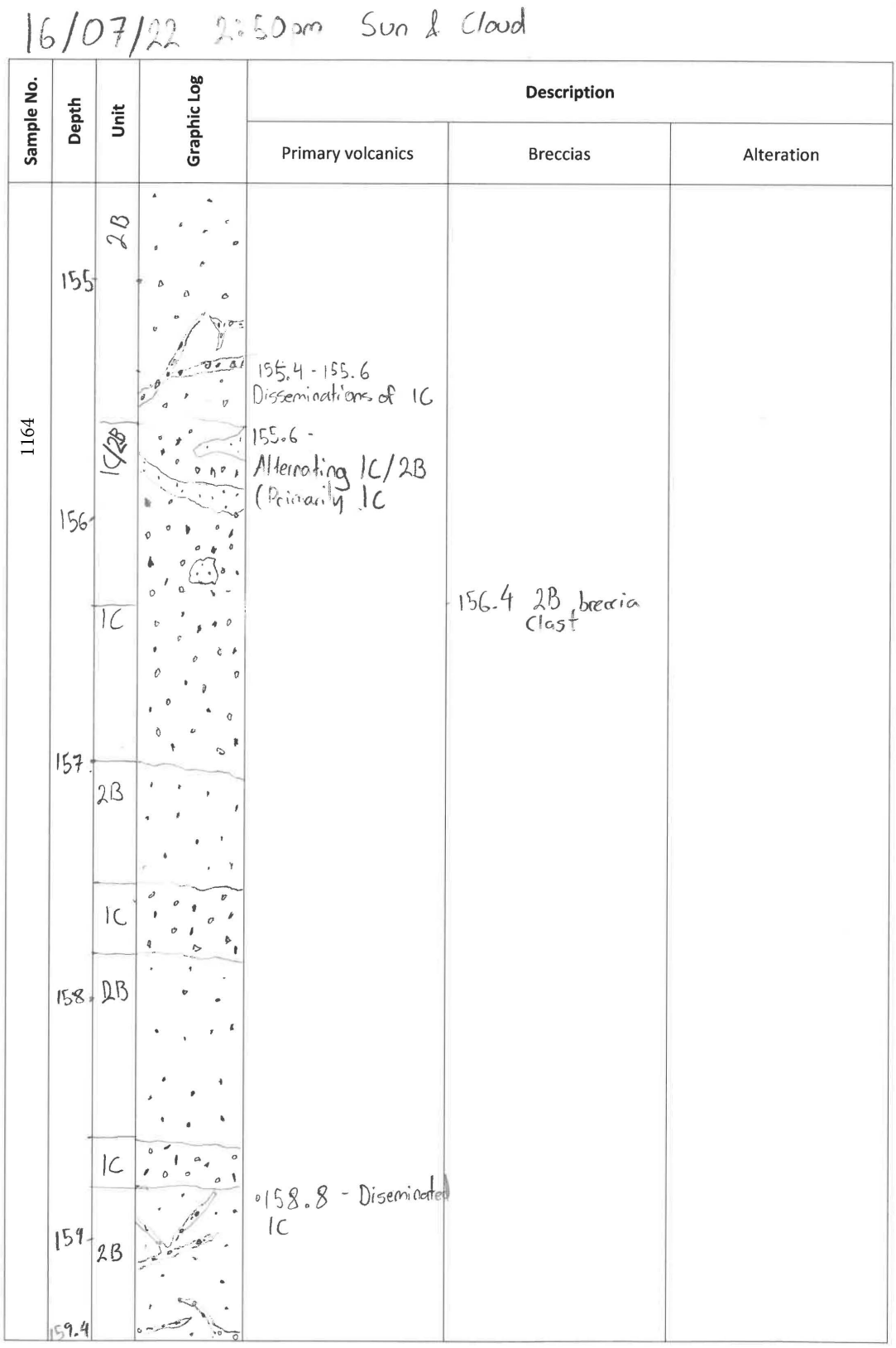

Figure 4: Figure showing core log for drill hole 1164 (3)

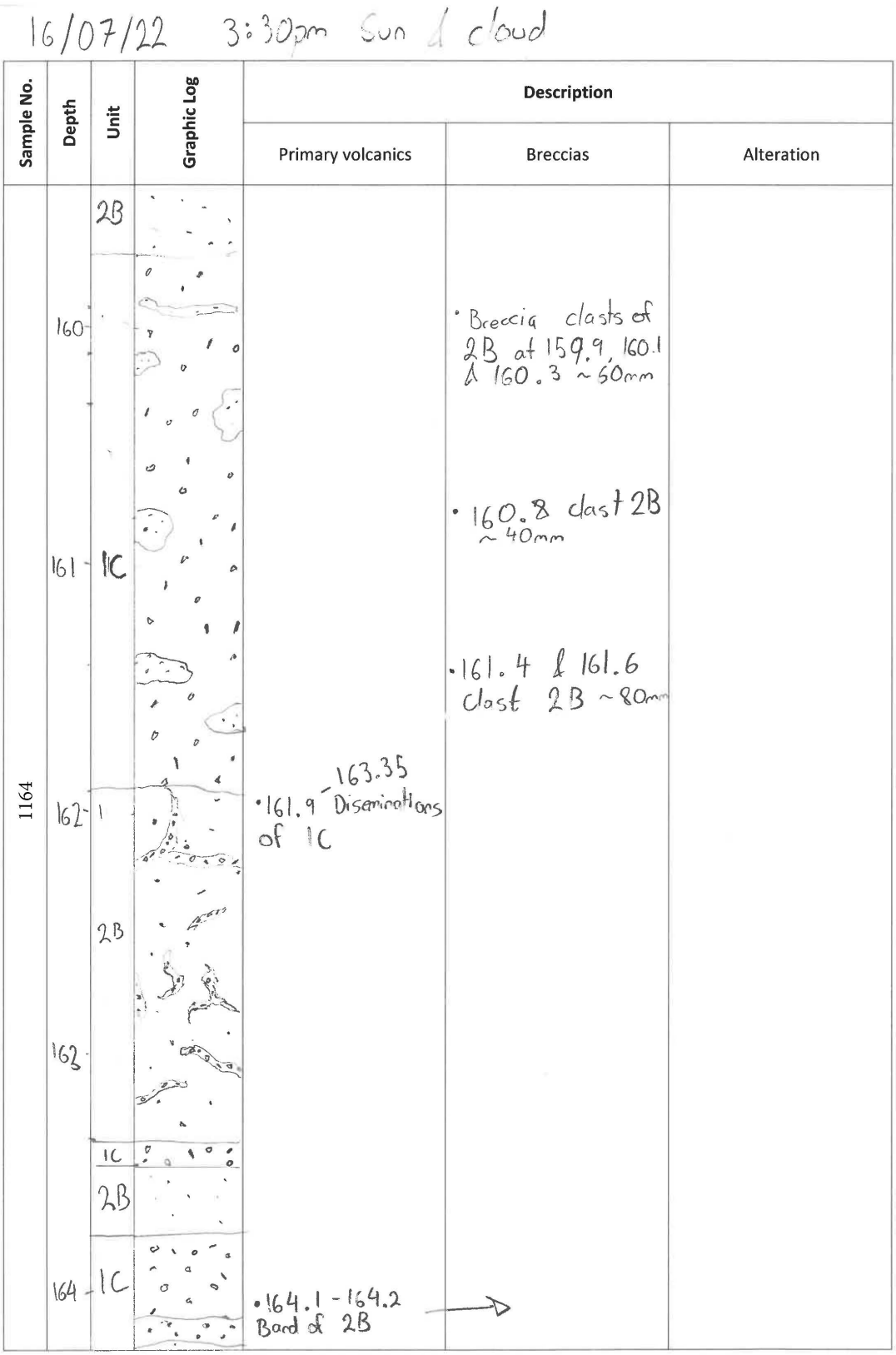

Figure 5: Figure showing core log for drill hole 1164 (4)

16/07/22 4:00pm Sun & cloud.

Sample No.	Depth	Unit	Graphic Log	Description		
				Primary volcanics	Breccias	Alteration
1164	165	1C	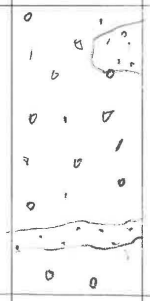		164.3 100mm 2B clast 164.95 - 165.05 Band of 2B clast ~100mm	

Figure 6: Figure showing core log for drill hole 1164 (6)

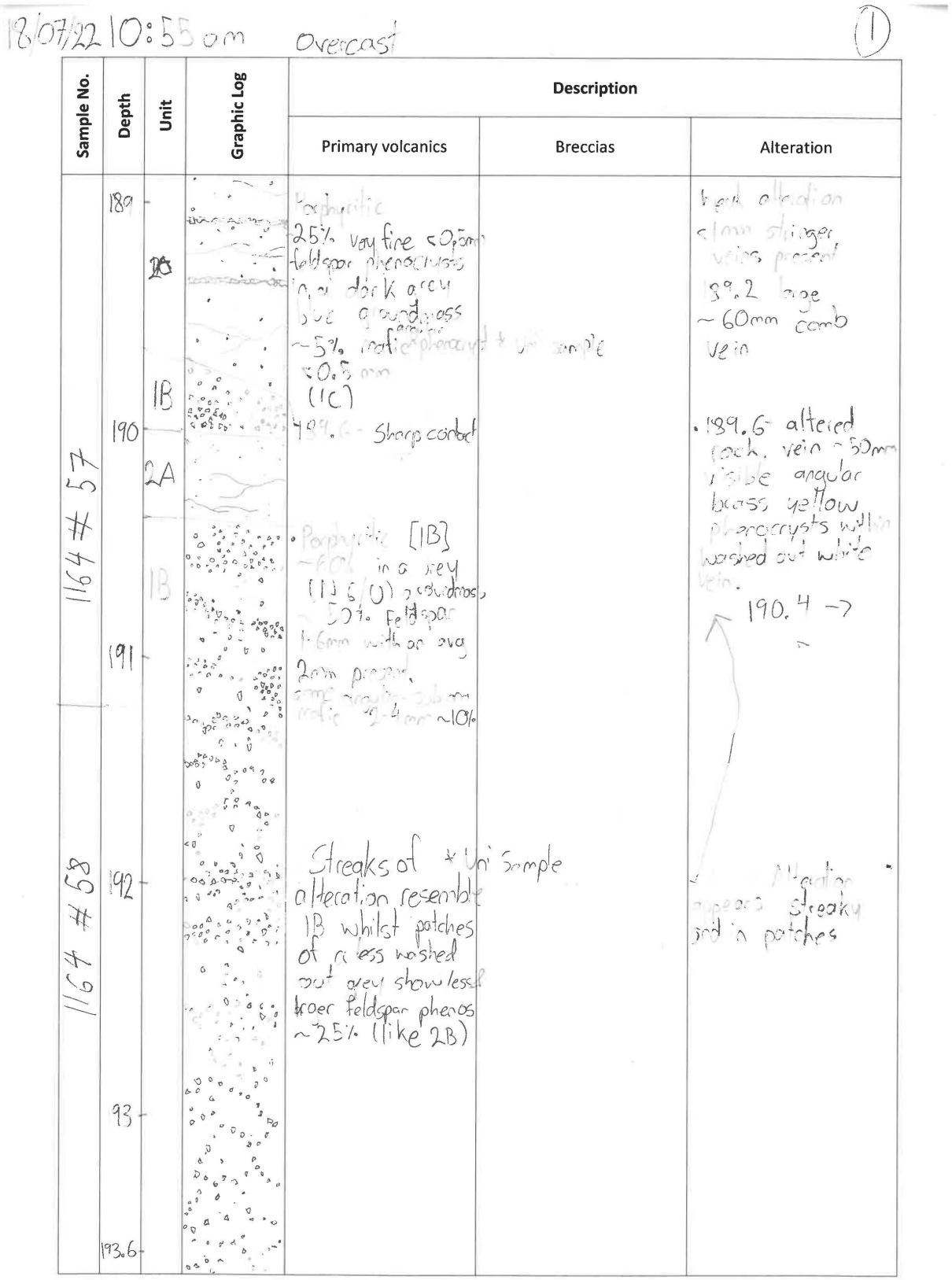

Figure 7: Figure showing core log for drill hole 1164 (7)

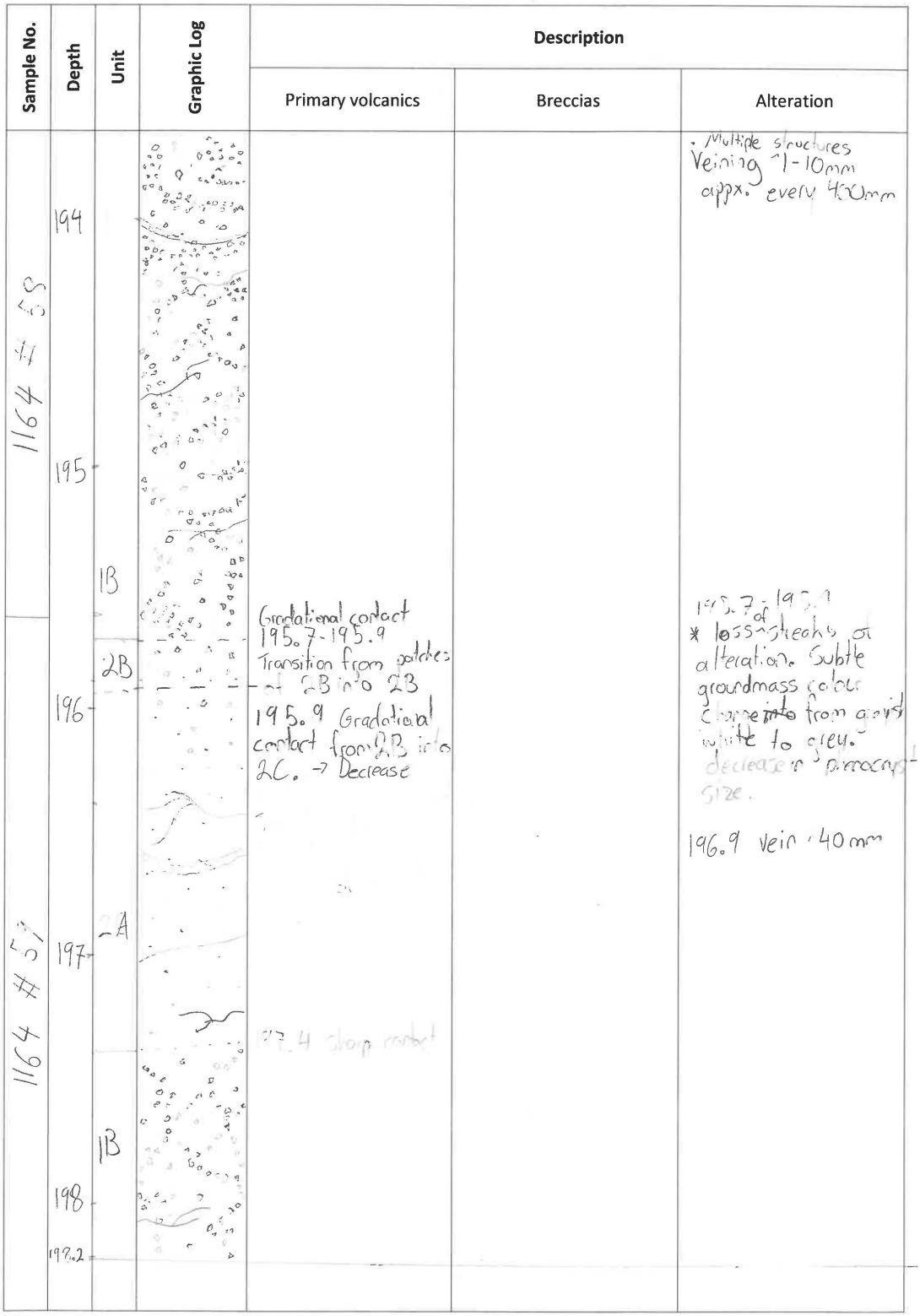

Figure 8: Figure showing core log for drill hole 1164 (8)

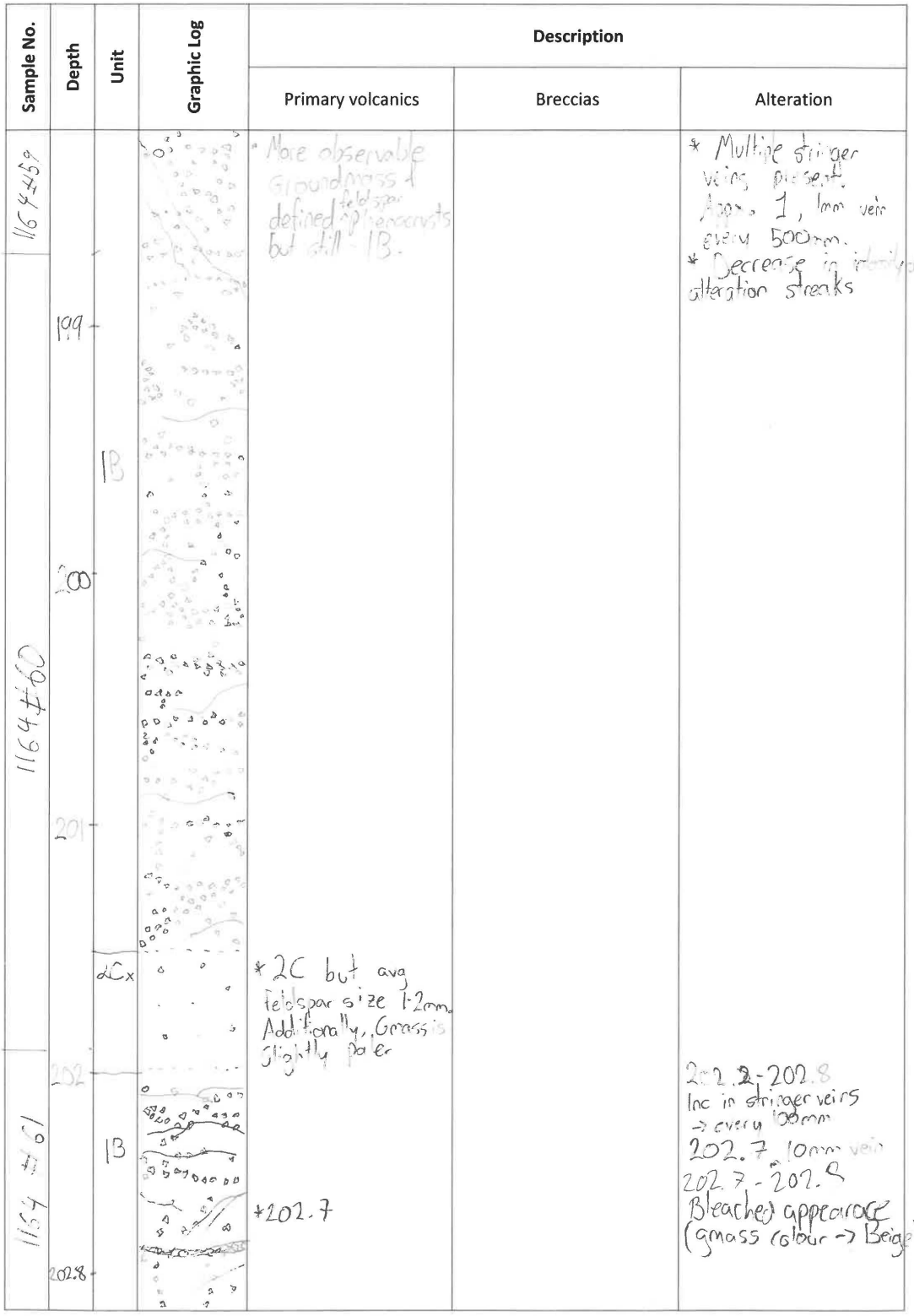

Figure 9: Figure showing core log for drill hole 1164 (9)

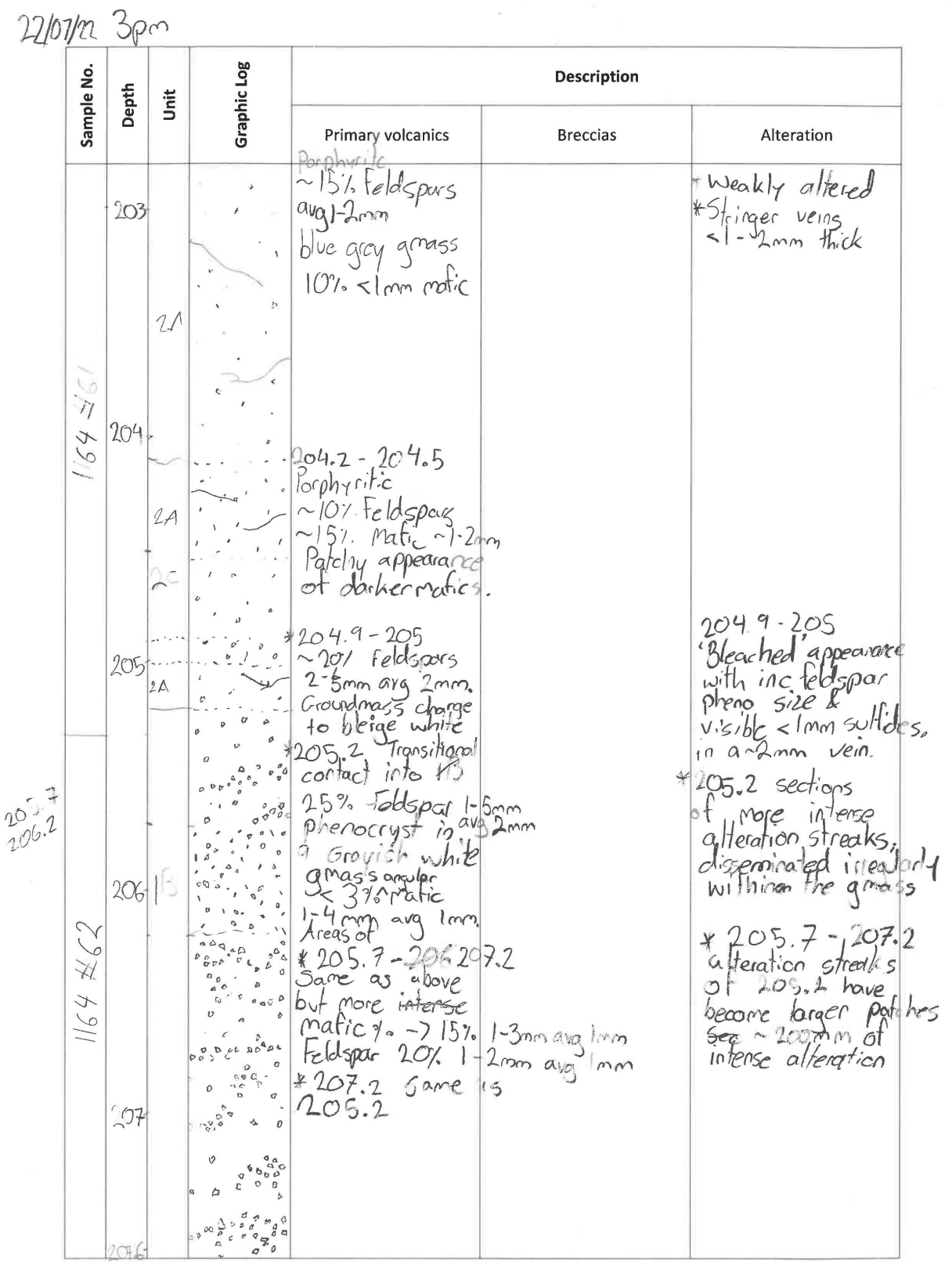

Figure 10: Figure showing core log for drill hole 1164 (10)

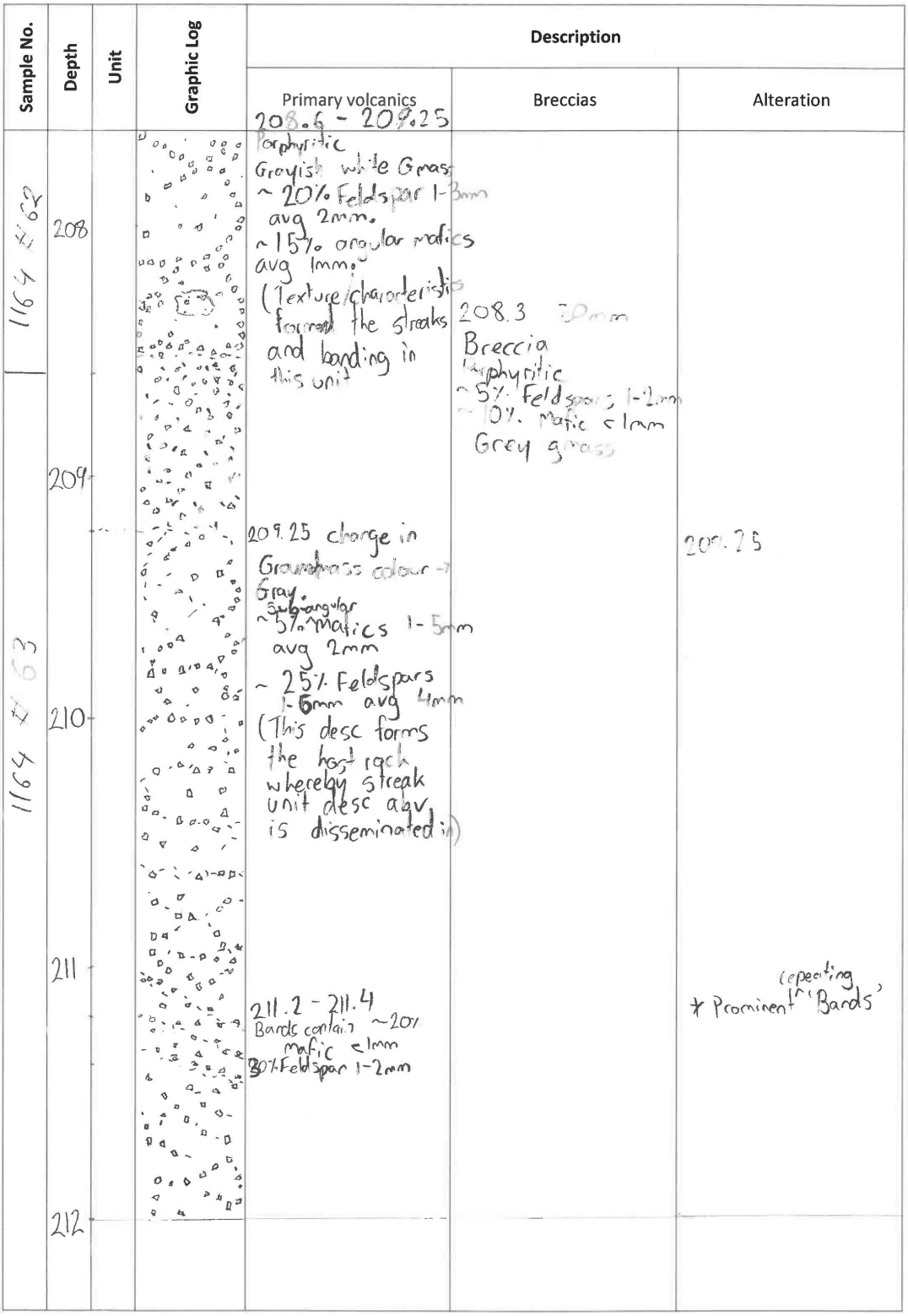

Figure 11: Figure showing core log for drill hole 1164 (11)

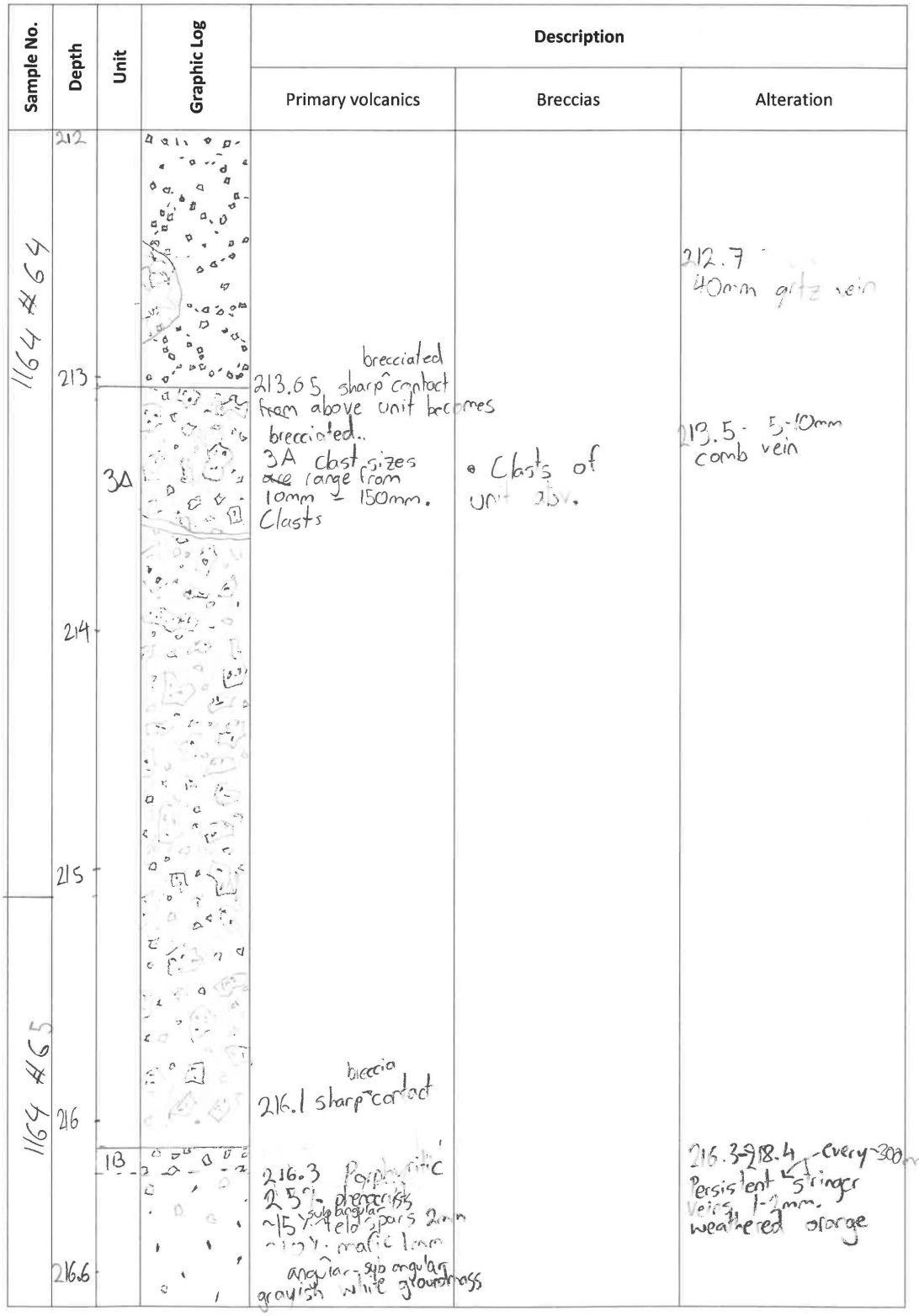

Figure 12: Figure showing core log for drill hole 1164 (12)

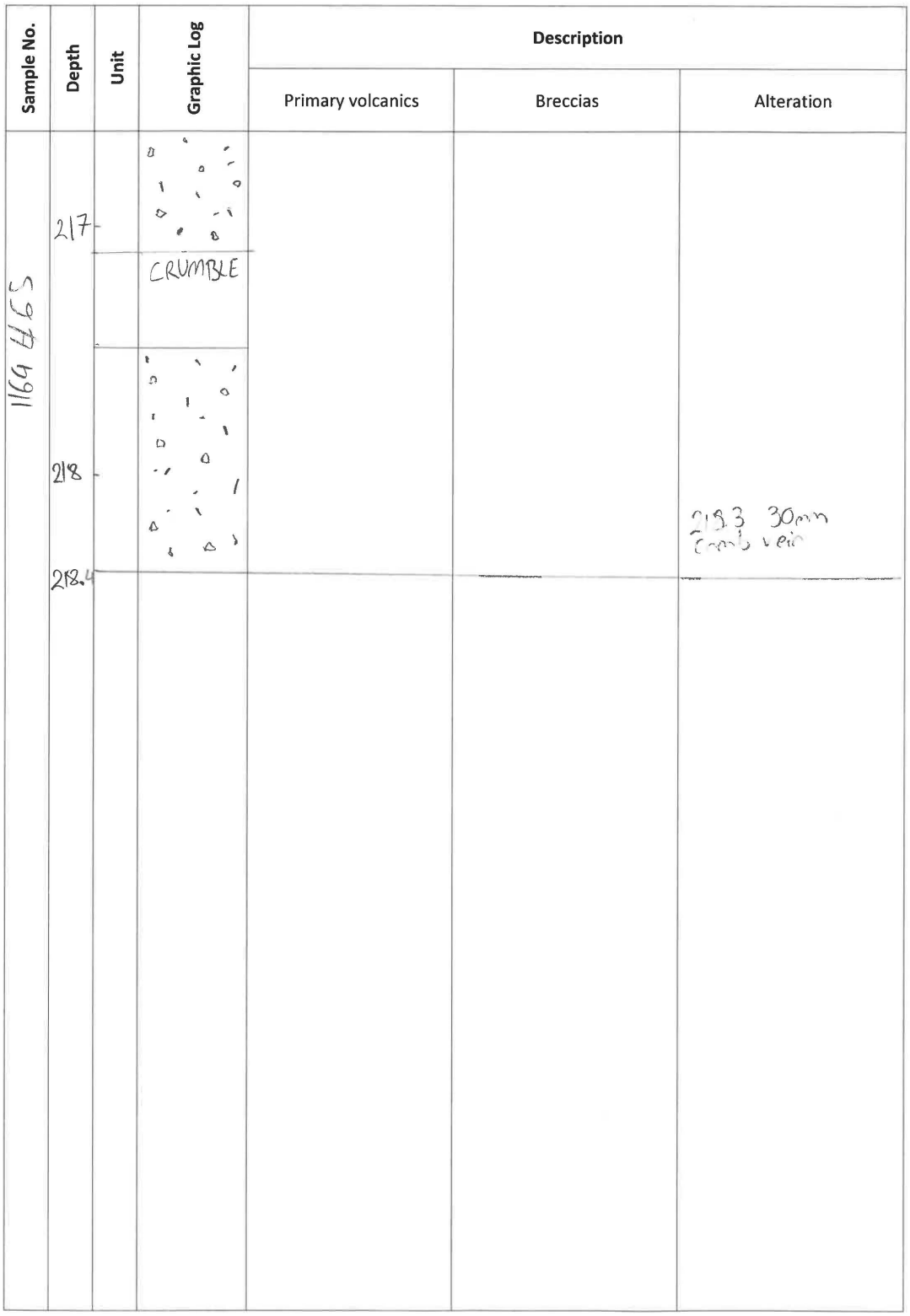

Figure 13: Figure showing core log for drill hole 1164 (13)

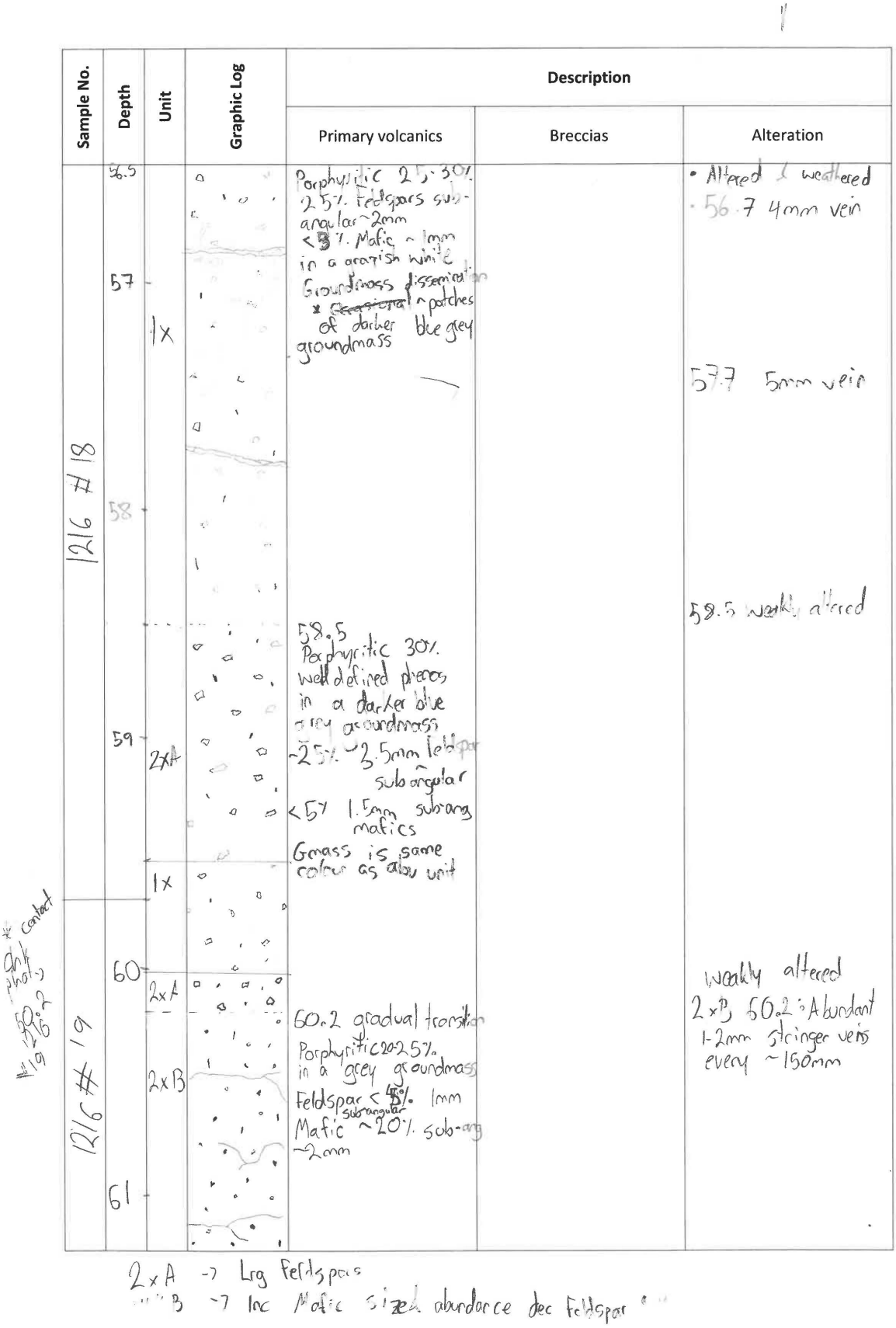

Figure 14: Figure showing core log for drill hole 1216 (1)

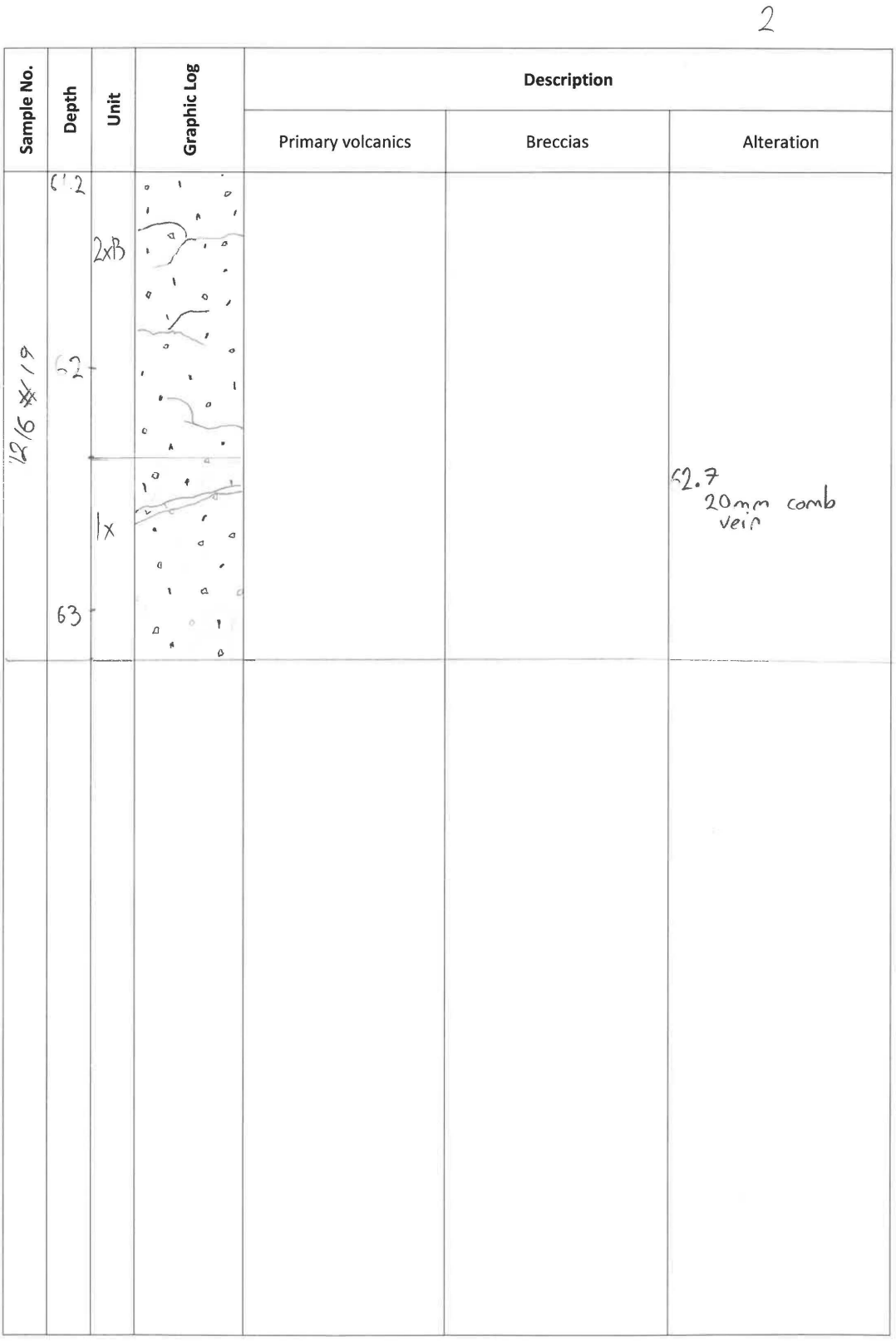

Figure 15: Figure showing core log for drill hole 1216 (2)

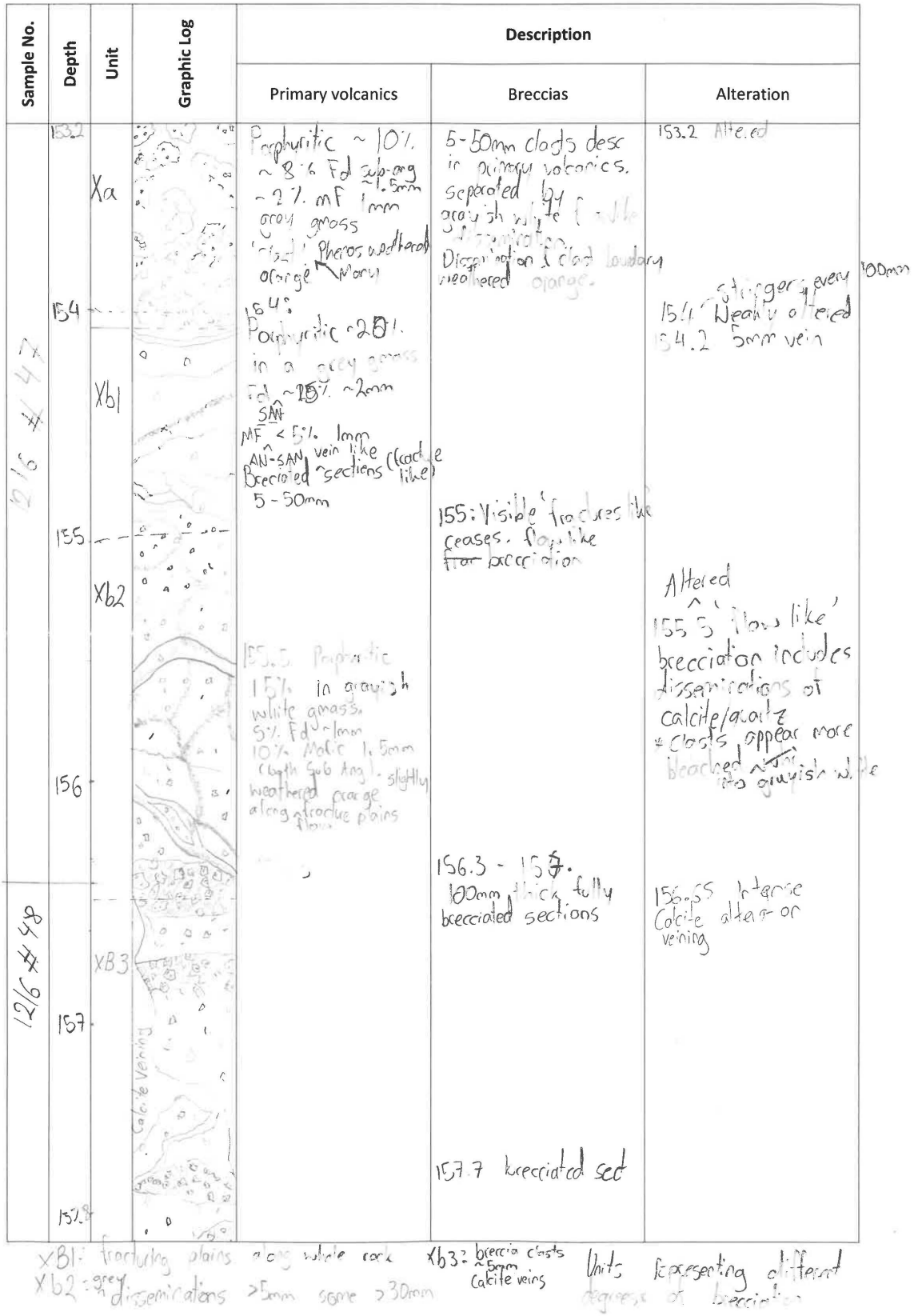

Figure 16: Figure showing core log for drill hole 1216 (3)

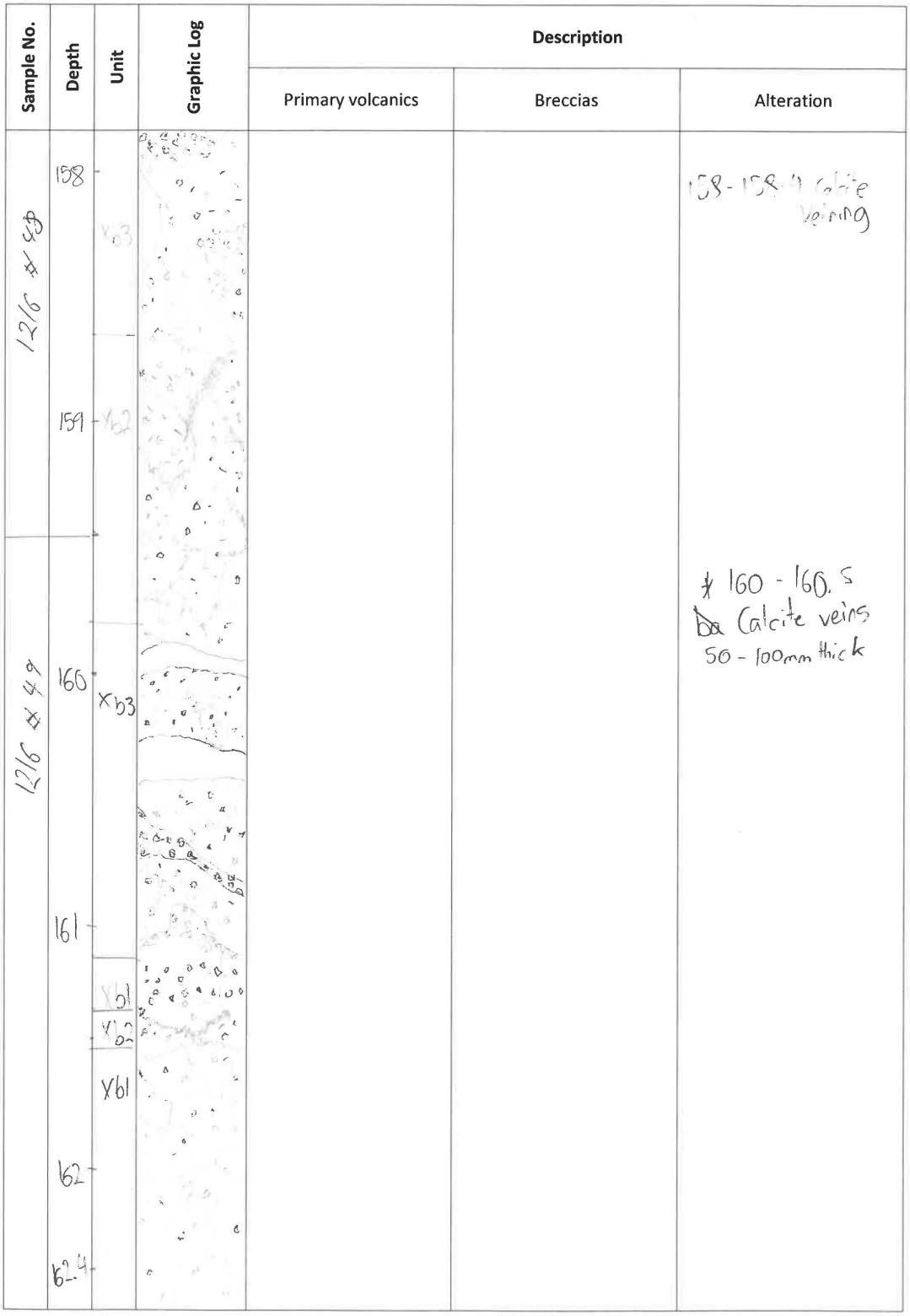

Figure 17: Figure showing core log for drill hole 1216 (4)

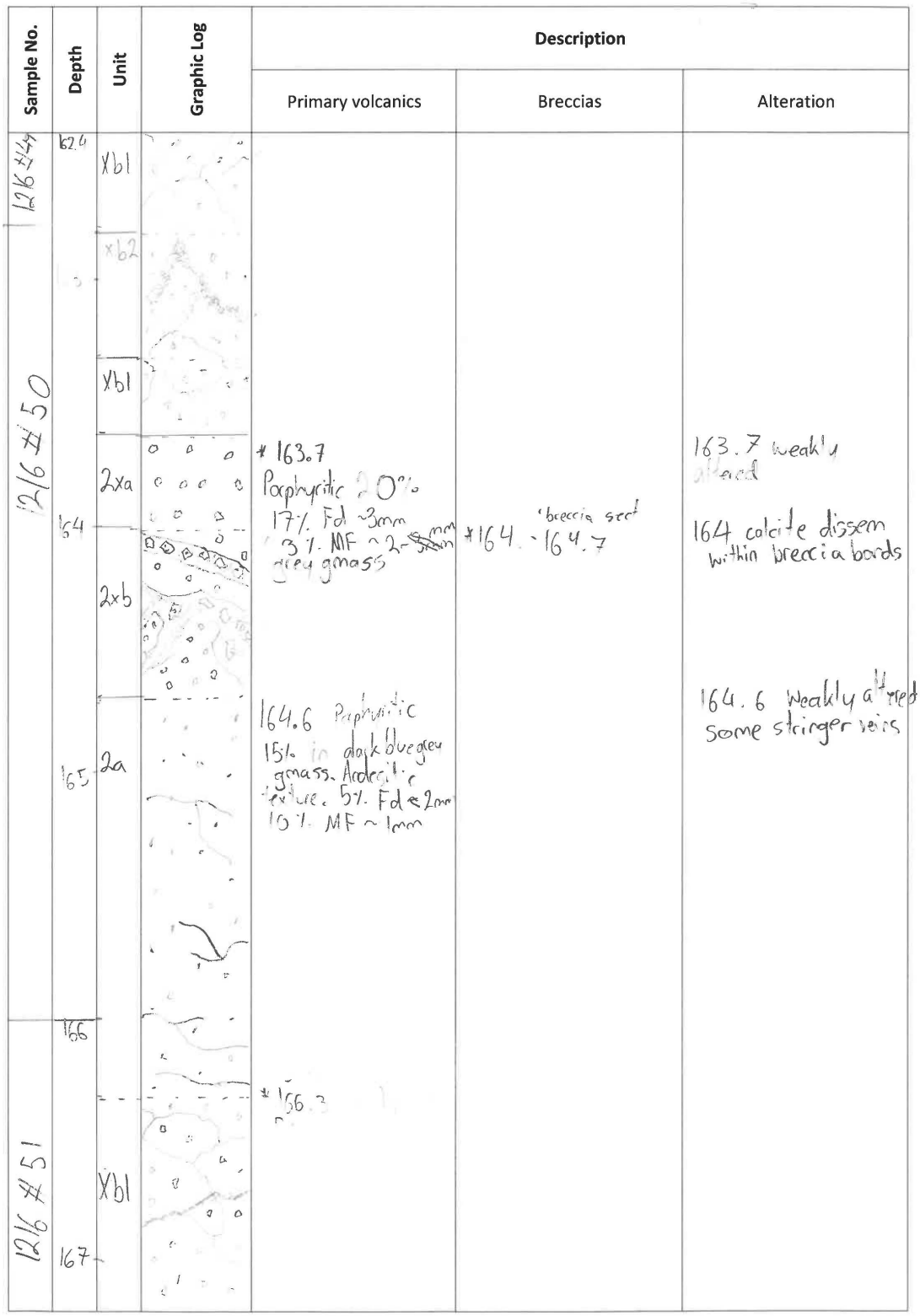

Figure 18: Figure showing core log for drill hole 1216 (5)

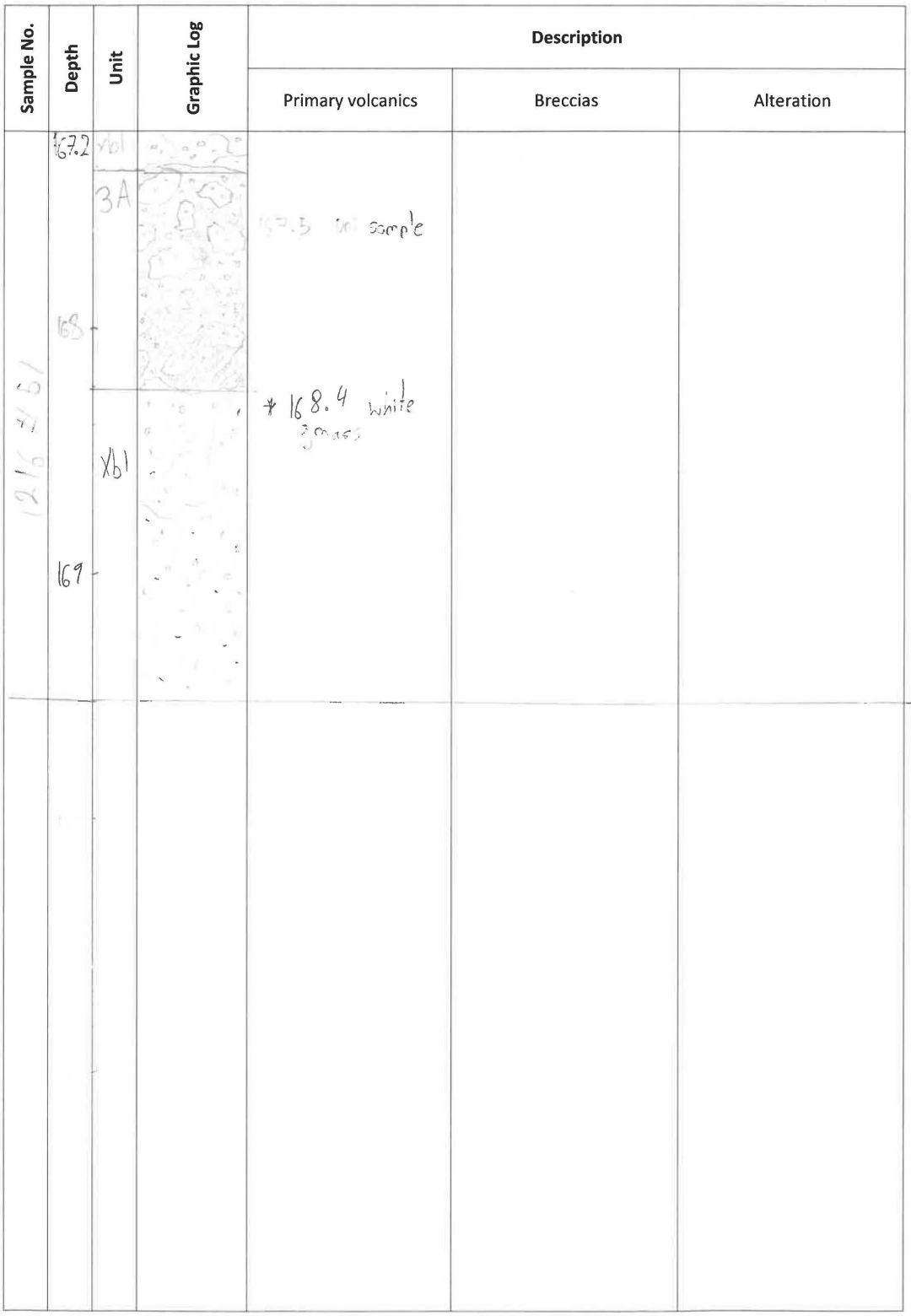

Figure 19: Figure showing core log for drill hole 1216 (6)

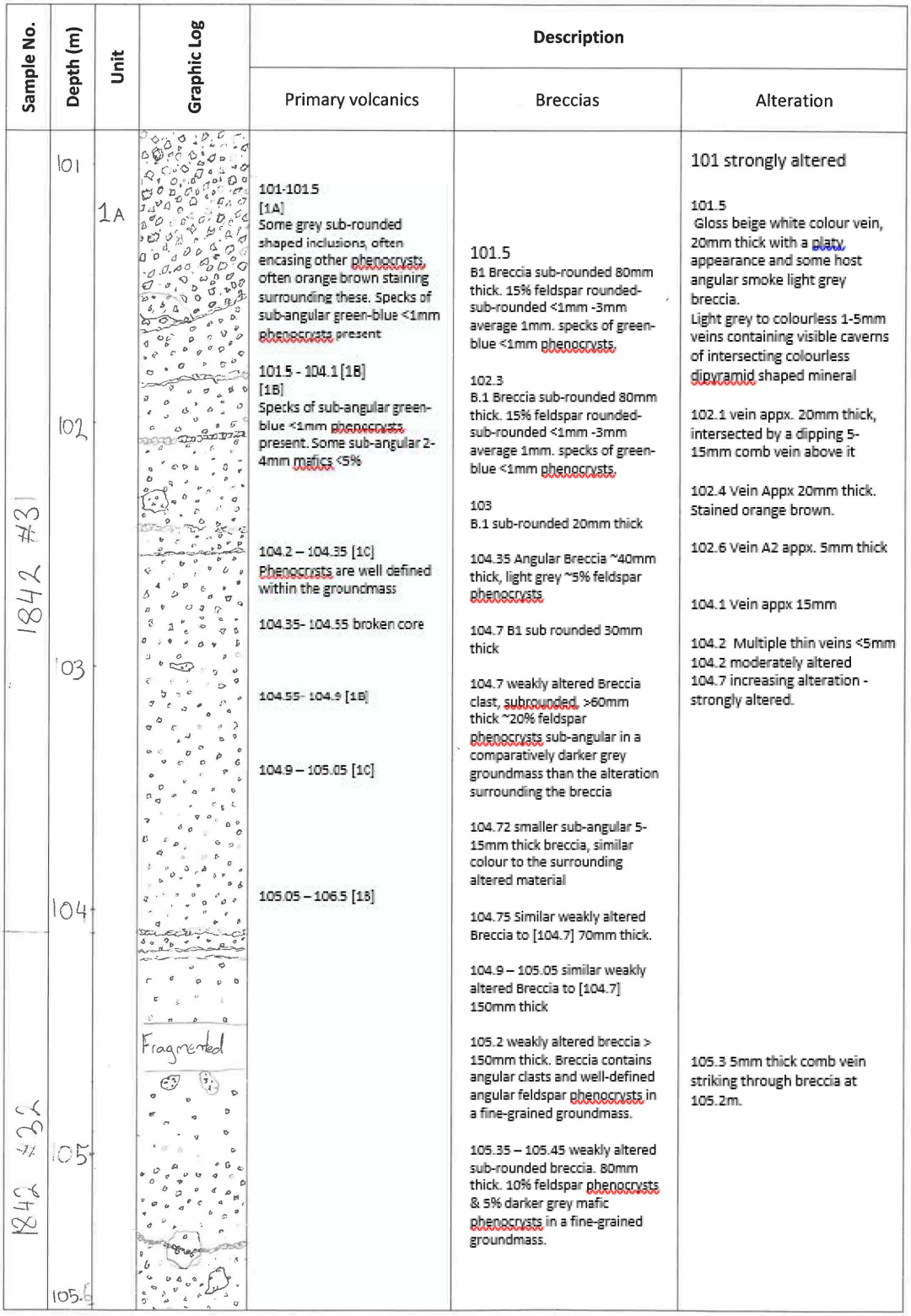

Figure 20: Figure showing core log for drill hole 1842 (1)

2

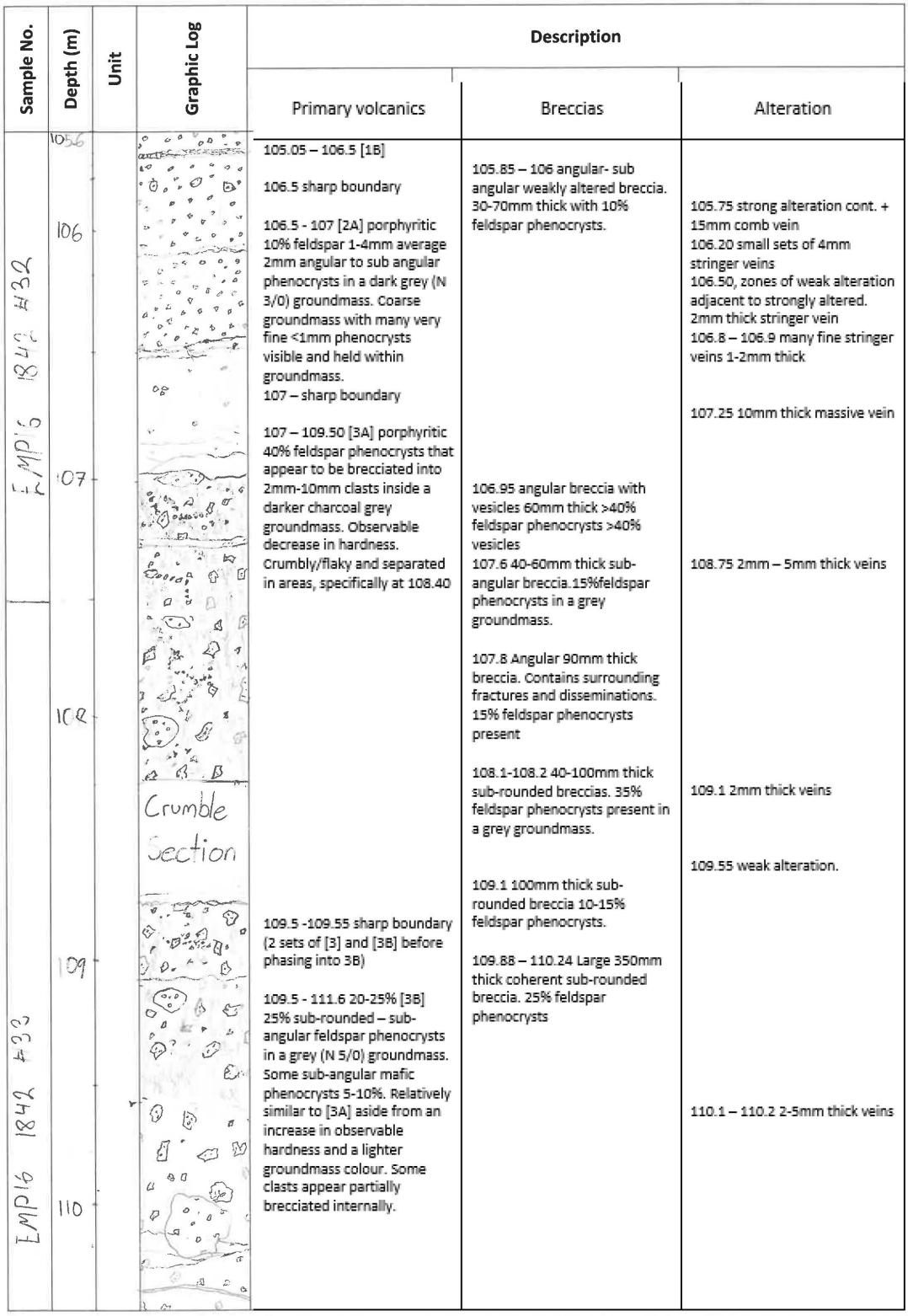

Figure 21: Figure showing core log for drill hole 1842 (2)

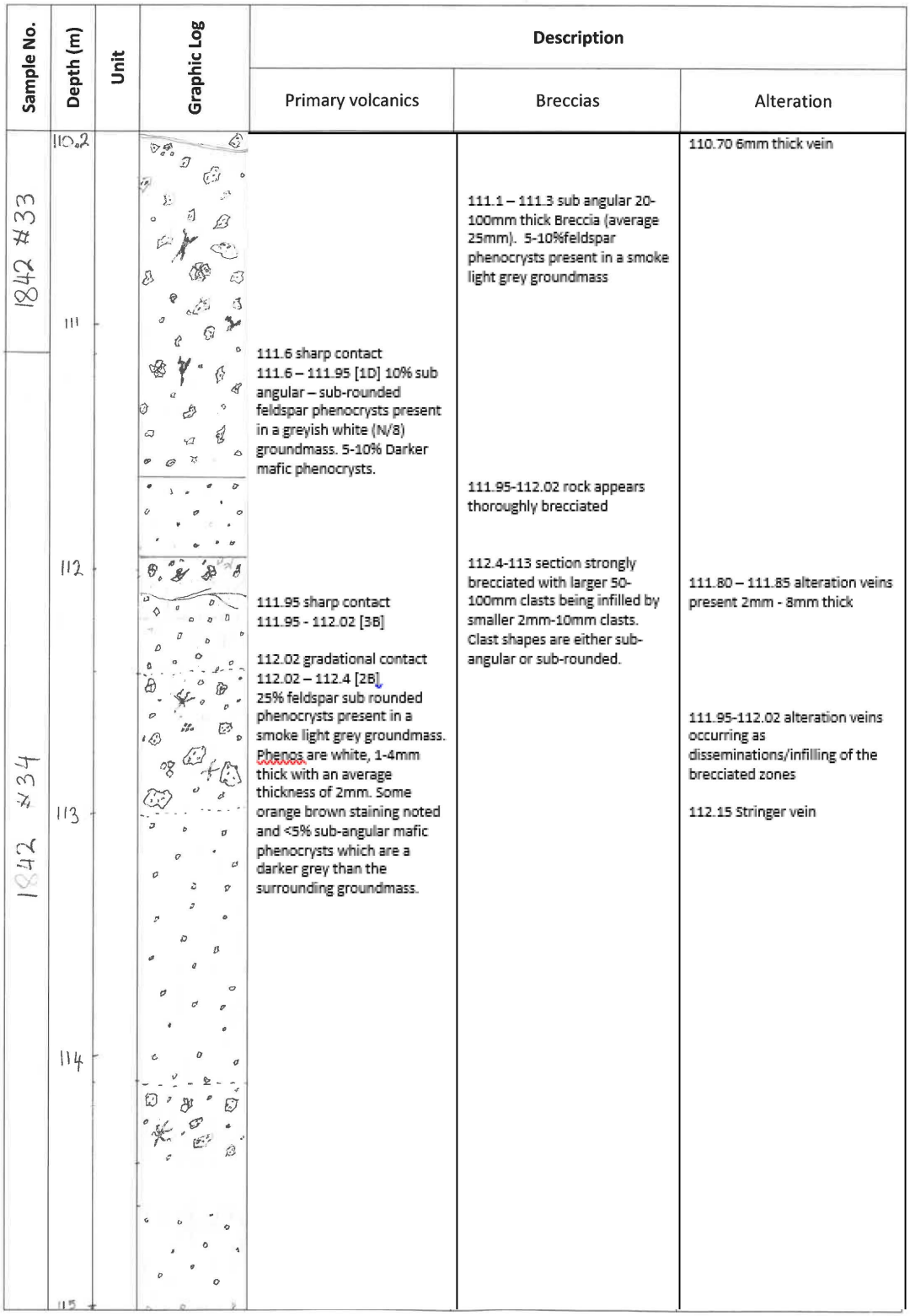

Figure 22: Figure showing core log for drill hole 1842 (3)

4

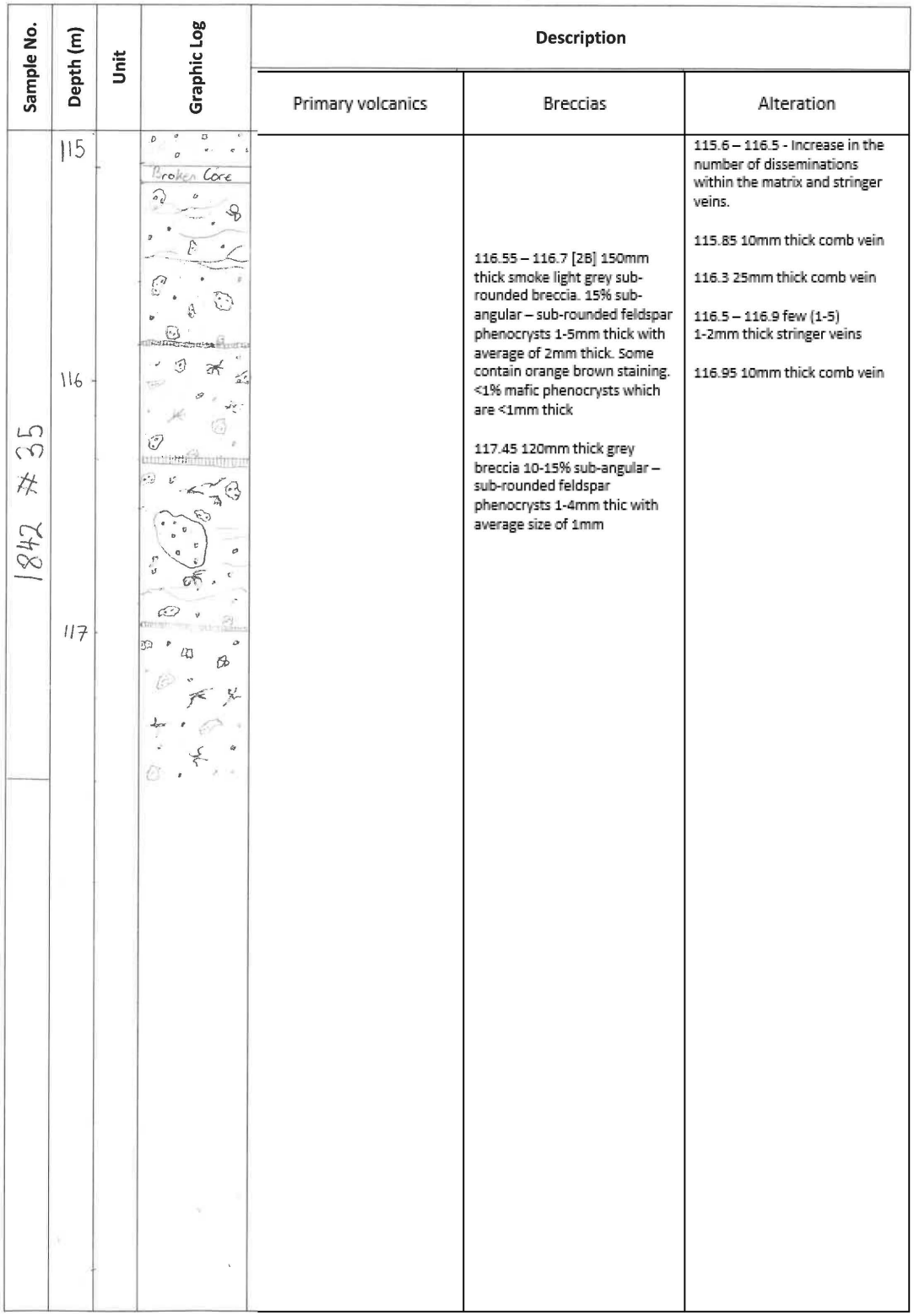

Figure 23: Figure showing core log for drill hole 1842 (4)

5

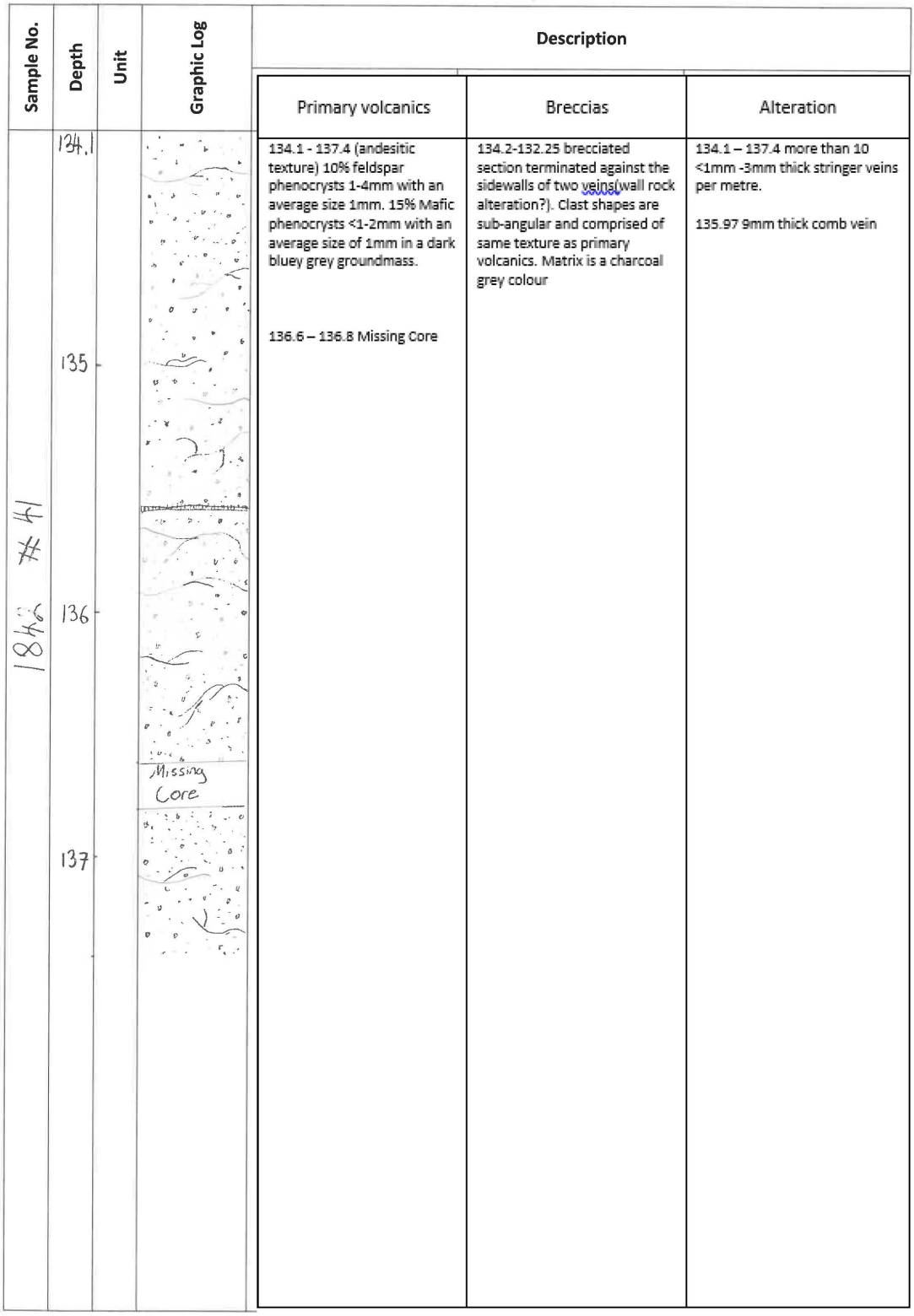

Figure 24: Figure showing core log for drill hole 1842 (5)

New Facies	Old Facies	Thin Sectio	Drill Hole	Depth
A1	1A	TZ:5	1842	101.2
A2	1B	TZ:2	1842	102
A2x	1Bb	TZ:4	1842	102.3
A3	1C	TX:4	1164	205.8
A3	1C	TX:12	1164	205.9
A3	1C	TX:6	1164	206.1
A3	1C	TZ:7	1842	104.2
A4	2A	TX:11	1164	189.3
A4	2A	TX:14	1164	192.1
A4	2A	TX:5	1164	203.1
A4	2A	TZ:3	1842	106.6
A5	2B	TZ:15	1842	113.8
A5	2Bx	TZ:10	1842	112.1
B1	2C	TZ:1	1842	136.2
B2	1D	TZ:14	1842	111.7
C1x	3Ac	TX:8	1216	168
C1	3A	TX:13	1216	168
C1	3A	TX:2	1164	213.8
C1	3A	TX:7	1164	214
C1	3A	TX:16	1164	214.5
C1	3A	TZ:11	1842	107.4
C1	3A	TX:3	1216	167.1
C1x	3A(c)	TX:15	1216	168
C1x	3A(c)	TX 18	1216	167.7
C2	3B	TZ:6	1842	111.37
C2	3Bx	TZ:13	1842	112.6
C2	3C	TZ:8	1842	114.4
C2x	3Bb	TZ:9	1842	111.25
C3b	3Db	TX:9	1216	162.2
C3c	3Dc	TX:1	1216	60.2

Table 1: Heavily altered, primary features thin section descriptions

Facie & Thin Section No.	Primary Textures
A1 [TZ 5]	Porphyritic ≈ 5% quartz, 0.7mm –5mm average size 1.5mm. Embayments & fractures <2% OPX 1mm, 85% heavily altered into a clay sized, grey amorphous fill.
A2 [TZ 2]	Porphyritic 8% anhedral white quartz phenocrysts average 1.5mm thick. Embayments. 15% grey – white euhedral– subhedral plagioclase average 2.4mm thick. Visible twinning/zonation 2% anhedral light orange brown – brown OPX average size 1mm <2% opaque minerals. Opaques consist predominantly of pyrite 0.2mm with smaller <0.01mm phenocrysts of pyrite being disseminated througout the groundmass
A2x [TZ4]	Porphyritic <4% subhedral plagioclase average 2mm thick. 2.5mm anhedral augite phenocryst
A3 [TZ 7]	"Porphyritic. 15% subhedral – anheral plagioclase phenocrysts average size 2.5mm. Common fracturing and light orange brown alteration within fractures/surrounding crystal boundaries. <4% individual anhedral quartz phenocrysts 1mm thick with embayments. 3% average size 2mm–0.40mm average size 0.80mm Opx.
A3 [TX 4]	Porphyritic. <5% anhedral – subhedral white – straw yellow quartz phenocrysts average 0.7mm thick. Straight extinction and embayments. 25–30% greyish white plagioclase with an average size of 1.6mm. Larger phenocrysts appear heavily altered in to a clay or calcite. <1% anhedral brown – green pleochroic hornblende. Average size 0.6mm. <2% anhedral – subhedral light brown – brown pleochroic Orthopyroxene, average size 0.35mm
A3 [TX 6]	Porphyritic. 8% anhedral white quartz phenocrysts average 2mm thick. 25–30% greyish white plagioclase with an average size of 2mm. Larger phenocrysts appear heavily altered in to a clay or calcite.
A3 [TX 12]	Porphyritic <4% anhedral white quartz phenocrysts average 0.8mm thick. 20–25% grey – white euhedral– subhedral plagioclase average 2mm thick within the altered calcite crystals. Visible twinning/zonation. 5 – 10% Orthopyroxene
A4 [TZ 3]	Porphyritic. 7% anhedral white quartz phenocrysts average 0.5mm thick. Embayments. 7% grey – white euhedral– subhedral plagioclase average 1.4mm thick. Visible twinning/zonation. 2% anhedral light orange brown – brown OPX average size 1mm. 15% 0.5mm – 2.5mm patches of opaque minerals. These larger patches of opaques consist predominantly of pyrite with very minor <1% smaller <0.01mm phenocryst inclusions of chalcopyrite+–arsenopyrite. Some anhedral 0.01mm patches of galena also present.
A4 [TX 5]	Porphyritic. <5% anhedral white quartz phenocrysts average 3.5mm thick. 25–30% greyish white plagioclase with an average size of 1.75mm. Evident twinning and zonation in most phenocrysts

A4 [TX 11]	Porphyritic. <4% anhedral white quartz phenocrysts average 0.8mm thick. 20–25% grey – white euhedral– subhedral plagioclase average 2mm thick within the altered calcite crystals. Visible twinning/zonation.
A5 [TZ 15]	Porphyritic20%. 15% subhedral – anhedral plagioclase. Phenocrysts size varies from 0.5mm – 4mm. Average size 1.2mm. Some plagioclase phenocrysts have a 0.05mm concentric rim of alteration 1. Some <0.25mm OPX inclusions within plagioclase phenocrysts.%OPX yellow,orange brown PPL. 1st order purple,blue,prange,yellow XPL. Average size 0.2mm. < 1 % opaque minerals mostly 0.1 mm pyrite disseminations and some sphalerite.
A5 [TZ 10]	Porphyritic 15%. 1% anhedral quartz. Average size 0.6mm. Single 4.5mm quartz phenocryst present. 8% subhedral–anhedral plagioclase 1mm. Twinning. 3% anhedral –subhedral OPX. Average size 0.5mm. Colourless – murky brown [PPL].1st order grey,yellow,reds [XPL]. Slighty pleochroic light brown to brown. <1% opaque minerals, predominantly disseminations of < 0.05mm pyrite.

Table 2: Heavily altered, groundmass/matrix descriptions

Facie & Thin Section No.	Groundmass / matrix
A1 [TZ 5]	Groundmass which consists of: 30–35% calcite disseminations 25–30%Very fine fragmented quartz grains 0.01 –0.05mm. Observable undulose extinction. <10% opaque euhedral–subhedral phenocrysts of pyrite concentrated in zones with an average size 0.4mm. Some galena and magnetite also present <1% 0.5mm. Sphaelerite <1% 0.1mm 25–30% <1micron clay sized amorphous grey pseudomorphs. Grey under PPL & XPL.
A2 [TZ 2]	"65–70% Groundmass which consists of: 20% calcite disseminations. 20% <1micron thick disseminations of a sooty amorphous clay sized brown specks. This clay sized speck is orange–yellow–grey under XPL and continuous as a sort of infilling within the groundmass. 25% anhedral white–grey mostly quartz+–plagioclase –prominent undulose extinction. 25–30% <1micron clay sized amorphous grey pseudomorphs. Grey under PPL & XPL. Often angular shaped phenocryst/microlite grains, that have been entirely altered to this matte grey. 10% opaque <0.01mm subhedral–anhedral phenocrysts of 'mostly' pyrite."
A3 [TZ 7]	Groundmass. 35–40% quartz +–plagioclase microlites. 40 – 45% <1micron clay sized amorphous grey under PPL & XPL. <5% opaque minerals (mostly pyrite) disseminated within the groundmass. 10% [PPL] light orange brown mineral appears fibrous with a concentric rim in [PPL] and [XPL].Visible individual grains are 5microns and grey with undulose extinction under [XPL].

A2x [TZ4]	"90% groundmass which consists of: 50–55% <1micron thick disseminations of a sooty amorphous clay sized brown filling. This clay sized fill is orange–yellow–brown–grey under XPL. 35% anhedral white–grey mostly serpentine+– quartz – prominent undulose extinction. 15% opaque <0.01mm subhedral–anhedral phenocrysts of 'mostly' pyrite.
A3 [TX 4]	Approx 55 – 60% matrix, of which: 40–45% white plagioclase microlites average 0.04mm thick. <5% calcite. 35–40% alteration 1. Dark yellow brown to grey patches in both [PPL] & [XPL] almost amorphous. Found as a patchy appearance within relict plagioclase microlites and phenocrysts. Clay like. 10–15% alteration 2. golden brown yellow clay like.
A3 [TX 6]	50% groundmass of which: 55–60% white plagioclase microlites average 0.05mm thick. 10–15% calcite. 35–40% alteration 1. Dark yellow brown to grey patches in both [PPL] & [XPL] almost amorphous. Found as patches/cement within the groundmass and surrounding some phenocrysts. Likely type of clay.
A3 [TX 12]	60 – 65% groundmass of which: 25 – 30% white plagioclase microlites average <0.1mm thick. 5% anhedral white quartz phenocrysts. 30 –35% grey patches in both [PPL] & [XPL] almost amorphous. Found as patches/cement within the groundmass and surrounding some phenocrysts. Likely type of clay. 5–10% anhedral yellow orange brown [PPL] & [XPL] almost amorphous. Some have a radial streaks of yellow brown stretching from a centre point. A potential type of clay. <5% calcite.
A4 [TZ 3]	65–70% Groundmass which consists of: 15% <1micron thick yellow–orange brown mineral. 35% anhedral beige white [PPL] white–grey mostly quartz+– plagioclase –prominent undulose extinction. 35% <1micron clay sized amorphous grey pseudomorphs. Grey under PPL & XPL. Often angular shaped phenocryst/microlite grains, that have been entirely altered to this matte grey. 15% opaque <0.01mm subhedral–anhedral phenocrysts of 'mostly' pyrite.
A4 [TX 5]	60 – 65% groundmass of which: 65 –70% white plagioclase microlites average 0.05mm thick. 15–20% calcite with a high birefringence colour showing an oil slick like appearance.
A4 [TX 11]	50 – 55% groundmass of which: 45 – 50% white plagioclase microlites average <0.1mm thick. 5% anhedral white quartz phenocrysts. 20 –25% grey patches in both [PPL] & [XPL] almost amorphous. Found as patches/cement within the groundmass and surrounding some phenocrysts. Likely type of clay. 10–15% yellow orange brown [PPL] & [XPL] almost amorphous. Radial streaks of gold brown stretching from a centre point. A potential type of clay. <5% calcite.
A5 [TZ 15]	35–40% anhedral plagioclase microlites with very altered mineral boundaries. 50–55% alteration 1 as an interstitial fill among microlites. 10% subhedral – anhedral OPX (as described in primary features). <5% Alteration 2.
A5 [TZ 10]	Groundmass 85%. Laths of plagioclase. Average size <0.25mm. 15% Alteration 1 30–35% Alteration 2 disseminations

Table 3: Heavily altered, alteration descriptions

Facie & Thin Section No.	Alteration
A1 [TZ 5]	Extremely altered thin section. Calcite present 20%. Speckled colourless to light yellow–brown mineral present 30%. Murky brown alteration 10% and grey amorphous disseminations 40%.
A2 [TZ 2]	Very altered thin section. Many plagioclase crystals are thoroughly fractured with calcite disseminations within the fracture points. 10% patches of calcite alteration patches within the plagioclase phenocrysts. As discussed within the groundmass section, there were two alteration minerals present <1micron thick, the sooty amorphous brown infill and the patchy amorphous grey under XPL and PPL. Barren 0.25mm vein of quartz.
A3 [TZ 7]	"Very altered thin section. 15% calcite alteration observed in plagioclase phenocrysts. Opx heavily altered into disseminations of a grey amorphous mineral [PPL&XPL] and a pervasive orange brown staining. Barren 9mm thick quartz vein. Barren 2.5mm thick quartz dissemination
A2x [TZ4]	Extremely altered thin section 15% calcite within the thin section with some calcite pseudomorphs and any relict plagioclase phenocrysts being almost entirely (>90%) altered to calcite. High presence of the sooty amorphous orange–yellow–brown clay sized mineral discussed in the groundmass. This mineral appears grey when concentrated and appears to fade in to a light orange–brown where the thin section is thinner.
A3 [TX 4]	Altered <10% calcite found as partial or complete alteration of plagioclase crystals. <2% 'opaque' mostly pyrite anhedral phenocrysts appearing as singular clasts dotted sporadically throughout the thin section. Alteration 1: Dark yellow brown to grey patches in both [PPL] & [XPL] almost amorphous. Found as a patchy appearance within relict plagioclase microlites and phenocrysts. Clay like. Alteration 2: golden brown yellow clay like.
A3 [TX 6]	Altered. 20 –25% calcite found as partial or complete alteration of plagioclase crystals. <4% 'opaque' anhedral phenocrysts, which consist of pyrite, galena, chalcopyrite, sphalerite. Alteration 1: Dark yellow brown to grey patches in both [PPL] & [XPL] almost amorphous. Found as patches/cement within the groundmass and surrounding some phenocrysts. Likely type of clay.

A3 [TX 12]	Very altered 5% anhedral calcite. <4% 'opaque' subhedral – anhedral pyrite 0.12mm thick located as sporadic phenocrysts throughout the thin section. More abundant within the veining section striking through the thin section. Some sphalerite present. Some minor concentrations of galena, average thickness <0.1mm. Yellow orange staining surrounding pyrite bearing veins. Alteration 1: grey patches in both [PPL] & [XPL] almost amorphous. Found as patches/cement within the groundmass and surrounding some phenocrysts. Clay–like. Alteration 2: anhedral yellow orange brown [PPL] & [XPL] almost amorphous. Some have a radial streaks of yellow brown stretching from a centre point. A potential type of clay.
A4 [TZ 3]	>80% Altered thin section. Plagioclase crystals are altered 15% into patches of calcite within the well defined phenocryst. As discussed within the groundmass section, there were two clay sized alteration minerals present <1micron thick. The amorhphous yellow–orange brown and the amorphous grey. High concentration of sulfides within the thin section.
A4 [TX 5]	Weakly altered 10% calcite found as partial or complete alteration of plagioclase phenocrysts and microlites. <3% 'opaque' anhedral phenocrysts, which consist of predominantly pyrite average thickness 0.12mm and some sphalerite & chalcopyrite. Alteration 1: 15–20% grey patches in both [PPL] & [XPL] almost amorphous. Found as patches/cement within the groundmass and surrounding some phenocrysts. Clay sized.
A4 [TX 11]	Altered groundmass, plagioclase phenocrysts still >90% intact 5% anhedral calcite. <4% 'opaque' subhedral – anhedral pyrite 0.12mm thick located as sporadic phenocrysts throughout the thin section. More abundant within the veining section striking through the thin section. Some minor concentrations of galena, average thickness <0.1mm. Yellow orange staining surrounding pyrite veining. Quartz veining. Alteration 1: grey patches in both [PPL] & [XPL] almost amorphous. Found as patches/cement within the groundmass and surrounding some phenocrysts. Likely type of clay. Alteration 2: yellow orange brown [PPL] & [XPL] almost amorphous. Radial streaks of gold brown stretching from a centre point. Clay–like.
A5 [TZ 15]	Very Altered 50–75%. Calcite partially altering 10% plagioclase phenocrysts. Alteration 1: amorphous grey – dark brown. Opaque to very dark grey under XPL. Alteration 2: Brown under PPL. Individual grains appx. 10microns and goes opaque with some orange colouration (internal reflections?).
A5 [TZ 10]	Very altered 50–75%. 5–15% Calcite alterating larger plagioclase phenocrysts. Alteration 1: Brown anhedral fibrous appearance mineral with extinction parallel to each fibrous strand under [XPL]. 30–35% Alteration 2: Grey – brown amorphous mineral. Average size <1micron. 5–10% OPX (same as described in primary features) 0.02mm – 0.10mm

Table 4: Weakly altered, primary texture descriptions

Facie & Thin Section No.	primary texture
B1 [TZ 1]	"Porphyritic <3% anhedral white quartz phenocrysts average 0.5mm thick. Embayments and slightly fractured. 20% grey – white subhedral with some anhedral plagioclase average 2mm thick. Visible twinning/zonation. 15% Mostly anhedral (some subhedral) grey – 1st order red OPX with an average size 1.8mm. olive green to lighter green pleochroism. Red orange discolouration as a centre fill in some grains. <1% anhedral Clinopyroxene 0.10mm. <1% Opaques, subhedral – anhedral <0.1mm pyrite +– Galena. There are also very few 0.01mm chalcopyrite inclusions.
B2 [TZ 14]	Porphyritic. 3% anhedral quartz. Average size 2mm. 15% subhedral–anhedral plagioclase. Size ranges from 0.5mm – 3mm with an average size 2mm. Some phenocrysts contain a concentric outer alteration rim. This rim is a partial 65% shade of an amorphous grey mineral. 8% subhedral–anhedral OPX. 0.25mm–1.5mm. Light brown – brown pleochroism. Low 1st order orange,yellow and greys under XPL. <2% opaque minerals, <0.1 mm pyrite and some sphalerite within crystal grains and groundmass.

Table 5: Weakly altered, groundmass / matrix descriptions

Facie & Thin Section No.	Groundmass / Matrix
B1 [TZ 1]	65% Groundmass which consists of: 70% <1mm thick laths of plagioclase. Laths appear as a fibrous texture in some areas of the thin section. 15% 0.1mm – 0.2mm anhedral Opx. <1% subhedral – anhedral Cpx average size of 0.1mm. 15% <1micron thick pervasive sooty amorphous charcoal grey–opaque patches under PPL & XPL. Strongly present within the groundmass and clouding the OPX phenocrysts – whilst rarely being observed over a plagioclase phenocryst.
B2 [TZ 14]	Groundmass 40–45%. Laths of plagioclase 0.01mm – 0.15mm. 5% alteration 1 <0.05mm 40–45% alteration 2. Interstitial mineral between other groundmass microlites. 5% OPX. (Same as larger phenocrysts described in primary features). Average size <0.25mm.

Table 6: Weakly altered, alteration descriptions

B1 [TZ 1]	weakly altered thin section. A hazy green brown concentric rim of alteration surrounding some plagioclase phenocrysts. 10–15% of larger phenocrysts contain disseminations of calcite as an alteration product. The pervasive sooty amorphous charcoal grey patches discussed in the groundmass section. 1mm calcite vein with 15% sub–hedral – anhedral quartz 0.45mm. There are also some sulfide inclusions within the vein centre. <2% 0.04mm anhedral pyrite and <1% 0.01mm chalcopyrite.
B2 [TZ 14]	Weakly altered 25% *No calcite alteration Alteration 1: orange brown–brown PPL, light orange, yellow and grey under XPL. Alteration 2. Amorphous grey – grey brown. Opaque with a brown tinge under XPL.

Table 7: Table description for breccia primary textures

Facie & Thin Section No.	Breccia primary texture
C1 [TZ 11]	Porphyritic. 2% anhedral quartz. Average size 0.25mm. <1% OPX rare and altered. 1% anhedral plagioclase 0.12mm fragments. 55% Breccia clasts <0.2mm – 2mm. Average size 0.8mm: Breccia 1: 2mm with; disseminated 5% Calcite 8% anhedral pseudomorphs of alteration 4. 15–20% subhedral – nahedral alteration 1. 60% colourless – brown groundmass [PPL] and opaque in XPL with <0.01mm fine grey inclusions showing no colour change with stage rotation. Anhedral pseudomorphs of alteration 2. Other Breccia clasts are mostly coherent fragments of alterations (1–4) described in the alteration section. Rare <1% opaque minerals. <0.01 mm pyrite pyrite disseminations with some 0.2 mm crystals. Some sphalerite <0.2 mm.
C1 [TX 2]	Porphyritic. 10% anhedral – subhedral white – straw yellow quartz phenocrysts average 0.25mm thick. Straight extinction present. Some phenocryst display embayment's <3% greyish white euhedral– subhedral plagioclase < 0.02mm thick within the altered calcite crystals. Visible twinning/zonation.
C1 [TX 7]	Porphyritic. 8% anhedral white quartz phenocrysts average 3.2mm thick. <10% greyish white plagioclase with an average size of 2mm. Larger phenocrysts appear heavily altered in calcite.
C1 [TX 13]	Porphyritic <3% anhedral white quartz phenocrysts average 0.7mm thick. Undulose extinction, prominent fractures. 20% grey – white euhedral– subhedral plagioclase average 1.6mm thick within the altered calcite crystals. Visible twinning/zonation. 15% anhedral yellow–orange brown Opx, 0.7mm thick.
C1 [TX 16]	Porphyritic 5% anhedral white quartz phenocrysts average 0.6mm thick. Fractures 20% grey – white euhedral– subhedral plagioclase average 0.9mm thick. Visible twinning/zonation. 2% anhedral light orange brown – brown OPX average size 0.35mm. 55% Breccia clasts: All clasts contain an interstitial fill of an amorphous grey mineral. Some clasts contain very fractured/disjointed average 0.2mm plagioclase phenocrysts with a prominent radial orange brown interstitial fill. Other clasts made up of 35% 0.5mm plagioclase phenocrysts and some larger 10% 1mm subhedral plagioclase phenocrysts. Other clasts contain 20% 2mm fractured plagioclase phenocrysts in a groundmass occupied by a mixture of <5% calcite and 35% 0.04mm feldspar +– quartz.
C1x [TX 8]	Porphyritic. <2% anhedral white quartz phenocrysts average 0.8mm thick. 30 – 35% greyish white euhedral– subhedral plagioclase 2.2mm thick within the altered calcite crystals. Visible twinning/zonation.
C1x [TX 15]	Porphyritic. <3% anhedral white quartz phenocrysts average 0.7mm thick. Undulose extinction, prominent fractures. 20% grey – white euhedral– subhedral plagioclase average 1.6mm thick within the altered calcite crystals. Visible twinning/zonation. 15% anhedral yellow–orange brown Opx, 0.7mm thick.

C2 [TZ 6]	Porphyritic 12% subhedral – anhedral plagioclase phenocrysts average size 1.7mm. <5% anhedral Quartz average size 0.8mm, showing some embayments and fracturing. <1% euhedral Cpx 0.1mm. <2% anhedral Opx 0.25mm. <3%% Opaque minerals; mostly consisting of pyrite <0.15mm. Some galena 0.05 – 0.1mm. Observed sphaelerite 0.1mm
C2x [TZ 9]	Porphyritic 10%. 7% subhedral–anhedral plagioclase. Average size <0.08mm. 3% anhedral quartz. Average size 0.7mm. Embayments.
C2 [TZ 13]	3% anhedral quartz. Average size 0.25mm. <2% anhedral plagioclase. Average size 0.2mm. Heavily altered to mostly calcite. Breccia clasts 65–70%. Breccia 1: 15% alteration 3 35–40% alteration 1. 40–45% interstitial laths of plagioclase 0.01mm – 0.02mm centrally concentrated in clasts. Breccia 1 within the thin section has an unusual 1mm thick intrusion penetrating the clast. The intrusion varies from other Breccia 1s as it has; no plagioclase and a groundmass similar to the matrix. 40–45% quartz. 30–35% alteration 3. 20% alteration 1. Other smaller clasts consist of less plagioclase laths and an increase in alteration 1. 5% opaque minerals. Predominantly 0.01 mm pyrite with some larger 0.5 mm. Some 0.1 mm sphalerite.
C2 [TZ 8]	Porphyritic. 15% Subhedral – anhedral 1.8mm plagioclase. 6% anhedral quartz average size 0.90mm thick.
C1 [TX 3]	Porphyritic. <5% anhedral – subhedral white – straw yellow quartz phenocrysts average 0.25mm thick. Straight extinction and embayments. 30–35% greyish white plagioclase with a varying average size. The larger, mostly intact subhedral – anhedral plagioclase crystals found are on average 1.25mm thick with twinning in some phenocrysts.
C3b [TX 9]	Porphyritic. 5% anhedral white quartz phenocrysts average 1.1mm thick. 15% greyish white euhedral– subhedral plagioclase 1.6mm thick within the altered calcite crystals. Visible twinning/zonation. Quartz veining.
C3c [TX 1]	Porphyritic. 20% Euhedral white–straw yellow plagioclase) phenocrysts average 3mm thick. Visible twinning present. <10% unaltered, grey – white, anhedral quartz present 0.5– 2mm thick (average 0.8mm) with visible embayments and some smaller phenocrysts showing zonation.

Table 8: Table description for breccia matrix

Facie & Thin Section No.	Groundmass / matrix
C1 [TZ 11]	"Matrix. <2% anhedral quartz <0.08mm 5% alteration 1. 5 – 10% alteration 2. 65% alteration 3. 20–25% anhedral colourless clasts with very light brown shade. Goes opaque under XPL with odd <0.01,, fine grey inclusions. Also found within Breccia 1.
C1 [TX 2]	Approx 30–35% matrix, of which; 40 – 45% alteration of amorphous murky brown disseminations <10% calcite. <5% unaltered quartz. 25% alteration of grey amorphous mineral. 7% radial golden brown disseminations.
C1 [TX 7]	55 – 60% groundmass of which: 50% alteration 1. grey patches in both [PPL] & [XPL] almost amorphous. Found as patches/cement within the groundmass and surrounding some phenocrysts. Clay–like. 20% alteration 2. Dark golden brown [PPL] & [XPL] almost amorphous. Radial streaks of gold brown stretching from a centre point. A potential type of clay. 15% calcite. 20% Murky brown alteration
C1 [TX 13]	50 – 55% matrix of which: <3% anhedral white quartz phenocrysts. 20 – 25% grey patches in both [PPL] & [XPL] almost amorphous. Found as patches/cement within the groundmass and surrounding some phenocrysts. Likely type of clay. 50 – 55% pervasive murky light brown. <5% calcite. 10% radial golden brown alteration
C1 [TX 16]	25% Matrix which consists of: 55–60% <1micron thick disseminations of a sooty amorphous clay sized brown speck. 10–15% Blebs of a light yellow brown concentric fibrous rim. 25–30% <1micron clay sized amorphous grey pseudomorphs. Grey under PPL & XPL. Often angular shaped phenocryst/microlite grains, that have been entirely altered to this matte grey.
C1x [TX 8]	60– 65% groundmass of which: 20–25% white plagioclase microlites average <0.1mm thick. 65–70% grey patches in both [PPL] & [XPL] almost amorphous. Found as patches/cement within the groundmass and surrounding some phenocrysts. Likely type of clay. 10% Dark golden brown [PPL] & [XPL] almost amorphous. Radial streaks of gold brown stretching from a centre point. A potential type of clay.
C1x [TX 15]	50 – 55% groundmass of which: 20–25% white plagioclase microlites average <0.1mm thick. <3% anhedral white quartz phenocrysts. 40 – 45% grey patches in both [PPL] & [XPL] almost amorphous. Found as patches/cement within the groundmass and surrounding some phenocrysts. Likely type of clay. 30–35% yellow brown under both PPL and XPL. Blotchy–smear like appearance, spanning <5mm in some areas. <4% calcite.

C2 [TZ 6]	"Groundmass 35–40%laths of plagioclase inerstitial. 35–40% <1micron clay sized amorphous grey under PPL & XPL. 5% finer <0.05mm opaque minerals (mostly pyrite) disseminated within the groundmass. 10% [PPL] light orange brown mineral with trachytic texture.Visible individual grains are 5microns and grey with undulose extinction under [XPL].
C2x [TZ 9]	Groundmass 90%. 55–60% Laths of plagioclase microlites. Average size <0.05mm. Some areas of the thin section, plagioclase abundance dereases 30–35%. <4% quartz fragments. Average size 0.12mm. 30–35% Alteration 1. Appears as a flow like concentration in some areas of the thin section. 25–30% Alteration 2. <5% Calcite diseminations concentrated in a single corner of the thin section.
C2 [TZ 13]	45% Matrix. 40–45% Matrix filling of very fine quartz 5–10microns disseminated intergranularly. 5% occasional calcite pseudomorphs. Average size 0.10mm. 35–40% breccia fragments of alteration 1. 10–15% fragments of alteration 3
C2 [TZ 8]	Matrix. 35–40% quartz +–plagioclase microlites. 40 – 45% <1micron clay sized amorphous grey under PPL & XPL. <5% opaque minerals (mostly pyrite) disseminated within the groundmass. 10% [PPL] light orange brown mineral appears fibrous with a concentric rim in [PPL] and [XPL].Visible individual grains are 5microns and grey with undulose extinction under [XPL].
C1 [TX 3]	Approx 35 – 40% matrix, of which; 25–30% Alteration 1 25–30% irregular Pervasive brownish–red altered interstitial material between matrix components and clasts. 5–10% Alteration 2. 50 – 55% patches of a grey mineral (presumably relict larger plagioclase crystals which have altered into a grey mineral/clay). Some of these patches found within plagioclase crystals contain a remaining 10–15% plagioclase adjacent to the altered grey mineral. <10% unaltered quartz.
C3b [TX 9]	60 – 65% groundmass of which: 40 – 45% white plagioclase microlites average <0.1mm thick. 25–30% grey patches in both [PPL] & [XPL] almost amorphous. Found as patches/cement within the groundmass and surrounding some phenocrysts. Likely type of clay. 10% Dark golden brown [PPL] & [XPL] almost amorphous. Radial streaks of gold brown stretching from a centre point. A potential type of clay.
C3c [TX 1]	Approx 65% Groundmass, of which; 50 – 55%% plagioclase microlites and 40–45% calcite pseudomorphs. Calcite is irregular patchy throughout groundmass.

Table 9: Table description for breccia alteration features

Facie & Thin Section No.	Alteration
C1 [TZ 11]	Entirely Altered Alteration 1: Colourless plagioclase phenocrysts with a clouding light orange brown alteration. This alteration is low 1st order greys, yellow orange under XPL with irregular extinction within <0.01mm grains. Alteration 2: Colourless – orange brown amorphous discolouration similar to alteration 1 under PPL but slightly more cloudy orange. Entire pseudomorph/mineral becomes a coherent grey fill under XPL. Alteration 3. Pervasive amorphous grey. Transitions to an orange–brown in some areas of the thin section [PPL]. Alteration 4: Coherent fill of charcoal grey – brown splotches with an ink spill appearance under [PPL. Brown with a darker orange brown centre under XPL.
C1 [TX 2]	Very altered. 15–20% subhedral – anhedral calcite pseudomorphs. 5% 'opaque' subhedral – anhedral mostly pyrite phenocrysts with an average size of 0.05mm. These appear either as clusters or scattered throughout the groundmass. 25–30% irregular Pervasive brownish–red altered interstitial material between matrix components and clasts. 15 – 20% almost amorphous, dark grey under both PPL and XPL. Found as a patchy appearance within relict plagioclase microlites and phenocrysts.
C1 [TX 7]	Altered 25 –30% calcite showing a high birefringence colour with an oil slick like appearance. Found as partial or complete alteration of plagioclase crystals. 6% 'opaque' anhedral phenocrysts, which consist of predominantly of larger pyrite phenocrysts average thickness 1mm and pyrite clusters of 0.11mm. There are also some chalcopyrite and sphalerite phenocrysts at low concentrations <0.05mm thick. Alteration 1: grey patches in both [PPL] & [XPL] almost amorphous. Found as patches/cement within the groundmass and surrounding some phenocrysts. Clay–like. Alteration 2: Dark golden brown [PPL] & [XPL] almost amorphous. Radial streaks of gold brown stretching from a centre point. A potential type of clay.
C1 [TX 13]	Altered matrix, intact plagioclase and opx phenocrysts with minor alteration. <5% anhedral calcite. 3% 'opaque' subhedral – anhedral pyrite 0.13mm thick located as sporadic phenocrysts throughout the thin section. Some chalcopyrite also present. Minor quartz veining. Alteration 1: grey patches in both [PPL] & [XPL] almost amorphous. Found as patches/cement within the groundmass and surrounding some phenocrysts. Likely type of clay. Alteration 2: pervasive murky light brown.

C1 [TX 16]	Altered thin section. Some plagioclase phenocrysts and microlites altered almost entirely in to calcite pseudomorphs. 50% of plagioclase altered. 55–60% <1micron thick disseminated amorphous clay sized brown specks which are opaque under XPL. Present in both breccia clasts and matrix. Blebs of a light yellow brown PPL which sometimes divide into laths of 1st order greys and yellows under XPL emitted from a centre point as a fibrous rim. <1micron clay sized amorphous grey. Grey under PPL & XPL. Often angular shaped phenocryst/microlite grains, that have been entirely altered to this matte grey. Present in both breccia clasts and the matrix. Barren 3mm comb vein with 1mm of calcite lining the centre.
C1x [TX 8]	Very altered 20 – 25% anhedral calcite showing high birefringence colours giving an 'oil slick' appearance under XPL. Presumably relict plagioclase crystals which have altered into calcite. <3% 'opaque' anhedral phenocrysts which consist of pyrite average size <0.05mm located sporadically through the thin section. Alteration 1: grey patches in both [PPL] & [XPL] almost amorphous. Found as patches/cement within the groundmass and surrounding some phenocrysts. Likely type of clay. Alteration 2: Dark golden brown [PPL] & [XPL] almost amorphous. Radial streaks of gold brown stretching from a centre point. A potential type of clay.
C1x [TX 15]	Altered, 50% of relict plagioclase still intact. <5% anhedral calcite. 3% 'opaque' subhedral – anhedral pyrite 0.13mm thick located as sporadic phenocrysts throughout the thin section. Some chalcopyrite also present. Minor quartz veining. Alteration 1: 40 – 45% grey patches in both [PPL] & [XPL] almost amorphous. Found as patches/cement within the groundmass and surrounding some phenocrysts. Likely type of clay. Alteration 2: yellow brown under both PPL and XPL. Blotchy–smear like appearance, spanning <5mm in some areas.
C2 [TZ 6]	"Very altered thin section. Plagioclase phenocrysts 15 – 90%altered to calcite. Altered groundmass of the amorphous grey and light orange brown mineral. Barren 0.3mm wide quartz vein
C2x [TZ 9]	Altered 50% 10–15% calcite altering larger plagioclase phenocrysts. Alteration 1: < 1micron grey– dark brown clay sized amorphous mineral. Opaque under XPL. Alteration 2: Patches/streaks of fine brown giving a 'dusty or dirty' mineral appearance. Under XPL, entire mineral becomes 1st order yellows. Found as a partial alteration of some plagioclase phenocrysts. Disseminations of opaque minerals < 3%, predominantly fine 0.05mm pyrite with some sphalerite.
C2 [TZ 13]	Very Altered 50–75%. Alteration 1: grey amorphous <micron under both PPL and XPL Alteration 2: Calcite alteration as disseminations and partial alteration of plagioclase phenocrysts >50%. Alteration 3 anhedral orange brown–brown alteration low 1st order grey,yellow,orange XPL. Individual grains 25microns and show individual slightly undulating extinction. Dusty or fibrous alteration texture under PPL.

C2 [TZ 8]	Very altered thin section. Plagioclase up to 20–80% altered into calcite. Barren 0.1mm anastomosing network of quartz veining.
C1 [TX 3]	Very altered. Alteration 1: irregular Pervasive brownish–red altered interstitial material between matrix components and clasts. Alteration 2: patches of a grey mineral (presumably relict larger plagioclase crystals which have altered into a grey mineral/clay). Some of these patches found within plagioclase crystals contain a remaining 10–15% plagioclase adjacent to the altered grey mineral. 5–8% 'opaque' anhedral phenocrysts which are golden yellow under reflective light. These appear as cement/disseminated within the matrix. <5% calcite averaging 0.02mm thick showing a high birefringence colour with an oil slick like appearance. Found as occasional alteration within the plagioclase crystals.
C3b [TX 9]	Altered. 15–20% anhedral calcite Presumably relict plagioclase crystals which have altered into calcite. <4% 'opaque' subhedral – anhedral pyrite located as either 0.1mm thick veins, >4mm long or as sporadic phenocrysts with an average size 0.1mm throughout the thin section. Some minor concentrations of galena, average thickness <0.1mm. Yellow orange staining surrounding pyrite veining. Alteration 1: grey patches in both [PPL] & [XPL] almost amorphous. Found as patches/cement within the groundmass and surrounding some phenocrysts. Likely type of clay. Alteration 2: Dark golden brown [PPL] & [XPL] almost amorphous. Radial streaks of gold brown stretching from a centre point. A potential type of clay.
C3c [TX 1]	Very altered. <4% (opaque) anhedral – subhedral mostly pyrite phenocrysts with an average size of 0.13mm. Majority of plagioclase phenocrysts have been altered into patches of calcite.

Name: Gian Date:

0.1-0.2g ammonium iodide

Sample type:

Flux Used	12:22	LM100	Andesites >57% SiO2 and rhyolites
		Type 12:22	Basalts and basaltic andesites (47-57% SiO2)
		Type 57:43	Ultramafic rocks, carbonates, iron ores and materials high in bases

Sample Name	Flux Used	Sample (0.8g)		Flux (8g)	LOI
		on boat	after boat Actual	in crucible Actual	
1A	12:22	0.804	0.8039	8.0015	7.409615697
1B	12:22	0.8029	0.8026	8.0026	5.239408373
1Bb	12:22	0.7996	0.7993	8.004	7.170646121
1D	12:22	0.8005	0.7997	7.9988	4.044352832
2A	12:22	0.8029	0.8026	7.9992	4.609497304
2B	12:22	0.8003	0.8	8.0011	4.801269205
2Bx	12:22	0.8015	0.8013	8.0023	3.842252092
2C	12:22	0.7986	0.798	8.0025	3.676649623
3B	12:22	0.7997	0.7987	7.9998	5.791505792
3C*	12:22	0.8021	0.8007	8.0013	6.168647425
3C	12:22	0.8022	0.802	8.001	6.751894664
3Db	12:22	0.8022	0.8019	7.9995	4.236507644
3Db(Repeat)	-	-	-	-	4.241527514

Figure 26: Figure showing fusion disk data for XRF

Sample Name	SiO2 (%)	Al2O3 (%)	TiO2 (%)	MnO (%)	Fe2O3 (%)	MgO (%)	CaO (%)	Na2O (%)
A1	58.73	15.21	0.49	0.10	4.27	1.12	4.45	0.08
A2	65.57	14.26	0.53	0.04	4.62	1.17	1.28	0.39
A2x	56.94	16.49	0.89	0.06	7.63	1.68	1.37	0.09
B2	59.10	17.23	0.66	0.24	5.23	6.78	0.66	3.64
A4	63.54	13.63	0.49	0.11	6.40	2.72	0.41	1.00
A5	60.11	16.04	0.61	0.19	5.22	5.45	0.89	2.85
B1	60.80	15.80	0.58	0.16	5.08	4.68	5.32	2.23
C2	60.61	13.61	0.50	0.13	6.22	3.41	2.17	1.99
C3b	63.11	15.33	0.58	0.11	4.48	3.62	3.87	2.76

Figure 27: Figure showing the raw XRF data generated (1/2).

K2O (%)	P2O5 (%)	SO3 (%)	SrO (Sr - PPM)	BaO (Ba - PPM)	LOI (%)	Sum (%)
6.85	0.10	6.14	63	772	7.41	105.04
5.56	0.09	7.15	42	647	5.24	105.958
5.99	0.15	6.46	32	696	7.17	104.993
3.12	0.13	0.15	214	540	4.04	101.048
6.36	0.07	6.95	94	973	4.61	106.42
4.21	0.11	2.67	179.5	587.5	4.32	102.742
2.31	0.11	0.23	168	469	3.68	101.049
4.30	0.11	6.64	121.67	459.00	6.24	105.978
2.36	0.12	2.07	170	524	4.24	102.724

Figure 28: Figure showing the raw XRF data generated (2/2).